

Ⅲ. 研究成果の刊行に関する一覧表

研究成果の刊行に関する一覧表

雑誌

発表者氏名	論文タイトル名	発表誌名	巻号	ページ	出版年
Kobayashi E, Kamihara Y, Arai M, Wada A, Kikuchi S, Hatano R, Iwao N, Susukida T, Ozawa T, Adachi Y, Kishi H, Dang NH, Yamada T, Hayakawa Y, Morimoto C, Sato T.	Development of a Novel CD26-Targeted Chimeric Antigen Receptor T-Cell Therapy for CD26-Expressing T-Cell Malignancies.	Cells.	12(16)	2059	2023
Kikuchi S, Wada A, Kamihara Y, Okazaki K, Jawaid P, Rehman MU, Kobayashi E, Susukida T, Minemura T, Nabe Y, Iwao N, Ozawa T, Hatano R, Yamada M, Kishi H, Matsuya Y, Mizuguchi M, Hayakawa Y, Dang NH, Sakamoto Y, Morimoto C, Sato T.	DPP8 Selective Inhibitor Tominostat as a Novel and Broad-Spectrum Anticancer Agent against Hematological Malignancies.	Cells.	12(7)	1100	2023
Koyanagi Y, Kawasaki T, Kasuya Y, Hatano R, Sato S, Takahashi Y, Ohnuma K, Morimoto C, Dudek SM, Tsumi K, Suzuki T.	Functional roles of CD26/DPP4 in bleomycin-induced pulmonary fibrosis.	Physiol Rep.	11(6)	E15645	2023

発表者氏名	論文タイトル名	発表誌名	巻号	ページ	出版年
Kobayashi S, Fu go K, Hatano R, Yamazaki K, M orimoto C, Tera waki H.	Anti-glomerular Baseme nt Membrane Disease Concomitant with MPO -ANCA Positivity Conc urrent with High Serum Levels of Interleukin-2 6 Following Coronaviru s Disease 2019 Vaccina tion.	Intern Med.	62(7)	1043-1048	2023
Fujimoto N.	Spare the lung: surgical treatment approach for malignant pleural mes othelioma.	Transl Lung Cancer Res.	12(2)	197-199	2023
Hasegawa S, Shi ntani Y, Takuwa T, Aoe K, Kato K, Fujimoto N, Hida Y, Morise M, Moriya Y, Morohoshi T, S uzuki H, Chida M, Endo S, Kad okura M, Okumu ra M, Hattori S, Date H, Yoshin o I.	Nationwide prospective registry database of pat ients with newly diagn osed untreated pleural mesothelioma in Japan.	Cancer Sci.	115(2)	507-528	2024
Okaya T, Kawasa ki T, Sato S, Ko yanagi Y, Tatsum i K, Hatano R, O hnuma K, Morim oto C, Kasuya Y, Hasegawa Y, Oh ara O, Suzuki T.	Functional roles of CD2 6/DPP4 in bleomycin-ind uced pulmonary hyperten sion associated with inte rstitial lung disease.	Int J Mol Sc i.	25(2)	748	2024
Nishida H, Suzuki R, Nakajima K, Hayashi M, Mori moto C, Yamada T.	HDAC inhibition involve s CD26 induction on m ultiple myeloma cells vi a the c-Myc/Sp1-mediate d promoter activation.	Cancer Res C ommun.	4(2)	349-364	2024

IV. 研究成果の別刷

Article

Development of a Novel CD26-Targeted Chimeric Antigen Receptor T-Cell Therapy for CD26-Expressing T-Cell Malignancies

Eiji Kobayashi ^{1,†}, Yusuke Kamihara ^{2,†} , Miho Arai ³, Akinori Wada ² , Shohei Kikuchi ² , Ryo Hatano ⁴ , Noriaki Iwao ⁵, Takeshi Susukida ⁶ , Tatsuhiko Ozawa ¹, Yuichi Adachi ³, Hiroyuki Kishi ¹ , Nam H. Dang ⁷, Taketo Yamada ⁸, Yoshihiro Hayakawa ⁶ , Chikao Morimoto ⁴ and Tsutomu Sato ^{2,*}

- ¹ Department of Immunology, Faculty of Medicine, Academic Assembly, University of Toyama, 2630 Sugitani, Toyama 930-0194, Japan; ekoba@med.u-toyama.ac.jp (E.K.); toz@med.u-toyama.ac.jp (T.O.); immkishi@med.u-toyama.ac.jp (H.K.)
 - ² Department of Hematology, Faculty of Medicine, Academic Assembly, University of Toyama, 2630 Sugitani, Toyama 930-0194, Japan; kamihara@med.u-toyama.ac.jp (Y.K.); akino@med.u-toyama.ac.jp (A.W.); skikuchi@med.u-toyama.ac.jp (S.K.)
 - ³ Department of Pediatrics, Faculty of Medicine, Academic Assembly, University of Toyama, 2630 Sugitani, Toyama 930-0194, Japan; mkg8092@yahoo.co.jp (M.A.); ydachi@icloud.com (Y.A.)
 - ⁴ Department of Therapy Development and Innovation for Immune Disorders and Cancers, Graduate School of Medicine, Juntendo University, 2-1-1, Hongo, Bunkyo-ku, Tokyo 113-8421, Japan; rhatano@juntendo.ac.jp (R.H.); morimoto@ims.u-tokyo.ac.jp (C.M.)
 - ⁵ Department of Hematology, Juntendo University Shizuoka Hospital, Izunokuni City, Shizuoka 410-2211, Japan; niwao@juntendo.ac.jp
 - ⁶ Division of Host Defences, Institute of Natural Medicine, University of Toyama, 2630 Sugitani, Toyama 930-0194, Japan; susukida@inm.u-toyama.ac.jp (T.S.); haya@inm.u-toyama.ac.jp (Y.H.)
 - ⁷ Division of Hematology/Oncology, University of Florida, Gainesville, FL 32610-0275, USA; namdang5@outlook.com
 - ⁸ Department of Pathology, Saitama Medical University, 38 Morohongo, Moroyama, Saitama 3500495, Japan; taketo@keio.jp
- * Correspondence: tsutomus@med.u-toyama.ac.jp; Tel.: +81-76-434-7232
 † These authors contributed equally to this work.



Citation: Kobayashi, E.; Kamihara, Y.; Arai, M.; Wada, A.; Kikuchi, S.; Hatano, R.; Iwao, N.; Susukida, T.; Ozawa, T.; Adachi, Y.; et al.

Development of a Novel CD26-Targeted Chimeric Antigen Receptor T-Cell Therapy for CD26-Expressing T-Cell Malignancies. *Cells* **2023**, *12*, 2059. <https://doi.org/10.3390/cells12162059>

Academic Editor: Subramaniam Malarkannan

Received: 16 July 2023

Revised: 11 August 2023

Accepted: 11 August 2023

Published: 14 August 2023



Copyright: © 2023 by the authors. Licensee MDPI, Basel, Switzerland. This article is an open access article distributed under the terms and conditions of the Creative Commons Attribution (CC BY) license (<https://creativecommons.org/licenses/by/4.0/>).

Abstract: Chimeric-antigen-receptor (CAR) T-cell therapy for CD19-expressing B-cell malignancies is already widely adopted in clinical practice. On the other hand, the development of CAR-T-cell therapy for T-cell malignancies is in its nascent stage. One of the potential targets is CD26, to which we have developed and evaluated the efficacy and safety of the humanized monoclonal antibody YS110. We generated second (CD28) and third (CD28/4-1BB) generation CD26-targeted CAR-T-cells (CD26-2G/3G) using YS110 as the single-chain variable fragment. When co-cultured with CD26-overexpressing target cells, CD26-2G/3G strongly expressed the activation marker CD69 and secreted IFN γ . In vitro studies targeting the T-cell leukemia cell line HSB2 showed that CD26-2G/3G exhibited significant anti-leukemia effects with the secretion of granzymeB, TNF α , and IL-8, with 3G being superior to 2G. CD26-2G/3G was also highly effective against T-cell lymphoma cells derived from patients. In an in vivo mouse model in which a T-cell lymphoma cell line, KARPAS299, was transplanted subcutaneously, CD26-3G inhibited tumor growth, whereas 2G had no effect. Furthermore, in a systemic dissemination model in which HSB2 was administered intravenously, CD26-3G inhibited tumor growth more potently than 2G, resulting in greater survival benefit. The third-generation CD26-targeted CAR-T-cell therapy may be a promising treatment modality for T-cell malignancies.

Keywords: CD26; CAR-T; T-cell malignancies; third-generation; fratricide

1. Introduction

CD26 is a 110-kDa surface glycoprotein with intrinsic dipeptidyl peptidase IV (DPP-IV) activity that is expressed on various cell types and has many biological functions [1]. An important aspect of CD26 biology is its peptidase activity and its functional and physical association with molecules with key roles in various cellular pathways and biological programs [2]. Immune system CD4 T-cells, especially Th1, Th2, Th17, and T_{EM} (effector memory) cells with high cell-surface CD26 expression, demonstrate anti-tumoral properties [3]. Recent work also suggests that CD26 has significant roles in tumor biology, being both a marker of disease behavior clinically as well as playing an important role in tumor pathogenesis and development [2]. Moreover, we have had a long-standing interest in the role of CD26 in cancer biology and its suitability as a novel therapeutic target in selected neoplasms [4], particularly in view of its expression in such tumors such as malignant pleural mesothelioma (MPM), renal cell carcinoma (RCC), and T-cell malignancies [5].

Regarding MPM and RCC, our previous work showed that cell lines of both tissue types were suitable targets for our mouse anti-CD26 monoclonal antibody 14D10 [6,7]. Based on the amino-acid sequence of 14D10, we produced the recombinant DNA-derived humanized anti-CD26 monoclonal antibody YS110, which is effective against MPM cell lines [7]. Importantly, YS110 exhibited anti-tumor activity in patients with MPM and RCC, as demonstrated in two Phase 1 clinical trials and one Phase 2 trial conducted by our group [8–10]. Furthermore, we have shown that CD26 expressed on T-anaplastic large cell lymphoma KARPAS299 cells was involved in cell adhesion and tumorigenicity [11] and that KARPAS299 tumor growth was efficiently suppressed by our anti-CD26 monoclonal antibody 1F7 [12], indicating that CD26 is also a suitable therapeutic target for T-cell malignancies. Given the aggressive nature of T-cell malignancies, the lack of effective treatment and the poor prognosis associated with these cancers [13], there is an urgent need to develop effective therapy for use in the clinical setting. We, therefore, decided to develop a chimeric antigen receptor (CAR)-T-cell therapy based on YS110 given the established efficacy of this treatment modality against B-cell malignancies, even in the refractory setting, to the treatment with tumor-targeting monoclonal antibodies [14].

T-cell aplasia may be a possible on-target, off-tumor toxicity (OTOT) with CAR-T-cell therapy for T-cell malignancies [15–17], with acceptance of this side effect likely dependent on severity and treatment efficacy. This scenario may be analogous to how the effectiveness of CAR-T-cell therapy for B-cell malignancies led to acceptance of B-cell aplasia as an OTOT [18].

To establish CAR-T-cells, patient-derived or donor-derived T-cells are transduced with the genetic construct of the CAR to express the single-chain variable fragment (scFv). The scFv is usually designed from efficient antibodies by connecting their variable light (VL) and variable heavy (VH) chain domains with a peptide flexible linker in order to capture a specific antigen expressed on the surface of malignant cells.

CAR-T-cell therapy targeting CD19 or B-cell maturation antigen (BCMA) on B-cell malignancies is already established as a successful treatment modality in the clinical setting [19,20]. Thus far, only the second-generation of CAR-T-cell therapy targeting these two molecules have been approved, with either CD28 or 4-1BB as costimulatory signals [21]. However, the potential benefits of the third-generation of CD19 CAR-T-cell therapy over the second-generation have been suggested in the setting of clinical trials [22].

Building on the success of this novel approach, we used our well-established anti-CD26 antibody YS110 to develop CD26-targeted CAR-T-cell therapy for T-cell malignancies, demonstrating a greater anti-tumor effect of the third generation compared to the second generation of CAR.

2. Materials and Methods

2.1. Cell Culture

The T-cell non-Hodgkin's lymphoma (CD30+ anaplastic large cell lymphoma) cell line KARPAS299 was supplied by the European Collection of Authenticated Cell Cultures

(ECACC, Salisbury, UK). The T-lymphoblastic leukemia cell line HSB2, - cell acute lymphocytic leukemia cell line PEER, and T-cell lymphoma cell line (CD30+) Ki-JK were supplied by the Japanese Collection of Research Bioresources Cell Bank (JCRB, Tokyo, Japan). Cutaneous T-cell lymphoma (mycosis fungoides) cell line H9 and T-cell acute lymphocytic leukemia cell line Jurkat were supplied by the American Type Culture Collection (ATCC, Manassas, VA). All cell lines were authenticated by short tandem repeat (STR) profiling and were tested for mycoplasma to be free from contamination at each company. The stable transfectant of Jurkat cells which overexpress CD26 (CD26-Jurkat) has been established as described previously [23,24]. All these cell lines were maintained in RPMI 1640 (Gibco BRL, Tokyo, Japan) supplemented with 10% heat-inactivated fetal bovine serum (Sigma, St. Louis, MO), 100 µg/mL streptomycin, and 100 U/mL penicillin.

2.2. Patient Samples

Among the patients diagnosed with T-cell malignancies between January 2010 and December 2019 at the Division of Hematology, Toyama University Hospital, we randomly picked up biopsy specimens of twenty-one patients which were examined to evaluate the expression of CD26 by immunohistochemistry. The patients' diagnoses were as follows: anaplastic large cell lymphoma (ALCL) ($n = 2$), angioimmunoblastic T-cell lymphoma (AITL) ($n = 4$), extranodal NK/T-cell lymphoma (NK/T) ($n = 5$), and peripheral T-cell lymphoma (PTCL) ($n = 10$). Lymphoma cells from one PTCL and one AITL patient among the twenty-one patients mentioned above were employed as target cells to evaluate the killing effects of CD26-targeted CAR-T-cells. The PTCL patient exhibited a leukemic phase with 82% lymphoma cell involvement in total white blood cell counts of peripheral blood. The AITL patient had massive infiltration of lymphoma cells in the bone marrow. These lymphoma cells in peripheral blood or bone marrow were separated by a standard Ficoll-Hypaque technique.

2.3. Ethics Approval and Consent to Participate

This study was conducted according to the Declaration of Helsinki and was approved by the ethics committees of Toyama University Hospital (reference number R2019161). Written informed consent was obtained from all patients prior to study participation.

2.4. Luciferase-Expression Vector

The luciferase-expression vector was constructed by the insertion of luciferase gene from the pGL3 Luciferase Reporter Vector Basic (Promega, Madison, WI) into the pMXs-internal ribosomal entry site (IRES)-Kusabira-Orange 2 (KO2), which was prepared by the exchange of green fluorescent protein (GFP) gene in the pMXs-IRES-GFP for the CoralHue[®] humanized monomeric KO2 gene in the phmKO2-MNL (MBL, Nagoya, Japan).

2.5. Flow Cytometry

For flow cytometric analyses, samples were collected using a FACSCanto II flow cytometer (BD Biosciences, San Jose, CA) and analyzed with FlowJo software (Treestar, Ashland, OR). Expression of YS110 scFv was analyzed by its binding with the recombinant human CD26 protein (Fc chimera) (Abcam, Cambridge, MA), which was detected using an APC anti-human IgG F(c) antibody, goat polyclonal (Rockland immunochemicals, Limerick, PA) (Figure S1). Expression of CD8, CD26, human CD45, or mouse CD45 was analyzed using an APC anti-human CD8, clone 3B5, antibody (Invitrogen, Carlsbad, CA), an APC anti-human CD26 antibody, clone BA5b (BioLegend, San Diego, CA), a PE-Cy7 anti-human CD45 antibody, clone 2D1 (BioLegend), or an APC anti-mouse CD45 antibody, clone 30-F11 (Biolegend), respectively.

2.6. Immunohistochemical Staining

Expression of CD26 on lymphoma cells in biopsy specimens was assessed by immunohistochemistry using the standard protocol. In brief, following deparaffinization and

rehydration, biopsy specimens were incubated with anti-human CD26 mouse monoclonal antibody U16-3 as we previously described [25]. The CD26/anti-CD26 antibody immune complex on the tissue section was detected with the use of the second antibody conjugated with biotin, which was visualized with the 3,3'-diaminobenzidine peroxidase substrate kit (Vector Labs, Burlington, ON). Among the many methods of evaluating and interpreting the immunohistochemical data, we selected the immunoreactive score (IRS) [26], which gives a range of 0–12 as a product of multiplication between (A) positive cells proportion score (0–4) and (B) staining intensity score (0–3). The final IRS score will be a value between 0 and 12; 0–1 = negative, 2–3 = mild, 4–8 = moderate, and 9–12 = strong.

2.7. Construction of CD26 CAR

The basic structures of CD26 CAR-expression vectors were the same as those of TR1 CAR-expression vectors as we previously described [27]. For the anti-CD26 scFv region, we used the VH and VL of our well-established anti-CD26 antibody YS110 [8]. The nucleotide sequences encoding VH (SEQ ID NO: 215, page 85) or VL (SEQ ID NO: 216, page 86) and the amino acid sequences of VH (SEQ ID NO:22; X384) or VL (SEQ ID NO:18; X379) of YS110 (X392 Fab, rhuMAb411) are provided in our patent (US8030469B2; <https://patents.google.com/patent/US8030469B2/en> accessed on 13 August 2023). The nucleotide fragments of CD26 2/3G and control CD8 2/3G were synthesized (GenScript, Piscataway, NJ) and inserted into the pMXs-IRES-GFP retroviral expression vector RTV-013 (Cell Biolabs, San Diego, CA). As shown in Figure 1A, the second-generation CD26 CAR (CD26 2G/YS110-CD28) contains the leader sequence of the human κ chain (h κ -signal peptide), the YS110 scFv region, the CD8 hinge and transmembrane regions (CD8 hinge-TM), the CD28 intracellular signaling domain (CD28 cyto), and the CD3 ζ signaling domain (CD3 ζ cyto), in this order. The third-generation CD26 CAR (CD26 3G/YS110-CD28-4-1BB) additionally has the 4-1BB signaling domain (4-1BB cyto) between CD28 cyto and CD3 ζ cyto. CD8 controls (CD8 2G/CD8-CD28 and CD8 3G/CD8-CD28-4-1BB) contain the CD8-signal peptide followed by the extracellular domain of human CD8 (CD8) in place of the h κ -signal peptide followed by YS110 scFv of CD26 CAR. The IRES and the GFP genes are linked to the CD26 2/3G and CD8 2/3G as the transduction marker.

2.8. Transduction and Expression of CD26 CAR

Retroviral transduction was performed as we previously described [27]. Briefly, expression vectors of CD26 2/3G and control CD8 2/3G were transfected into Phoenix-A cells (kindly provided by Dr. G. Nolan, Stanford University) using FuGENE[®]6 (Promega). Culture supernatants were collected 72 h following transfection. For retroviral infection into peripheral blood mononuclear cells (PBMCs), retrovirus in the culture supernatants were spin-loaded into 24-well culture plate coated with 20 μ g/mL retronectin (TaKaRa, Kyoto, Japan) by centrifugation for 2 h at 2000 \times g at 32 °C according to the manufacturer's instructions. PBMCs (5×10^5 cells) in 1 mL of medium, which have been stimulated with Dynabeads CD3/CD28 T-Cell Expander (Invitrogen Dynal AS, Oslo, Norway) at a concentration of 25 μ L/ 1×10^6 cells and 30 U/mL of recombinant human interleukin-2 (rhIL-2) (PeproTech Rocky Hill, NJ) for two days, were added to the retrovirus-loaded 24-well culture plate and spun down at 500 \times g at 22 °C for 10 min, followed by incubation at 37 °C. Following three days of incubation, the cells were transferred into a 25 cm² cell culture flask, and medium containing 30 U/mL of rhIL-2 was added. At day 5 following retroviral transfection, 25 μ L of Dynabeads CD3/CD28 T-Cell Expander was added to each cell culture flask.

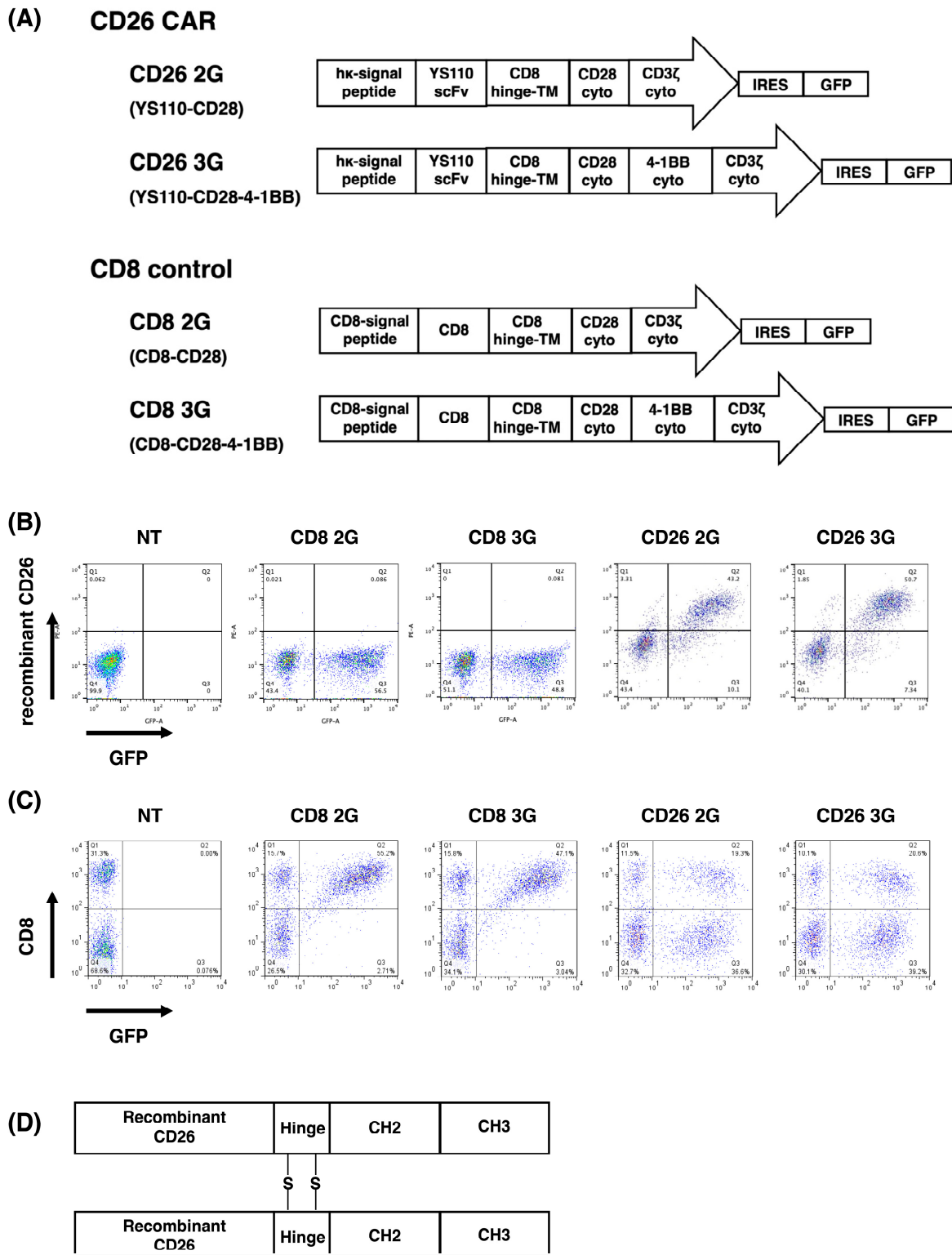


Figure 1. Transduction and expression of CD26 CAR. Gene transduction of CD26 2/3G and control CD8 2/3G into PBMCs was confirmed by GFP marker fluorescence three days following retroviral infection. **(A)** Schematic diagram of CD26 CAR and CD8 control. **(B)** Expression of YS110 scFv on CD26 2/3G-transfected PBMCs was confirmed by binding to Fc-tagged recombinant CD26, which was detected by the anti-Fc antibody conjugated with PE. **(C)** Expression of CD8 on control CD8 2/3G-transfected PBMCs was confirmed with the anti-CD8 antibody conjugated with PE. **(D)** Construct schema for rh-CD26 FC-chimera. Data are representative of three independent experiments ($n = 3$).

2.9. Activation of CD26 CAR-T-Cells

CD26 2/3G CAR-T-cells and CD8 2/3G control cells were placed onto a 96-well culture plate (1×10^5 cells/well) as the effector cells and were co-cultured overnight with CD26-Jurkat or HSB2 cells as the target cells. For positive controls of the activated effector cells, effector cells were incubated with both 10 ng/mL of phorbol-12-myristate 13-acetate (PMA) (FUJIFILM Wako, Osaka, Japan) and 500 ng/mL of ionomycin (Merck, Darmstadt, Germany) for the same period without the target cells. CD69 expression on effector cells, which were selected from the target cells by gating on marker fluorescence GFP, was then analyzed by flow cytometry using an APC anti-human CD69 antibody, clone FN50 (BioLegend). Furthermore, concentrations of interferon gamma (IFN- γ) and granzyme B in the culture supernatants secreted by the effector cells were measured by the Enzyme-Linked Immuno Sorbent Assay (ELISA) method using a Human IFN-gamma DuoSet ELISA (R&D Systems, Minneapolis, MN) and a Human Granzyme B DuoSet ELISA (R&D Systems). The concentrations of tumor necrosis factor-alpha (TNF α) and interleukin-8 (IL-8) were also measured by flow cytometry using a BDTM Cytometric Bead Array (CBA) Kit (BD Biosciences) according to the manufacturer's instructions.

2.10. In Vitro Anti-Tumor Activity of CD26 CAR-T-Cells

HSB2, H9, and KARPAS299 target cells were retrovirally transduced with the luciferase gene by the same method as described above to transduce CD26 2/3G into PBMCs. These target cells were placed onto a 96-well culture plate (1×10^4 cells/well). CD26 2/3G CAR-T-cells or CD8 2/3G control cells were then co-cultured as the effector cells with the target cells for 24 h. The luciferase from the target cells was measured using a Steady-Glo Luciferase Assay System (Promega). For blocking experiments, KARPAS299 target cells were treated with 1 μ g/mL of control IgG or YS110 2 h prior to co-culturing. KARPAS299 cells were then co-cultured with CD26 3G CAR-T-cells or CD8 3G control cells for 6 h.

2.11. In Vivo Anti-Tumor Activity of CD26 CAR-T-Cells

In vivo experiments were performed as we previously described [28,29]. NOD.Cg-Prkdc^{scid}Il2rg^{tm1Wjl}/SzJ (NSG) female mice of age (6–7 weeks) and weight (19–21 g) were obtained from Charles River Japan Inc. (Kanagawa, Japan). The mice were kept under specific pathogen-free conditions with a 12 h day and night cycle with free access to food and water, and received humane care in compliance with Institutional Guidelines. All experiments were approved by the animal care and use committee of Toyama University (reference number A2022MED-14). In order to examine the anti-lymphoma activity of CD26 CAR-T-cells, KARPAS299 and HSB2 cells were retrovirally transduced with pMXs luciferase-IRES-KO2 vector mentioned above. Subsequently, 1×10^6 of KARPAS299 cells were transplanted subcutaneously into NSG mice at day 0. 1×10^7 of CD26 2/3G CAR-T-cells or CD8 2/3G control cells were then injected intravenously through the lateral tail veins twice at day 6 and day 13. Tumor volume (mm³) was calculated by the formula: $\frac{1}{2}$ (length \times width²). Luciferase luminescence was estimated using the IVIS Imaging System (PerkinElmer, Waltham, MA) to monitor tumor growth. Signal intensity of the tumor burdens was expressed in Luminescence (photon/sec). To model systemic dissemination, 1×10^6 of HSB2 cells were transplanted intravenously into NSG mice at day 0. 1×10^7 of CD26 2/3G CAR-T-cells or CD8 2/3G control cells were then injected intravenously once at day 1. To monitor tumor growth, bioluminescence imaging using IVIS was performed. Survival of mice was also monitored. In order to identify CD26 3G CAR-T-cells injected into mice, peripheral blood of mice was collected at day 15. Human cells such as CD26 3G CAR-T-cells and HSB2 cells were selected by flow cytometry from live lymphocytes as both human CD45-positive and mouse CD45-negative cells. In human cells, HSB2 cells were identified as the KO2-positive cells and CD26 3G CAR-T-cells were identified as the GFP-positive cells.

2.12. *In Vitro* Anti-Tumor Activity of CD26 CAR-T-Cells against Patient Samples

Lymphoma cells from the patients (1×10^5) mentioned above were co-cultured with CD26 2/3G CAR-T-cells or CD8 2/3G control cells (1×10^6) for 24 h. CD26 2/3G CAR-T-cells and CD8 2/3G control cells were pre-stained with CellTrace™ Oregon Green® 488 Carboxylic Acid Diacetate Succinimidyl Ester (CTOG) (Thermo Fisher Scientific, Ogden, UT, USA) to distinguish these cells from the lymphoma cells by flow cytometry as Alexa Fluor 488-positive cells. The percentage of CD26-positive cells in the Alexa Fluor 488-negative lymphoma cells was a measurement of the anti-tumor effect of CD26 CAR-T-cells. Dead cells were excluded with the staining of Fixable Viability Dye-eFluor™ 780 (eBioscience, Waltham, MA, USA).

2.13. Statistical Analysis

All statistical analyses were performed using GraphPad Prism 9 (GraphPad Software, La Jolla, CA, USA). Statistical significance was determined using Student's t-test. To analyze the statistical significance of differences in survival curves constructed using the Kaplan–Meier method, the log-rank test was used. Statistical significance was defined as $p < 0.05$.

3. Results

3.1. Transduction and Expression of CD26 CAR

The basic structures of CD26 CAR-expression vectors were the same as those of TR1 CAR-expression vectors as we previously described [27]. For the anti-CD26 scFv region, we used VH and VL of our well-established anti-CD26 antibody YS110 [8] as shown in Figure 1A. Evaluation of GFP fluorescence of PBMCs as the marker of transduction three days following retroviral infection showed a transduction efficacy of approximately 50% for CD26 2/3G and control CD8 2/3G (Figure 1B,C). For these studies, we employed T-cells expressing CD8-signal peptide on the cell surface (CD8 2/3G control cells) as a control for CD26 2/3G CAR-T-cells expressing YS110 scFv. The appropriateness of this control was shown in our previous report [27]. We also examined the expression of YS110 scFv on PBMCs transduced with CD26 2/3G by its binding with the recombinant human CD26 protein (Fc chimera) (Figure 1D). As shown in Figure 1B, almost all of the GFP-positive cells bound to recombinant CD26, as detected by an anti-Fc antibody. CD8 expression on PBMCs transduced with control CD8 2/3G was also confirmed since no CD8-negative cells were detected in the GFP-positive cell population (Figure 1C). As a side note, approximately 30% of cells were CD8-positive in the “no transduction (NT)” PBMCs.

3.2. Expansion of CD26 CAR-T-Cells

As shown in Figure 2A, PBMC cell numbers gradually increased following retroviral infection of CD26 2/3G and control CD8 2/3G from day 0 (0.5×10^6 cells) until day 9 ($10\text{--}20 \times 10^6$ cells). We did observe that the number of cells transduced with CD26 2/3G was lower than that of control CD8 2/3G at day 6, likely due to the phenomenon of “fratricide” in the CD26 2/3G CAR-T-cell population [30,31]. Nevertheless, CD26 3G CAR-T-cell level was similar to CD8 3G control cell level by day 9. On the other hand, the CD26 2G CAR-T-cell number was higher than the CD8 2G control cell number at day 9, but then rapidly decreased over the following days. Cells were, therefore, stored on day 9 or 10 and used for subsequent experiments. In order to further analyze the fratricide phenomenon, we assessed CD26 expression at day 3, 6, 9, and 12 (Figure 2B). In contrast to the high level of CD26 expression in the CD8 2/3 control cell population, there was no CD26 expression on CD26 2/3G CAR-T-cells. Our findings were similar to previous work showing loss of CD5 on CD5 2G CAR-T-cells due to fratricide during the expansion process [32].

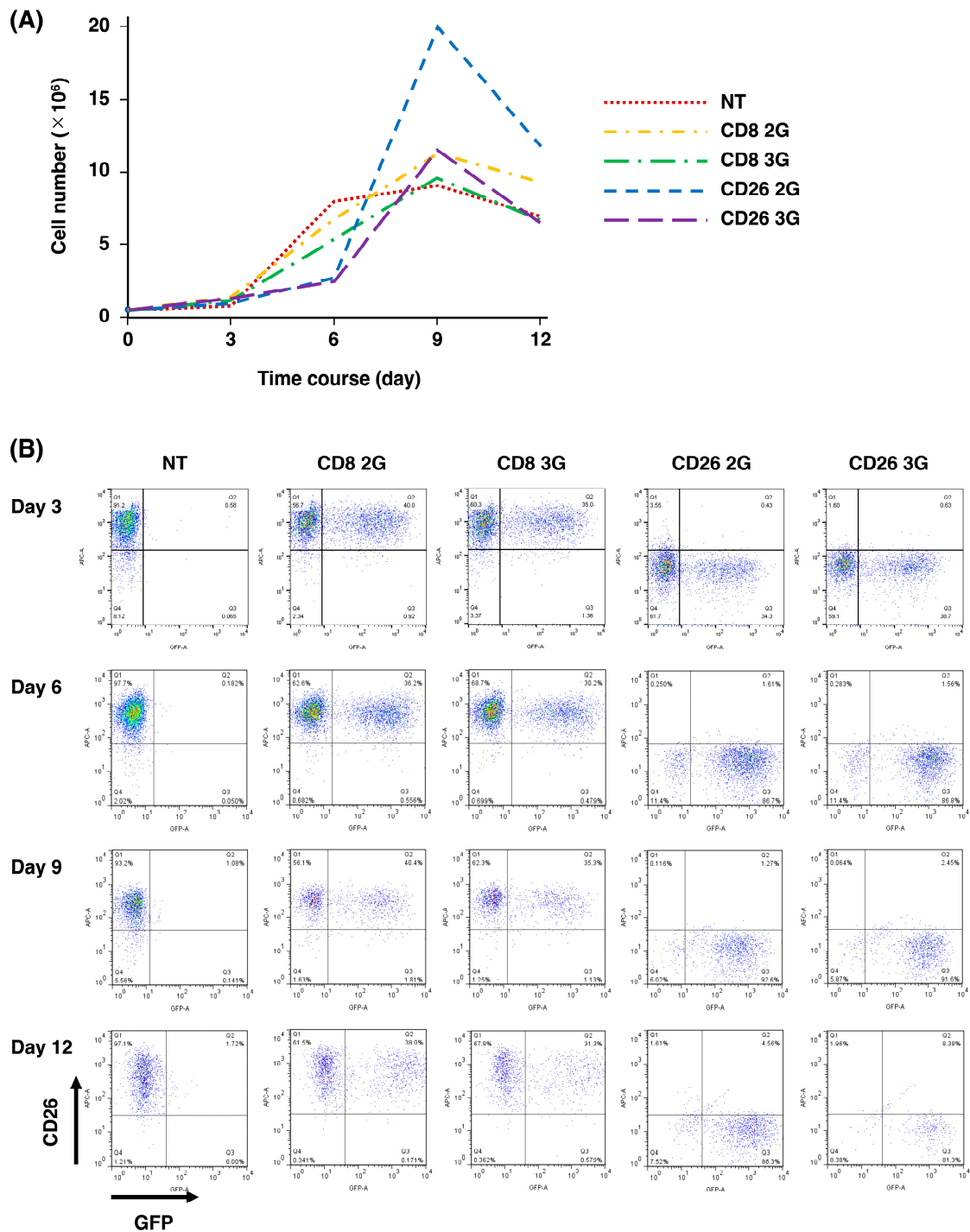


Figure 2. Expansion of CD26 CAR-T-cells. **(A)** Cell numbers of CD26 2/3G CAR-T-cells and CD8 2/3G control cells were determined at day 3, 6, 9 and 12 following retroviral infection. **(B)** CD26 expression on CD26 2/3G CAR-T-cells and CD8 2/3G control cells was analyzed at day 3, 6, 9, and 12 by flow cytometry. Data are representative of three independent experiments ($n = 1$).

3.3. Activation of CD26 CAR-T-Cells

CD26 2/3G CAR-T-cells and CD8 2/3G control cells were fully stimulated by PMA and ionomycin (P/I), as demonstrated by the high level of CD69 expression and IFN- γ secretion (Figure S2). Meanwhile, co-culture with CD26-Jurkat cells overexpressing CD26 artificially as the target cells (Figure S3A) resulted in activation of the CD26 2/3G CAR-T-cell population, as demonstrated by CD69 expression (Figure S2A) and IFN- γ secretion

(Figure S2B). However, such effects were not observed on the CD8 2/3G control cells. Furthermore, the secretion of granzyme B, TNF α , and IL-8 of CD26 3G CAR-T-cells was much higher than that of CD26 2G CAR-T-cells with the statistical significance (Figure 3) when we used a malignant T-cell line, HSB2 cells expressing CD26 originally (Figure S3B) as the target cells.

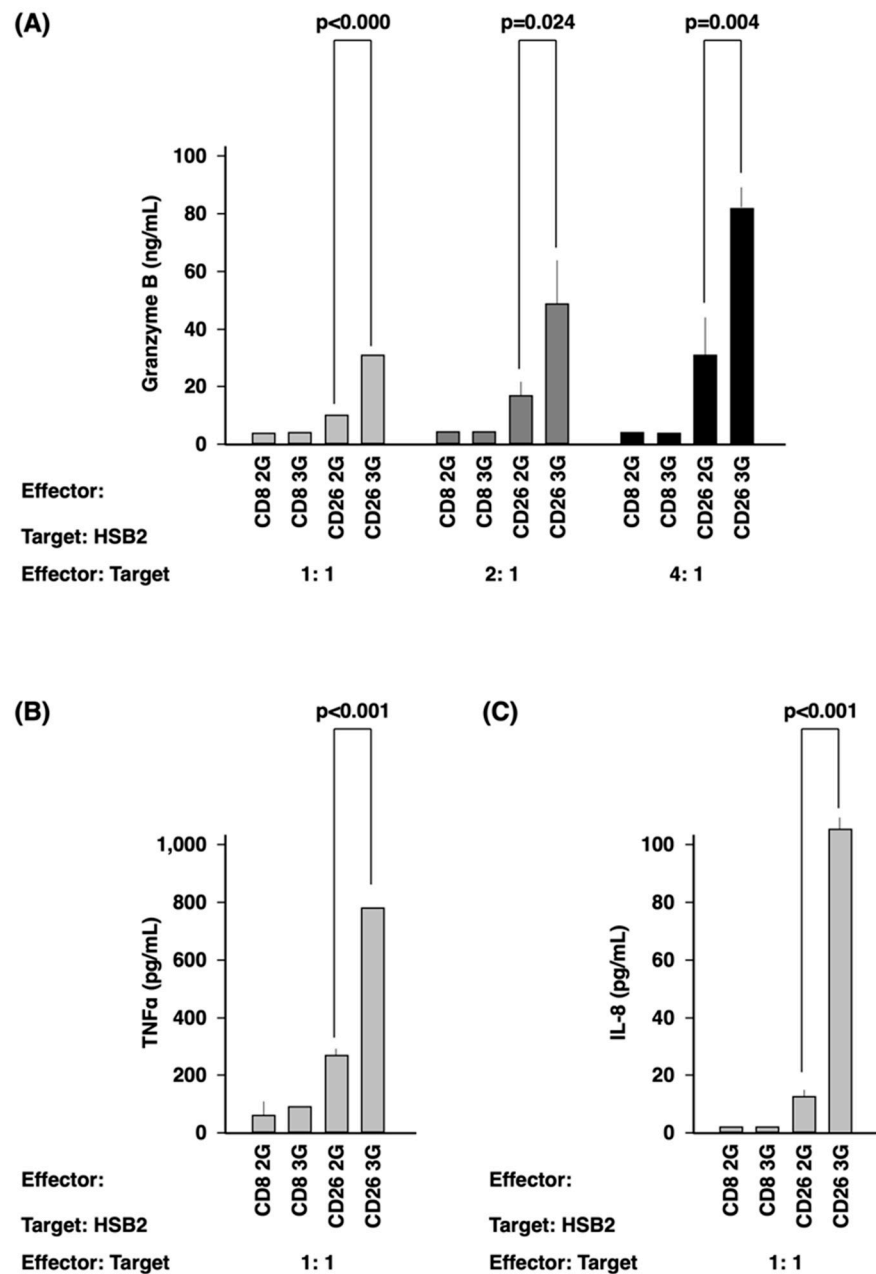


Figure 3. Activation of CD26 CAR-T-cells. Effector cells (CD26 2/3G CAR-T-cells and CD8 2/3G control cells) were cultured with HSB2 cells as target cells at an effector:target ratio of 1:1, 2:1, and 4:1. (A) Secretion of granzyme B was evaluated by ELISA assay. (B,C) Secretion of TNF α (B) and IL-8 (C) were evaluated by flow cytometry. Data are representative of three independent experiments ($n = 3$).

3.4. In Vitro Anti-Tumor Activity of CD26 CAR-T-Cells

Then, we examined the anti-tumor effect of CD26 CAR-T-cells on HSB2 cells. CD26 3G CAR-T-cells demonstrated greater anti-tumor activity than CD26 2G CAR-T-cells at both 1:1 and 5:1 effector:target cells ratios ($p < 0.001$ and 0.004 , respectively) (Figure 4A). As shown in Figure 4B, the anti-tumor activity of CD26 3G CAR-T-cells was further confirmed

with the other CD26-expressing T-cell lines (Figure S3B), H9 and KAPPA299. The anti-tumor effect of CD26 3G CAR-T-cells was completely abrogated by pretreatment of the target KARPAS299 cells with anti-CD26 antibody YS110 prior to co-culture (Figure S4).

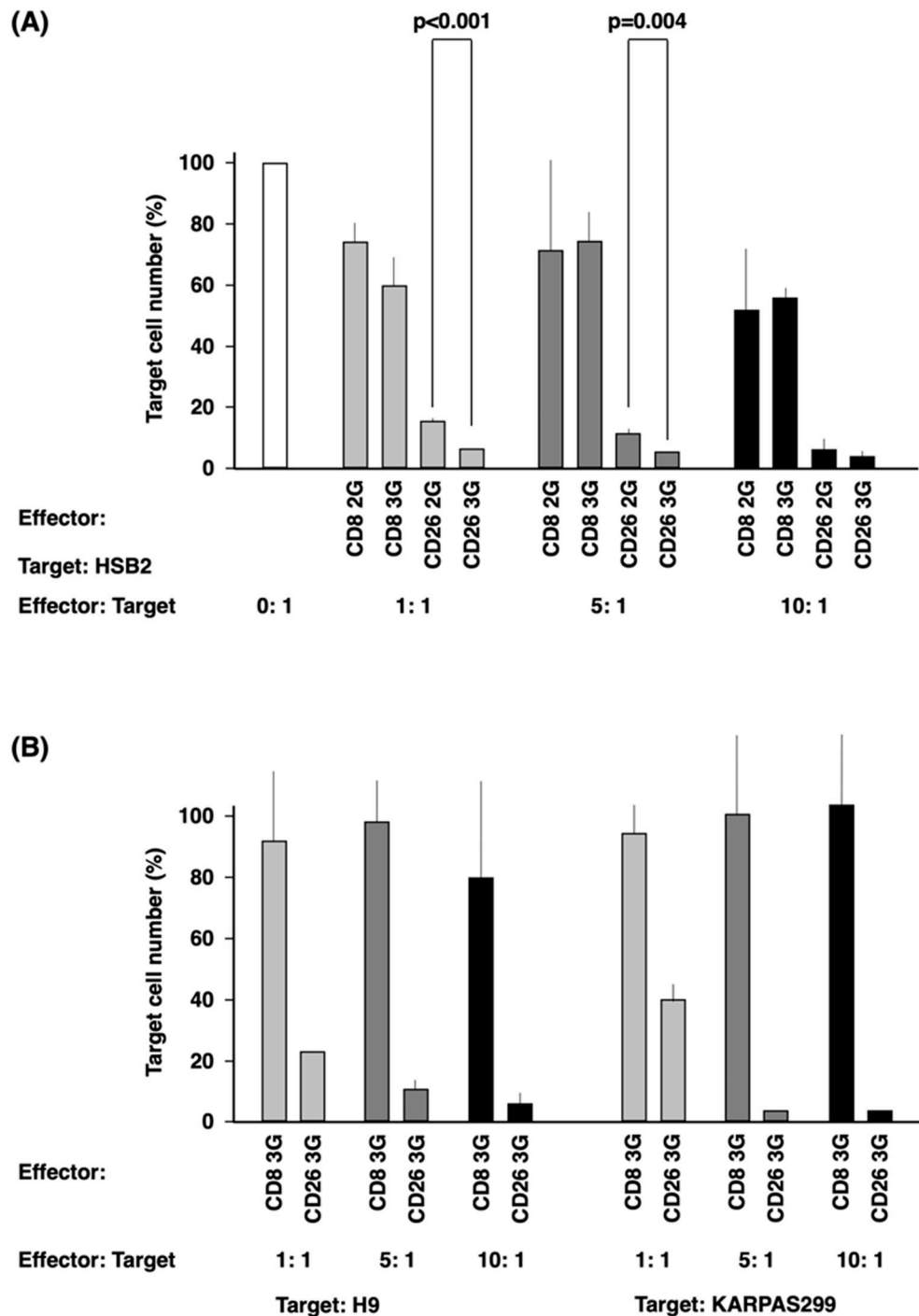


Figure 4. In vitro anti-tumor activity of CD26 CAR-T-cells. **(A)** Target cells (HSB2 cells) were co-cultured with effector cells (CD26 2/3G CAR-T-cells or CD8 2/3G control cells) at an effector:target ratio of 0:1, 1:1, 5:1, and 10:1. **(B)** Target cells (H9 and KARPAS299 cells) were co-cultured with effector cells (CD26 3G CAR-T-cells or CD8 3G control cells) at an effector:target ratio of 1:1, 5:1, and 10:1. Anti-tumor activity of effector cells was evaluated by measurement of luciferase activity from the target cells. Data are representative of three independent experiments ($n = 3$).

3.5. In Vivo Anti-Tumor Activity of CD26 CAR-T-Cells

Using a subcutaneous tumor model with the T-lymphoma cell line KARPAS299 (Figure 5A,B), our studies showed that there was no difference in the effect of CD26 2G CAR-T-cells and CD8 2G control cells on tumor growth. In contrast, CD26 3G CAR-T-cells displayed statistically significant anti-lymphoma activity compared with CD8 3G control cells ($p = 0.019$ in Figure 5A and $p = 0.029$ in Figure 5B). We then employed a systemic dissemination model with the T-leukemia cell line HSB2, as described previously [33], with the tumor cells being administered through the tail vein (Figure 5C–E). CD26 2/3G CAR-T-cells significantly inhibited leukemic dissemination compared with CD8 2/3G control cells at day 7 ($p = 0.000$ and $p = 0.002$, respectively) (Figure 5C and Figure S5). The presence of circulating live CD26 3G CAR-T-cells in the mouse peripheral blood was confirmed at day 15 (Figure S6). At day 21, the relative leukemic burden in mice treated with CD26 3G CAR-T-cells was significantly less than mice treated with CD26 2G CAR-T-cells ($p = 0.026$) (Figure 5D). The median survival period of mice treated with CD26 3G CAR-T-cells was 37 days, which was significantly longer than the median of 32 days for mice treated with CD26 2G CAR-T-cells ($p = 0.002$) (Figure 5E).

3.6. Anti-Tumor Activity of CD26 CAR-T-Cells against Patient Samples

CD26 expression was detected through immunohistochemical staining on all the biopsy specimens of patients with T-cell malignancies ($n = 21$), which were randomly selected (Table 1). The intensity of staining was mild in five, moderate in nine, and strong in seven samples (typical staining results are demonstrated in Figure S7). Furthermore, lymphoma cells from the peripheral blood of one CD26-positive (moderate) PTCL patient with leukemic phase involvement and from the bone marrow of one CD26-positive (moderate) AITL patient with massive bone marrow involvement were co-cultured as the target cells with CD26 2/3G CAR-T-cells or CD8 2/3G control cells (Figure 6). The level of CD26-positive cells from the PTCL sample were 50–70% following co-culturing with CD8 2/3G control cells while co-culturing with CD26 2/3G CAR-T-cells reduced the level of CD26-positive cells to 1–2% (Figure 6A). Similar results were obtained with the AITL sample (Figure 6B). As supplemental data, CD26 expression across various immature and mature T-cell malignancies are presented in Table S1.

Table 1. The immunoreactive score (IRS) of CD26 in mature T- and NK-cell neoplasms.

	Negative	Positive		
		Mild	Moderate	Strong
ALCL ($n = 2$)	0	0	2	0
AITL ($n = 4$)	0	0	4	0
NK/T ($n = 5$)	0	3	0	2
PTCL ($n = 10$)	0	2	3	5

ALCL, anaplastic large cell lymphoma; AITL, angioimmunoblastic T-cell lymphoma; NK/T, extranodal NK/T-cell lymphoma; and PTCL, peripheral T-cell lymphoma.

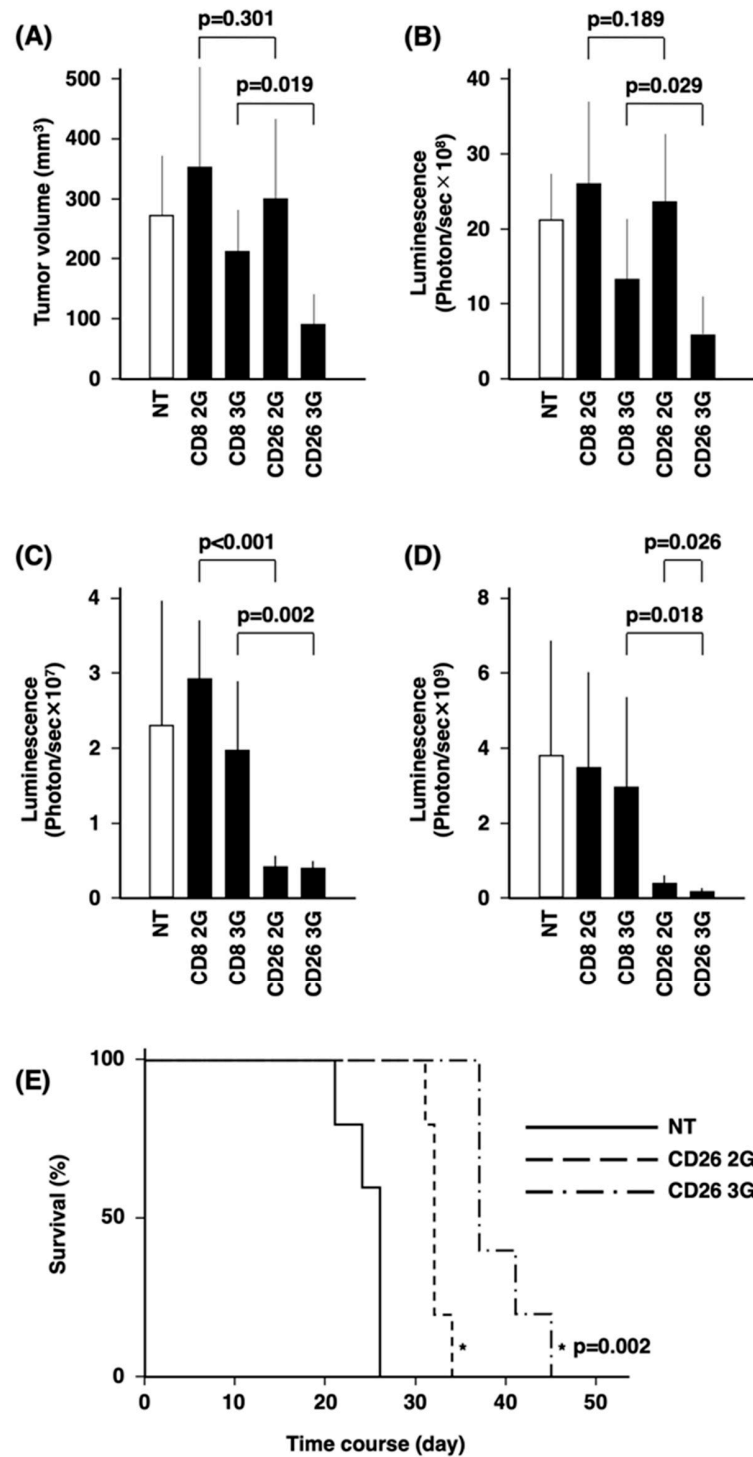


Figure 5. In vivo anti-tumor activity of CD26 CAR-T-cells. (A,B) KARPAS299 cells transduced with luciferase gene were transplanted subcutaneously into NSG mice at day 0. CD26 2/3G CAR-T-cells or CD8 2/3G control cells were then injected intravenously twice at day 6 and day 13. Tumor volume (mm³) (A) and luminescence (photon/sec) (B) at day 20 are presented (*n* = 6). (C–E) HSB2 cells transduced with the luciferase gene were transplanted intravenously into NSG mice at day 0 as a murine model of systemic dissemination. CD26 2/3G CAR-T-cells or CD8 2/3G control cells were then injected intravenously once at day 1. Luminescence (photon/sec) at day 7 (C) and day 21 (D) are presented (*n* = 6). For the same model of systemic dissemination, CD26 2/3G CAR-T-cells were injected intravenously once at day 1 and survival of mice was monitored (*n* = 5) (E).

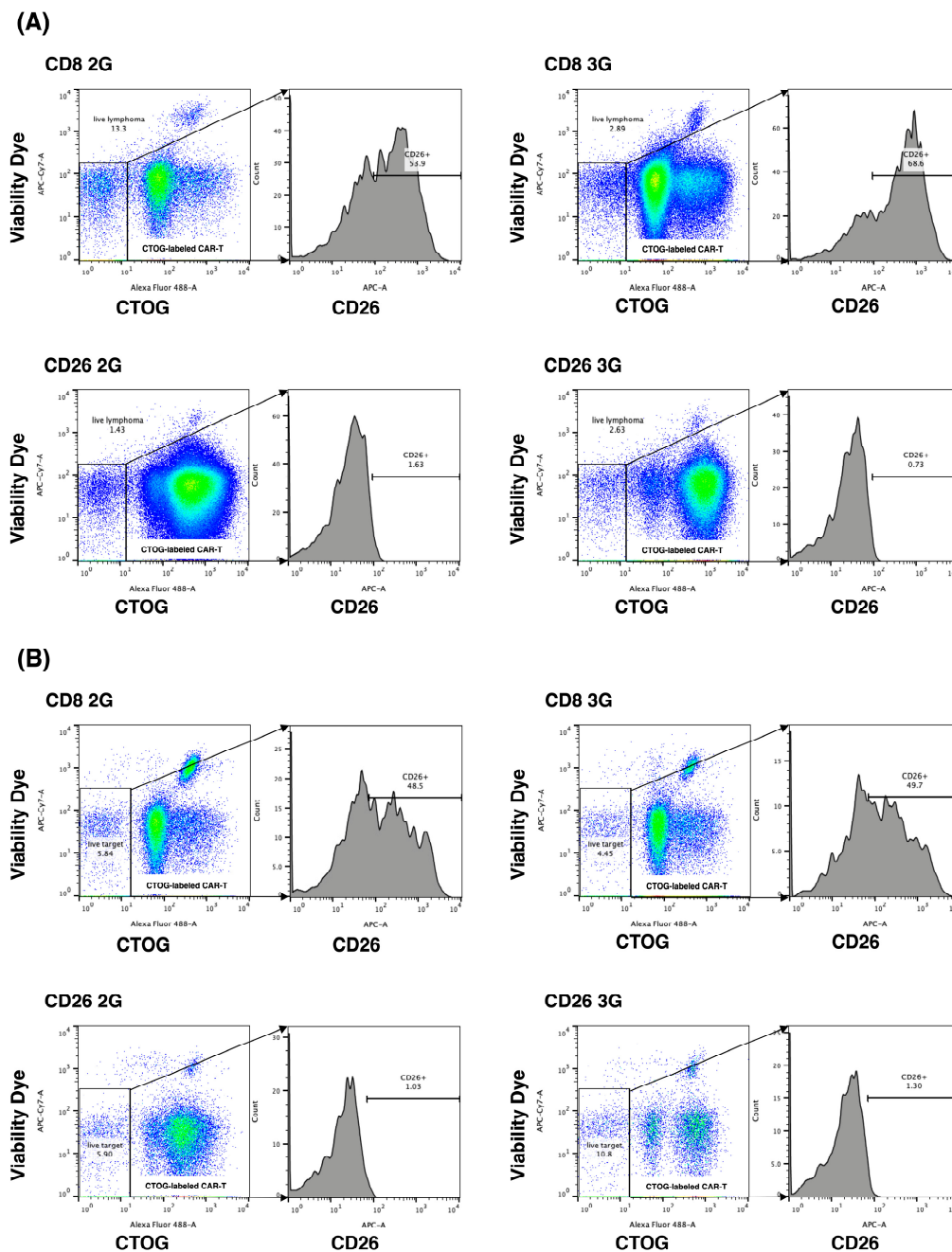


Figure 6. In vitro anti-tumor activity of CD26 CAR-T-cells against patient lymphoma samples. CD26-expressing lymphoma cells from patients with PTCL (A) ($n = 1$) or AITL (B) ($n = 1$) were co-cultured with CD26 2/3G CAR-T-cells or CD8 2/3G control cells. CD26 2/3G CAR-T-cells or CD8 2/3G control cells were pre-stained with CTOG and were distinguished from lymphoma cells by flow cytometry as the Alexa Fluor 488-positive cells. CD26 expression was evaluated in the Alexa Fluor 488-negative lymphoma cells. Data are representative of three independent experiments ($n = 3$).

4. Discussion

In the present study, we have demonstrated that the novel CD26-targeted CAR-T therapy based on our previously developed YS110 antibody may be a promising treatment modality for CD26-expressing T-cell malignancies, particularly third-generation CAR-T-cells containing both CD28 and 4-1BB as co-stimulatory domains.

The CD28 co-stimulatory domain in CD19 2G CAR-T-cells results in the rapid expansion and immediate differentiation into short-lived T effector cells, whereas 4-1BB in

CD19 2G CAR-T-cells induces limited T-cell differentiation with the development of central memory T-cells and longer immune control. Despite these differences in biological activity, it is heretofore unclear as to which co-stimulatory domain produces superior clinical outcomes [30]. Of course, the functionality of CAR depends not only on co-stimulation molecules but also the combination of these with scFv, the linker, and the hinge-final 3D configuration. The CD19 CAR-T-cells currently used in the clinical setting are the second-generation products, which have as their co-stimulatory domain either CD28 (axicabtagene ciloleucel; axi-cel) or 4-1BB (tisagenlecleucel; tisa-cel and lisocabtagene maraleucel; liso-cel). However, CD28 and 4-1BB signal through different pathways and may have complementary functions. Indeed, previous studies have demonstrated that CD20 3G (CD28 and 4-1BB) CAR-T-cells exhibited greater activation of intracellular signaling pathways, more potent antitumor activity, and longer in vivo persistence than CD20 2G (CD28) CAR-T-cells [34,35]. The potential superiority of CD19 3G has been suggested in a clinical trial, in which CD19 2G CAR-T-cells (CD28) and CD19 3G CAR-T-cells (CD28 and 4-1BB) were infused simultaneously in 16 patients with relapsed or refractory non-Hodgkin's lymphoma. This trial demonstrated that CD19 3G CAR-T-cells had superior expansion and greater persistence than CD19 2G CAR-T-cells [22]. However, more work still needs to be done to determine whether CD19 3G is clinically superior to CD19 2G.

The nature of the co-stimulatory domain of CAR is an important issue in the usage of CAR-T-cell therapy in T-cell malignancies, since normal T-cells share most targetable surface antigens with T-cell malignancies. Therefore, CAR-T-cells targeting T-cell malignancies also target each other, resulting in the phenomenon of "fratricide". This problem was well-described in previous work involving CD5 CAR-T-cells [30]. CD5 2G (4-1BB) CAR-T-cells failed to expand due to fratricide since the TRAF signaling from 4-1BB upregulated the level of intercellular adhesion molecule 1, which stabilized the fratricidal immunologic synapse between CD5 CAR-T-cells [30]. In contrast, the limited fratricide associated with CD5 2G (CD28) CAR-T-cells allowed for sufficient cellular expansion to exert antitumor activity toward T-cell malignancies [32]. Interestingly, the expansion of CD5 CAR-T-cells was accompanied by the downregulation of CD5, possibly facilitating the expansion of CD5 CAR-T-cells and limiting fratricide. Of note is that CD5 downregulation possibly occurred at the translational and/or post-translational level since overall transcription of the CD5 gene was unaltered [32]. This point is particularly important because downregulation of the cognate antigen on tumor cells is a mechanism of escape, and may partly explain the decreased level of target-bearing cells, in addition to direct cell killing effect of CAR-T.

Similar results have been described with YS110-based CD26 2G CAR-T-cells by other researchers [31,36]. Their work showed that CD26 2G (4-1BB) CAR-T-cells exhibited poor viability, multiple cytokine secretion, and direct cytotoxicity against themselves, resulting in fratricide [31]. In contrast, the initial expansion of CD26 2G (CD28) CAR-T-cells were delayed due to transient fratricide, but subsequent expansion of CAR-T-cells was accelerated with the downregulation of CD26. These CD26 2G (CD28) CAR-T-cells displayed cytotoxicity against CD26-positive malignant cells, activated multiple effector functions in co-culture assays, and limited tumor progression in a mouse model [36].

Expansion of both CD26 2G (CD28) CAR-T and CD26 3G (CD28 and 4-1BB) CAR-T-cells associated with CD26 downregulation was also observed in our experiments. Both CD26 2/3G CAR-T-cell populations might undergo transient fratricide at the beginning of culture (Figure 2), consistent with previous reports [32,36]. Similar to CD5, downregulation of CD26 could possibly result from translational or post-translational modifications [32]. Another potential mechanism for decreased CD26 surface expression may involve CD26 intracellular translocation upon YS110 stimulation [37].

In addition, we also observed the accelerated expansion and rapid decrease of CD26 2G CAR-T-cells compared with CD26 3G CAR-T-cells and CD8 2/3G control cells (Figure 2A). This phenomenon may be caused by the stimulatory effects of YS110 scFv itself. We previously reported that crosslinking of CD26 and CD3 with solid-phase immobilized monoclonal antibodies could induce T-cell activation and interleukin-2 production and that

anti-CD26 antibody treatment of T-cells enhanced the tyrosine phosphorylation of signaling molecules such as CD3 ζ and p56^{lck} [38–42]. YS110 scFv might stimulate CD26 2G CAR-T-cells prior to the downregulation of CD26 in combination with Dynabeads CD3/CD28 and rhIL-2, resulting in the rapid expansion and subsequent exhaustion of the cell population. On the other hand, YS110 scFv-mediated stimulation in the CD26 3G CAR-T-cells might be stabilized by signaling from 4-1BB since 4-1BB activates the noncanonical nuclear factor κ B (ncNF- κ B) signaling cascade, which is necessary for the survival and persistence of CD19 CAR-T-cells [43]. It is our hypothesis that the lack of ncNF- κ B activation could likely result in overstimulation of CD26 2G CAR-T-cells from CD26-mediated signaling.

Most importantly, our present findings demonstrated the successful development of a third-generation CD26-targeted CAR-T with superior *in vitro* and *in vivo* activity than the second-generation product against T-cell malignancies. This difference may partly be due to the longer survival of CD26 3G CAR-T-cells compared to CD26 2G CAR-T-cells since our data demonstrated a sharp decline following a significant increase after day 6 of CD26 2G CAR-T-cells (Figure 2A); however, CD26 3G CAR-T-cells were detected in mouse peripheral blood after 15 days post-administration (Figure S6) as well as CD26 2G CAR-T-cells.

Based on previous work, it is our hypothesis that the superior efficacy of CD26 3G CAR-T-cells against T-cell malignancies as compared to CD26 2G CAR-T-cells is at least partially due to 4-1BB-mediated ncNF- κ B activation [43]. The 4-1BB/ncNF- κ B signaling cascade might affect the degree of CAR-T-cell activation. In our present study, we have clearly demonstrated that the secretion of granzyme B, TNF α , and IL-8 by CD26 3G CAR-T-cells was higher than that seen with CD26 2G CAR-T-cells (Figure 3). This result was compatible with a previous report demonstrating that CD20 3G CAR-T-cells secreted much higher levels of IFN- γ than CD20 2G (CD28) CAR-T-cells [35]. Given the aggressive nature of T-cell malignancies, the lack of effective treatment and the poor prognosis associated with these cancers [13], a novel therapy that is effective can potentially be very beneficial in the clinical setting. While the *in vivo* survival-prolonging effect of CD26 3G CAR-T-cells may be modest, our data do not preclude the possible use of CD26 3G CAR-T-cell therapy in the clinical setting. Of note is that while CD19 2G (CD28) CAR-T-cell therapy prolonged mouse survival by only one week compared to controls [44], it has demonstrated impressive efficacy in real-world clinical practice, as noted above. While the CD26-targeting CAR-T-cell therapy was highly efficient in the subcutaneous model, it prolonged the survival of mice in the intravenous model for 5 days, which would be equivalent to approximately 6 months for humans. These findings would suggest that the novel therapy may be more appropriate for T-cell lymphoma subtypes rather than for leukemic T-cell malignancies.

The development of CAR-T-cell therapy for T-cell malignancies is underway, with CD5, CD7, and CD30 being targeted in these efforts [21]. In particular, Phase 1 trial of CD7 CAR-T-cell therapy has been completed and excellent response rates have been reported [45]. In this context, a potential advantage of CD26 over CD5, CD7, and CD30 as a target is its expression frequency in T-cell malignancies. CD5, CD7, and CD30 expression levels in PTCL were 85%, 50%, and 16%, respectively; in AITL, 96%, 57%, and 32–50%, respectively; in ALCL, 30%, 32–54%, and 93%, respectively [46]. On the other hand, as shown in Table 1, all 21 patients with PTCL, AITL, ALCL, and NK/T tested expressed CD26, ranging from mild to strong intensity. This ubiquitous expression of CD26 in T-cell malignancies may result in high level of efficacy for CD26 CAR-T-cell therapy in the clinical setting. Of note, our immunostaining assays used the anti-human CD26 mouse monoclonal antibody U16-3, which was developed by our group with high sensitivity and specificity in formalin-fixed, paraffin-embedded samples [25].

A concern for the practical application of CD26 CAR-T-cell therapy in the clinical setting is CD26 expression in normal tissues. Since CD26 is highly expressed on normal T lymphocytes [47], lymphopenia is an expected side effect of CD26 CAR-T-cell therapy. Cordero and colleagues demonstrated that most human CD26-negative CD4 T-cells in circulating lymphocytes are central memory cells while CD26-high expression is present

on effector Th1, Th2, Th17, and TEM (effector memory) cells. Therefore, future clinical trials should monitor the levels of these cell types [3]. In addition, since CD26 expression is observed in salivary glands and smooth muscle [47], salivary gland inflammation and gastrointestinal symptoms may potentially be associated with CD26 CAR-T-cell therapy. In the Phase 2 study of YS110, lymphopenia was [3] seen in 45% of patients, while diarrhea and nasopharyngitis were observed in 13% of patients [9]. Furthermore, soluble CD26 level and associated DPPIV activity may be reduced with CD26 CAR-T-cell therapy, findings which were observed with the administration of YS110 [9]. A potential clinical manifestation of this phenomenon may be hypoglycemia, an infrequent side effect associated with administration of DPPIV inhibitors to diabetic patients [48]. Clinical trials are needed to determine the side effect profiles of CD26 CAR-T-cell therapy, particularly since YS110 does not bind to mouse CD26 (unpublished data), hence preventing the assessment of adverse events associated with CD26 CAR-T-cell therapy in a mouse model.

In summary, CD26-targeting CAR-T-cell therapy is a promising therapeutic alternative against T-cell malignancies. Our findings indicate that a third-generation CAR-T product combining both CD28 with 4-1BB co-stimulatory domains displays more anti-tumor activity than the second-generation product harboring CD28 alone. We plan to further validate our conclusion in future studies involving multiple patient donors.

5. Conclusions

In this study, we developed and evaluated the efficacy and safety of CD26-targeted CAR-T-cell therapy for T-cell malignancies using YS110 as the single-chain variable fragment. We demonstrated that CD26 3G CAR-T-cells exhibited superior anti-leukemia effects than CD26 2G CAR-T-cells in vitro and in vivo. Our findings suggest that CD26 3G CAR-T-cells are promising candidates for the treatment of T-cell malignancies, which are currently challenging to treat with conventional therapies. However, further studies are needed to optimize the design and delivery of CD26-targeted CAR-T-cells, as well as to assess their long-term safety and efficacy in clinical settings.

Supplementary Materials: The following are available online at <https://www.mdpi.com/article/10.3390/cells12162059/s1>, Figure S1: Schematic diagram describing the method to detect expression of YS110 scFv. Figure S2: Activation of CD26 CAR-T-cells. Effector cells (CD26 2/3G CAR-T-cells and CD8 2/3G control cells) were cultured with both PMA and ionomycin (P/I) as positive controls or with CD26-Jurkat cells as target cells at an effector: target ratio of 1:1. (A) CD69 expression on effector cells was analyzed by flow cytometry. (B) Secretion of IFN- γ was evaluated by ELISA assay. Figure S3: Expression of CD26 on various T-cell lines. Figure S4: Blocking effect of YS110 against CD26 3G CAR-T-cells. Target cells (KARPAS299 cells) were co-cultured with effector cells (CD26 3G CAR-T-cells or CD8 3G control cells) at an effector:target ratio of 1:1, 5:1, and 10:1 with control IgG or YS110. Anti-tumor activity of effector cells was evaluated by measurement of luciferase activity from the target cells. Figure S5: Monitoring of mice transplanted with HSB2 cells by IVIS. Actual photographic data of luciferase luminescence of Figure 5C. Figure S6: Identification of CD26 3G CAR-T-cells in mice. In experiments described in Figure 5C–E, CD26 3G CAR-T-cells injected into mice were identified. (A) In peripheral blood of mice collected at day 15, human cells were selected by flow cytometry from live lymphocytes as both human CD45-positive and mouse CD45-negative cells. (B,C). In human cells, HSB2 cells were identified as the KO2-positive cells and CAR-T-cells were identified as the GFP-positive cells. (B) Control mice without injection of CD26 3G CAR-T-cells (NT). (C) Mice with injection of CD26 3G CAR-T-cells. Figure S7: Expression of CD26 on lymphoma cells in patient samples. Biopsy specimens of patients with T-cell malignancies were stained for CD26 by immunohistochemistry. Four typical results of staining assays are demonstrated. (A) ALCL patient with “moderate” staining intensity. (B) AITL patient with “moderate” staining intensity. (C) NK/T patient with “strong” staining intensity. (D) PTCL patient with “strong” staining intensity. Table S1: CD26 expression across various immature and mature T-cell malignancies.

Author Contributions: Investigation, methodology, Y.K., M.A., A.W., S.K., R.H., N.I., T.S. (Takeshi Susukida), T.O., T.Y. and Y.H.; supervision, Y.A., H.K. and C.M.; writing—review and editing, N.H.D.;

funding acquisition, writing—original draft: E.K. and T.S. (Tsutomu Sato). All authors have read and agreed to the published version of the manuscript.

Funding: This research was supported by Japan Science and Technology Agency (JST) Moonshot R&D Grant Number JPMJMS2021, Japan Agency for Medical Research and Development (AMED) Grant Number 21lm0203005j0005 (A145), 22ym0126807j0001 (A160), 21am0401024h0003, and Japan Society for the Promotion of Science (JSPS) Grant-in-Aid for Scientific Research Grant Number 21K07237, 21H02782.

Institutional Review Board Statement: This study was approved by the ethics committees of Toyama University Hospital (reference number R2019161) and by the animal care and use committee of Toyama University (reference number A2022MED-14).

Informed Consent Statement: Informed consent was obtained from all subjects involved in the study.

Data Availability Statement: Data are available on reasonable request. All data relevant to the study are included in the article.

Acknowledgments: We gratefully thank Toyomi Kozawa, Mai Sasai, and, Toshiyuki Fujiwara for their help in performing this study.

Conflicts of Interest: The authors declare no conflict of interest.

References

- Ohnuma, K.; Hosono, O.; Dang, N.H.; Morimoto, C. Dipeptidyl Peptidase in Autoimmune Pathophysiology. *Adv. Clin. Chem.* **2011**, *53*, 51–84.
- Thompson, M.; Ohnuma, K.; Abe, M.; Morimoto, C.; Dang, N. CD26/Dipeptidyl Peptidase IV as a Novel Therapeutic Target for Cancer and Immune Disorders. *Mini-Rev. Med. Chem.* **2007**, *7*, 253–273. [[CrossRef](#)] [[PubMed](#)]
- Cordero, O.J.; Rafael-Vidal, C.; Varela-Calviño, R.; Calviño-Sampedro, C.; Malvar-Fernández, B.; García, S.; Viñuela, J.E.; Pego-Reigosa, J.M. Distinctive CD26 Expression on CD4 T-Cell Subsets. *Biomolecules* **2021**, *11*, 1446. [[CrossRef](#)] [[PubMed](#)]
- Ohnuma, K.; Hatano, R.; Komiya, E.; Otsuka, H.; Itoh, T.; Iwao, N.; Kaneko, Y.; Yamada, T.; Dang, N.H.; Morimoto, C. A Novel Role for CD26/Dipeptidyl Peptidase IV as a Therapeutic Target. *Front. Biosci.* **2018**, *23*, 1754–1779. [[CrossRef](#)] [[PubMed](#)]
- Havre, P.A.; Abe, M.; Urasaki, Y.; Ohnuma, K.; Morimoto, C.; Dang, N.H. The Role of CD26/Dipeptidyl Peptidase IV in Cancer. *Front. Biosci.* **2008**, *13*, 1345–1351. [[CrossRef](#)]
- Inamoto, T.; Yamochi, T.; Ohnuma, K.; Iwata, S.; Kina, S.; Inamoto, S.; Tachibana, M.; Katsuoka, Y.; Dang, N.H.; Morimoto, C. Anti-CD26 Monoclonal Antibody-Mediated G1-S Arrest of Human Renal Clear Cell Carcinoma Caki-2 Is Associated with Retinoblastoma Substrate Dephosphorylation, Cyclin-Dependent Kinase 2 Reduction, P27kip1 Enhancement, and Disruption of Binding to the Extracellular Matrix. *Clin. Cancer Res.* **2006**, *12*, 3470–3477. [[PubMed](#)]
- Inamoto, T.; Yamada, T.; Ohnuma, K.; Kina, S.; Takahashi, N.; Yamochi, T.; Inamoto, S.; Katsuoka, Y.; Hosono, O.; Tanaka, H.; et al. Humanized Anti-CD26 Monoclonal Antibody as a Treatment for Malignant Mesothelioma Tumors. *Clin. Cancer Res.* **2007**, *13*, 4191–4200. [[CrossRef](#)]
- Angevin, E.; Isambert, N.; Trillet-Lenoir, V.; You, B.; Alexandre, J.; Zalcman, G.; Vielh, P.; Farace, F.; Valleix, F.; Podoll, T.; et al. First-in-Human Phase 1 of YS110, a Monoclonal Antibody Directed against CD26 in Advanced CD26-Expressing Cancers. *Br. J. Cancer* **2017**, *116*, 1126–1137. [[CrossRef](#)]
- Nakagawa, K.; Kijima, T.; Okada, M.; Morise, M.; Kato, M.; Hirano, K.; Fujimoto, N.; Takenoyama, M.; Yokouchi, H.; Ohe, Y.; et al. Phase 2 Study of YS110, a Recombinant Humanized Anti-CD26 Monoclonal Antibody, in Japanese Patients With Advanced Malignant Pleural Mesothelioma. *JTO Clin. Res. Rep.* **2021**, *2*, 100178. [[CrossRef](#)]
- Takeda, M.; Ohe, Y.; Horinouchi, H.; Hida, T.; Shimizu, J.; Seto, T.; Nosaki, K.; Kishimoto, T.; Miyashita, I.; Yamada, M.; et al. Phase I Study of YS110, a Recombinant Humanized Monoclonal Antibody to CD26, in Japanese Patients with Advanced Malignant Pleural Mesothelioma. *Lung Cancer* **2019**, *137*, 64–70. [[CrossRef](#)]
- Sato, T.; Yamochi, T.; Yamochi, T.; Aytac, U.; Ohnuma, K.; McKee, K.S.; Morimoto, C.; Dang, N.H. CD26 Regulates P38 Mitogen-Activated Protein Kinase-Dependent Phosphorylation of Integrin B1, Adhesion to Extracellular Matrix, and Tumorigenicity of T-Anaplastic Large Cell Lymphoma Karpas 299. *Cancer Res.* **2005**, *65*, 6950–6956. [[CrossRef](#)] [[PubMed](#)]
- Ho, L.; Aytac, U.; Stephens, L.C.; Ohnuma, K.; Mills, G.B.; McKee, K.S.; Neumann, C.; LaPushin, R.; Cabanillas, F.; Abbruzzese, J.L.; et al. In Vitro and in Vivo Antitumor Effect of the Anti-CD26 Monoclonal Antibody 1F7 on Human CD30+ Anaplastic Large Cell T-Cell Lymphoma Karpas 299. *Clin. Cancer Res.* **2001**, *7*, 2031–2040. [[PubMed](#)]
- Escalón, M.P.; Liu, N.S.; Yang, Y.; Hess, M.; Walker, P.L.; Smith, T.L.; Dang, N.H. Prognostic Factors and Treatment of Patients with T-Cell Non-Hodgkin Lymphoma: The M.D. Anderson Cancer Center Experience. *Cancer* **2005**, *103*, 2091–2098. [[CrossRef](#)] [[PubMed](#)]

14. Schuster, S.J.; Tam, C.S.; Borchmann, P.; Worel, N.; McGuirk, J.P.; Holte, H.; Waller, E.K.; Jaglowski, S.; Bishop, M.R.; Damon, L.E.; et al. Long-Term Clinical Outcomes of Tisagenlecleucel in Patients with Relapsed or Refractory Aggressive B-Cell Lymphomas (JULIET): A Multicentre, Open-Label, Single-Arm, Phase 2 Study. *Lancet Oncol.* **2021**, *22*, 1403–1405. [[CrossRef](#)] [[PubMed](#)]
15. Flugel, C.L.; Majzner, R.G.; Krenciute, G.; Dotti, G.; Riddell, S.R.; Wagner, D.L.; Abou-el-Enein, M. Overcoming On-Target, off-Tumour Toxicity of CAR T Cell Therapy for Solid Tumours. *Nat. Rev. Clin. Oncol.* **2023**, *20*, 49–62. [[CrossRef](#)] [[PubMed](#)]
16. Safarzadeh Kozani, P.; Safarzadeh Kozani, P.; Rahbarizadeh, F. CAR-T Cell Therapy in T-Cell Malignancies: Is Success a Low-Hanging Fruit? *Stem Cell Res. Ther.* **2021**, *12*, 527. [[CrossRef](#)]
17. Fleischer, L.C.; Spencer, H.T.; Raikar, S.S. Targeting T Cell Malignancies Using CAR-Based Immunotherapy: Challenges and Potential Solutions. *J. Hematol. Oncol.* **2019**, *12*, 141. [[CrossRef](#)]
18. Safarzadeh Kozani, P.; Safarzadeh Kozani, P.; Rahbarizadeh, F. Optimizing the Clinical Impact of CAR-T Cell Therapy in B-Cell Acute Lymphoblastic Leukemia: Looking Back While Moving Forward. *Front. Immunol.* **2021**, *12*, 765097. [[CrossRef](#)]
19. Mohanty, R.; Chowdhury, C.R.; Arega, S.; Sen, P.; Ganguly, P.; Ganguly, N. CAR T Cell Therapy: A New Era for Cancer Treatment (Review). *Oncol. Rep.* **2019**, *42*, 2183–2195. [[CrossRef](#)]
20. Rinaldi, I.; Muthalib, A.; Edina, B.C.; Wiyono, L.; Winston, K. Role of Anti-B-Cell Maturation Antigen (BCMA) in the Management of Multiple Myeloma. *Cancers* **2022**, *14*, 3507. [[CrossRef](#)]
21. Barros, L.R.C.; Couto, S.C.F.; da Silva Santurio, D.; Paixão, E.A.; Cardoso, F.; da Silva, V.J.; Klinger, P.; Ribeiro, P.d.A.C.; Rós, F.A.; Oliveira, T.G.M.; et al. Systematic Review of Available CAR-T Cell Trials around the World. *Cancers* **2022**, *14*, 2667. [[CrossRef](#)] [[PubMed](#)]
22. Ramos, C.A.; Rouce, R.; Robertson, C.S.; Reyna, A.; Narala, N.; Vyas, G.; Mehta, B.; Zhang, H.; Dakhova, O.; Carrum, G.; et al. In Vivo Fate and Activity of Second- versus Third-Generation CD19-Specific CAR-T Cells in B Cell Non-Hodgkin's Lymphomas. *Mol. Ther.* **2018**, *26*, 2727–2737. [[CrossRef](#)] [[PubMed](#)]
23. Aytac, U.; Claret, F.X.; Ho, L.; Sato, K.; Ohnuma, K.; Mills, G.B.; Cabanillas, F.; Morimoto, C.; Dang, N.H. Expression of CD26 and Its Associated Dipeptidyl Peptidase IV Enzyme Activity Enhances Sensitivity to Doxorubicin-Induced Cell Cycle Arrest at the G(2)/M Checkpoint. *Cancer Res.* **2001**, *61*, 7204–7210.
24. Aytac, U.; Sato, K.; Yamochi, T.; Yamochi, T.; Ohnuma, K.; Mills, G.B.; Morimoto, C.; Dang, N.H. Effect of CD26/Dipeptidyl Peptidase IV on Jurkat Sensitivity to G2/M Arrest Induced by Topoisomerase II Inhibitors. *Br. J. Cancer* **2003**, *88*, 455–462. [[CrossRef](#)] [[PubMed](#)]
25. Hatano, R.; Yamada, T.; Madokoro, H.; Otsuka, H.; Komiya, E.; Itoh, T.; Narita, Y.; Iwata, S.; Yamazaki, H.; Matsuoka, S.; et al. Development of Novel Monoclonal Antibodies with Specific Binding Affinity for Denatured Human CD26 in Formalin-Fixed Paraffinembedded and Decalcified Specimens. *PLoS ONE* **2019**, *14*, e0218330. [[CrossRef](#)] [[PubMed](#)]
26. Fedchenko, N.; Reifemath, J. Different Approaches for Interpretation and Reporting of Immunohistochemistry Analysis Results in the Bone Tissue—A Review. *Diagn. Pathol.* **2014**, *9*, 221. [[CrossRef](#)]
27. Kobayashi, E.; Kishi, H.; Ozawa, T.; Hamana, H.; Nakagawa, H.; Jin, A.; Lin, Z.; Muraguchi, A. A Chimeric Antigen Receptor for TRAIL-Receptor 1 Induces Apoptosis in Various Types of Tumor Cells. *Biochem. Biophys. Res. Commun.* **2014**, *453*, 798–803. [[CrossRef](#)]
28. Ono, K.; Sato, T.; Iyama, S.; Tatekoshi, A.; Hashimoto, A.; Kamihara, Y.; Horiguchi, H.; Kikuchi, S.; Kawano, Y.; Takada, K.; et al. A Novel Strategy Inducing Autophagic Cell Death in Burkitt's Lymphoma Cells with Anti-CD19-Targeted Liposomal Rapamycin. *Blood Cancer J.* **2014**, *4*, e180. [[CrossRef](#)]
29. Sato, T.; Tatekoshi, A.; Takada, K.; Iyama, S.; Kamihara, Y.; Jawaid, P.; Rehman, M.U.; Noguchi, K.; Kondo, T.; Kajikawa, S.; et al. DPP8 Is a Novel Therapeutic Target for Multiple Myeloma. *Sci. Rep.* **2019**, *9*, 18094. [[CrossRef](#)]
30. Mamonkin, M.; Mukherjee, M.; Srinivasan, M.; Sharma, S.; Gomes-Silva, D.; Mo, F.; Krenciute, G.; Orange, J.S.; Brenner, M.K. Reversible Transgene Expression Reduces Fratricide and Permits 4-1BB Costimulation of CAR T Cells Directed to T-Cell Malignancies. *Cancer Immunol. Res.* **2018**, *6*, 47–58. [[CrossRef](#)]
31. Zhou, S.; Zhu, X.; Shen, N.; Li, Q.; Wang, N.; You, Y.; Zhong, Z.; Cheng, F.; Zou, P.; Zhu, X. T Cells Expressing CD26-Specific Chimeric Antigen Receptors Exhibit Extensive Self-Antigen-Driven Fratricide. *Immunopharmacol. Immunotoxicol.* **2019**, *41*, 490–496. [[CrossRef](#)] [[PubMed](#)]
32. Mamonkin, M.; Rouce, R.H.; Tashiro, H.; Brenner, M.K. A T-Cell-Directed Chimeric Antigen Receptor for the Selective Treatment of T-Cell Malignancies. *Blood* **2015**, *126*, 983–992. [[CrossRef](#)]
33. Flavell, D.J.; Boehm, D.A.; Okayama, K.; Kohler, J.A.; Flavell, S.N.U. Therapy of Human T-cell Acute Lymphoblastic Leukaemia in Severe Combined Immunodeficient Mice with Two Different Anti-CD7-saporin Immunotoxins Containing Hindered or Non-hindered Disulphide Cross-linkers. *Int. J. Cancer* **1994**, *58*, 407–414. [[CrossRef](#)] [[PubMed](#)]
34. Enblad, G.; Karlsson, H.; Gammelgård, G.; Wenthe, J.; Lövgren, T.; Amini, R.M.; Wikstrom, K.I.; Essand, M.; Savoldo, B.; Hallböök, H.; et al. A Phase I/IIa Trial Using CD19-Targeted Third-Generation CAR T Cells for Lymphoma and Leukemia. *Clin. Cancer Res.* **2018**, *24*, 6185–6194. [[CrossRef](#)] [[PubMed](#)]
35. Wang, J.; Jensen, M.; Lin, Y.; Sui, X.; Chen, E.; Lindgren, C.G.; Till, B.; Raubitschek, A.; Forman, S.J.; Qian, X.; et al. Optimizing Adoptive Polyclonal T Cell Immunotherapy of Lymphomas, Using a Chimeric T Cell Receptor Possessing CD28 and CD137 Costimulatory Domains. *Hum. Gene Ther.* **2007**, *18*, 712–725. [[CrossRef](#)]
36. Zhou, S.; Li, W.; Xiao, Y.; Zhu, X.; Zhong, Z.; Li, Q.; Cheng, F.; Zou, P.; You, Y.; Zhu, X. A Novel Chimeric Antigen Receptor Redirecting T-Cell Specificity towards CD26+ Cancer Cells. *Leukemia* **2021**, *35*, 119–129. [[CrossRef](#)]

37. Yamada, K.; Hayashi, M.; Madokoro, H.; Nishida, H.; Du, W.; Ohnuma, K.; Sakamoto, M.; Morimoto, C.; Yamada, T. Nuclear Localization of CD26 Induced by a Humanized Monoclonal Antibody Inhibits Tumor Cell Growth by Modulating of POLR2A Transcription. *PLoS ONE* **2013**, *8*, e62304. [[CrossRef](#)]
38. Dang, N.H.; Torimoto, Y.; Sugita, K.; Daley, J.F.; Schow, P.; Prado, C.; Schlossman, S.F.; Morimoto, C. Cell Surface Modulation of CD26 by Anti-1F7 Monoclonal Antibody. Analysis of Surface Expression and Human T Cell Activation. *J. Immunol.* **1990**, *145*, 3963–3971. [[CrossRef](#)]
39. Hegen, M.; Kameoka, J.; Dong, R.P.; Schlossman, S.F.; Morimoto, C. Cross-Linking of CD26 Antibody Induces Tyrosine Phosphorylation and Activation of Mitogen-Activated Protein Kinase. *Immunology* **1997**, *90*, 257–264. [[CrossRef](#)]
40. Morimoto, C.; Torimoto, Y.; Levinson, G.; Rudd, C.E.; Schrieber, M.; Dang, N.H.; Letvin, N.L.; Schlossman, S.F. 1F7, a Novel Cell Surface Molecule, Involved in Helper Function of CD4 Cells. *J. Immunol.* **1989**, *143*, 3430–3439. [[CrossRef](#)]
41. Ohnuma, K.; Takahashi, N.; Yamochi, T.; Hosono, O.; Dang, N.H.; Morimoto, C. Role of CD26/Dipeptidyl Peptidase IV in Human T Cell Activation and Function. *Front. Biosci.* **2008**, *13*, 2299–2310. [[CrossRef](#)] [[PubMed](#)]
42. Tanaka, T.; Camerini, D.; Seed, B.; Torimoto, Y.; Dang, N.H.; Kameoka, J.; Dahlberg, H.N.; Schlossman, S.F.; Morimoto, C. Cloning and Functional Expression of the T Cell Activation Antigen CD26. *J. Immunol.* **1992**, *149*, 2090. [[CrossRef](#)]
43. Philipson, B.I.; O'Connor, R.S.; May, M.J.; June, C.H.; Albelda, S.M.; Milone, M.C. 4-1BB Costimulation Promotes CAR T Cell Survival through Noncanonical NF-KB Signaling. *Sci. Signal.* **2020**, *13*, eaay8248. [[CrossRef](#)]
44. Zhao, X.; Yang, J.; Zhang, X.; Lu, X.A.; Xiong, M.; Zhang, J.; Zhou, X.; Qi, F.; He, T.; Ding, Y.; et al. Efficacy and Safety of CD28- or 4-1BB-Based CD19 CAR-T Cells in B Cell Acute Lymphoblastic Leukemia. *Mol. Ther.-Oncolytics* **2020**, *18*, 272–281. [[CrossRef](#)] [[PubMed](#)]
45. Pan, J.; Tan, Y.; Wang, G.; Deng, B.; Ling, Z.; Song, W.; Seery, S.; Zhang, Y.; Peng, S.; Xu, J.; et al. Donor-Derived CD7 Chimeric Antigen Receptor T Cells for T-Cell Acute Lymphoblastic Leukemia: First-in-Human, Phase I Trial. *J. Clin. Oncol.* **2021**, *39*, 3340–3351. [[CrossRef](#)]
46. Polgárová, K.; Otáhal, P.; Šálek, C.; Pytlík, R. Chimeric Antigen Receptor Based Cellular Therapy for Treatment Of T-Cell Malignancies. *Front. Oncol.* **2022**, *12*, 876758. [[CrossRef](#)]
47. Su, A.I.; Wiltshire, T.; Batalov, S.; Lapp, H.; Ching, K.A.; Block, D.; Zhang, J.; Soden, R.; Hayakawa, M.; Kreiman, G.; et al. A Gene Atlas of the Mouse and Human Protein-Encoding Transcriptomes. *Proc. Natl. Acad. Sci. USA* **2004**, *101*, 6062–6067. [[CrossRef](#)] [[PubMed](#)]
48. Florentin, M.; Kostapanos, M.S.; Papazafiropoulou, A.K. Role of Dipeptidyl Peptidase 4 Inhibitors in the New Era of Antidiabetic Treatment. *World J. Diabetes* **2022**, *13*, 85–96. [[CrossRef](#)]

Disclaimer/Publisher's Note: The statements, opinions and data contained in all publications are solely those of the individual author(s) and contributor(s) and not of MDPI and/or the editor(s). MDPI and/or the editor(s) disclaim responsibility for any injury to people or property resulting from any ideas, methods, instructions or products referred to in the content.

Article

DPP8 Selective Inhibitor Tominostat as a Novel and Broad-Spectrum Anticancer Agent against Hematological Malignancies

Shohei Kikuchi ^{1,†} , Akinori Wada ^{1,†} , Yusuke Kamihara ¹, Kosuke Okazaki ², Paras Jawaid ¹, Mati Ur Rehman ³, Eiji Kobayashi ⁴, Takeshi Susukida ⁵, Tomoki Minemura ¹, Yoshimi Nabe ¹, Noriaki Iwao ⁶, Tatsuhiko Ozawa ⁴, Ryo Hatano ⁷ , Mitsugu Yamada ⁸, Hiroyuki Kishi ⁴, Yuji Matsuya ⁹, Mineyuki Mizuguchi ⁹, Yoshihiro Hayakawa ⁵ , Nam H. Dang ¹⁰, Yasumitsu Sakamoto ¹¹, Chikao Morimoto ⁷ and Tsutomu Sato ^{1,*}

- ¹ Department of Hematology, Faculty of Medicine, Academic Assembly, University of Toyama, 2630 Sugitani, Toyama 930-0194, Japan
 - ² Center for Clinical Research, Toyama University Hospital, 2630 Sugitani, Toyama 930-0194, Japan
 - ³ Department of Biological and Biomedical Sciences, The Aga Khan University, Karachi 74800, Pakistan
 - ⁴ Department of Immunology, Faculty of Medicine, Academic Assembly, University of Toyama, 2630 Sugitani, Toyama 930-0194, Japan
 - ⁵ Section of Host Defences, Institute of Natural Medicine, University of Toyama, 2630 Sugitani, Toyama 930-0194, Japan
 - ⁶ Department of Hematology, Juntendo University Shizuoka Hospital, 1129 Nagaoka, Izunokuni City, Shizuoka 410-2295, Japan
 - ⁷ Department of Therapy Development and Innovation for Immune Disorders and Cancers, Graduate School of Medicine, Juntendo University, 2-1-1 Hongo Bunkyo-ku, Tokyo 113-8421, Japan
 - ⁸ JEM Utilization Center Human Spaceflight Technology Directorate, Japan Aerospace Exploration Agency (JAXA), 2-1-1 Sengen, Tsukuba-shi 305-8505, Japan
 - ⁹ Faculty of Pharmaceutical Sciences, University of Toyama, 2630 Sugitani, Toyama 930-0194, Japan
 - ¹⁰ Division of Hematology/Oncology, University of Florida, Gainesville, FL 32610, USA
 - ¹¹ School of Pharmacy, Iwate Medical University, 1-1-1 Idaidori, Yahaba 028-3694, Japan
- * Correspondence: tsutomus@med.u-toyama.ac.jp; Tel.: +81-76-434-7232
- † These authors contributed equally to this work.



Citation: Kikuchi, S.; Wada, A.; Kamihara, Y.; Okazaki, K.; Jawaid, P.; Rehman, M.U.; Kobayashi, E.; Susukida, T.; Minemura, T.; Nabe, Y.; et al. DPP8 Selective Inhibitor Tominostat as a Novel and Broad-Spectrum Anticancer Agent against Hematological Malignancies. *Cells* **2023**, *12*, 1100. <https://doi.org/10.3390/cells12071100>

Academic Editor:
Mustapha Kandouz

Received: 5 March 2023
Revised: 29 March 2023
Accepted: 4 April 2023
Published: 6 April 2023



Copyright: © 2023 by the authors. Licensee MDPI, Basel, Switzerland. This article is an open access article distributed under the terms and conditions of the Creative Commons Attribution (CC BY) license (<https://creativecommons.org/licenses/by/4.0/>).

Abstract: DPP8/9 inhibition induces either pyroptotic or apoptotic cell death in hematological malignancies. We previously reported that treatment with the DPP8/9 inhibitor 1G244 resulted in apoptotic cell death in myeloma, and our current study further evaluates the mechanism of action of 1G244 in different blood cancer cell lines. Specifically, 1G244 inhibited DPP9 to induce GSDMD-mediated-pyroptosis at low concentrations and inhibited DPP8 to cause caspase-3-mediated-apoptosis at high concentrations. HCK expression is necessary to induce susceptibility to pyroptosis but does not participate in the induction of apoptosis. To further characterize this DPP8-dependent broad-spectrum apoptosis induction effect, we evaluated the potential antineoplastic role for an analog of 1G244 with higher DPP8 selectivity, tominostat (also known as 12 m). In vitro studies demonstrated that the cytotoxic effect of 1G244 at high concentrations was enhanced in tominostat. Meanwhile, in vivo work showed tominostat exhibited antitumor activity that was more effective on a cell line sensitive to 1G244, and at higher doses, it was also effective on a cell line resistant to 1G244. Importantly, the weight loss morbidity associated with increasing doses of 1G244 was not observed with tominostat. These results suggest the possible development of novel drugs with antineoplastic activity against selected hematological malignancies by refining and increasing the DPP8 selectivity of tominostat.

Keywords: DPP8; inhibitor; anticancer agent; hematological; malignancies

1. Introduction

The S9b serine protease family has the ability to cleave Xaa-Pro dipeptides from N-termini of their substrates, and these enzymatic members include dipeptidyl peptidase-4 (DPP4), DPP8, DPP9, and fibroblast activation protein (FAP) [1].

For example, DPP4 cleaves the pancreatic polypeptide family, including neuropeptide Y and peptide YY, several members of the glucagon family, and certain chemokines as natural substrates [2,3]. Of these substrates, insulino-tropic hormone (incretin) glucagon-like peptide 1 (GLP-1) is of particular interest, which is cleaved and inactivated by DPP4 to antagonize insulin secretion. Small-molecule inhibitors of DPP4 have been developed as well-established therapies for the treatment of type II diabetes [4]. DPPs are therefore an important class of enzymes that are potential therapeutic targets for human diseases due to their highly selective and limited proteolytic activities.

Several proteins have been identified as substrates of DPP8 and DPP9 [1,5–10]. DPP8 substrates include inflammatory protein-10 (IP10), interfering T-cell chemokines (ITAC), and chemokines stromal cell-derived factor (SDF-1) [10], while DPP9 cleaves C-X-C motif chemokine 10 (CXCL10/IP10), S100-A10, SET, nucleobindin-1 (NUCB1), and interleukin-1 receptor antagonist protein (IL-1RA) as substrates [8]. In addition, numerous studies have shown that DPP8/9 is involved in immune system regulation and inflammation by the cleavage of these substrates [11].

DPP8 and DPP9 localize intracellularly in contrast to DPP4, which has an extracellular catalytic domain. With significant homology among these enzymes (79% amino acid similarity and 61% amino acid identity) [12], no small-molecule compounds have heretofore been identified to selectively inhibit only one of these proteins. On the other hand, inhibitors which simultaneously inhibit both DPP8 and DPP9 have been demonstrated to be potential therapeutic agents for selected hematologic malignancies, as described below.

The DPP family nonselective inhibitor Val-boroPro (talabostat) triggers a lytic form of programmed cell death known as pyroptosis in human acute myeloid leukemia (AML) cell lines and primary AML samples, an effect that is dependent on DPP9 inhibition [13]. The inhibition of DPP9 in mouse monocytes and macrophages by talabostat causes the autoproteolysis of the function-to-find (FIIND) domain in the inflammasome sensor protein, nucleotide-binding domain, and leucine-rich repeat pyrin containing 1b (Nlrp1b) and the cleavage of gesdermin D (GSDMD) by caspase-1 activated by this autoproteolysis induces pyroptosis [14]. Interestingly, DPP9 functions as an endogenous inhibitor of Nlrp1b rather than as a protease in this series of reactions [15]. In human AML cells, NLRP1 and caspase recruitment domain family member 8 (CARD8) function as human homologs of mouse Nlrp1b, and the expression levels of caspase-1 and CARD8 determine the sensitivity to talabostat [13].

Alternatively, 1G244 is a specific inhibitor of DPP8 and DPP9 [11]. We have reported that 1G244 triggers caspase-3-activation-mediated apoptosis in multiple myeloma (MM) cell lines and primary MM samples, and that this effect may be dependent on DPP8 inhibition [16]. However, cell death induced by 1G244 in the AML cell line THP-1 is not dependent on DPP8/9 inhibition but is the result of an unidentified off-target effect [14]. In view of these contradictory findings, we conducted the studies described in this paper to further investigate 1G244-induced cell death.

On the other hand, 12 m, a 1G244 methylpiperazine analog, has been reported to be highly selective for DPP8 [17]. Based on our hypothesis that the antitumor effect of 1G244 depends on DPP8 inhibition, we would expect 12 m to exhibit potent antineoplastic activity. For our current work, we have named 12 m as tominostat and have investigated its potential role as an anticancer drug.

In this study, we found that high concentrations of 1G244 induce caspase-3-activation-mediated apoptosis that is dependent on DPP8 inhibition. We also demonstrated that the higher level of selectivity for DPP8 by tominostat enhances its apoptotic effect and that it may be a more potent anticancer drug with an improved in vivo weight loss toxicity profile.

2. Materials and Methods

2.1. Cell Culture

T cell non-Hodgkin's lymphoma cell line KARPAS299 was supplied by the European Collection of Authenticated Cell Cultures (ECACC). Multiple myeloma cell lines, MM.1S and RPMI8226; Burkitt's lymphoma cell lines, Daudi, Raji, and NAMALWA; the acute

myelogenous leukemia cell line, KG1; the acute T cell leukemia cell line, Jurkat; and the chronic myelogenous leukemia cell line, K562, were supplied by American Type Culture Collection (ATCC). Acute monocytic leukemia cell lines, THP-1, MOLM-13, and NOMO-1; and the myelodysplastic syndrome cell line, SKM-1, were supplied by Japanese Collection of Research Bioresources Cell Bank (JCRB). All these cell lines were maintained in RPMI 1640 (Gibco BRL) supplemented with 10% heat-inactivated fetal bovine serum (Sigma), 100 µg/mL streptomycin, and 100 U/mL penicillin.

2.2. Lentivirus and Transduction

The shRNA lentivirus, MISSION Lentiviral Transduction Particles, SHCLNV was purchased from Sigma-Aldrich. The lentivirus vector system is composed of the vector pLKO.1-Puro-CMV-tGFP. The control is MISSION pLKO.1-Puro-CMV-tGFP Positive Control Transduction Particles, SHC003V. DPP8 KD1, TRCN0000300778; DPP8 KD2, TRCN0000300777. DPP9 KD1, TRCN0000075265; DPP9 KD2, TRCN0000075264. HCK KD1, TRCN0000320535; HCK KD2, TRCN0000381826. The human HCK gene overexpressing lentivirus, HCK (NM_002110) Human Tagged ORF Clone Lentiviral Particle, RC217022L4V was purchased from OriGene. The lentivirus vector system is composed of the vector pLenti-C-mGFP-P2A-Puro. The control is Lenti ORF control particles of pLenti-C-mGFP-P2A-Puro, PS100093V. Lentivirus transduction and stable cell line selection were performed according to the manufacturer's instructions.

2.3. Reagents

Puromycin and 1G244 were purchased from Sigma-Aldrich. Talabostat, Disulfiram, and Necrostatin-1 were purchased from MedChemexpress. Necrosulfonamide was purchased from Santa Cruz Biotechnology. Z-DEVD-FMK and Z-VAD-FMK were purchased from Medical & Biological Laboratories. Tominostat (12 m) was prepared according to previously published work [17].

2.4. Cellular Cytotoxicity

The viable cell number was quantified using a Premix WST-1 Cell Proliferation Assay System (TaKaRa, Shiga, Japan) according to the manufacturer's instructions. The level of cytotoxicity was also quantified by measuring the level of lactate dehydrogenase (LDH) released from damaged cells using a Cytotoxicity LDH Assay Kit-WST (Dojindo, Kumamoto, Japan) according to the manufacturer's instructions.

2.5. Western Blot Analyses

Cells were lysed in a buffer containing 1% sodium dodecyl sulfate (SDS); 20 mM Tris-HCl, pH 7.4; 5 µg/mL pepstatin A; 10 µg/mL leupeptin; 5 µg/mL aprotinin; and 1 mM phenyl-methylsulfonyl fluoride and then heated for 5 min. After passage through a 20-gauge needle ten times and centrifugation at 15,000 rpm at 4 °C for 30 min, the aliquot was boiled in a standard reducing sample buffer for 3 min and subjected to SDS-polyacrylamide gel electrophoresis. This was followed by transfer to an Immobilon-P membrane (Millipore, Burlington, MA, USA) and hybridization with an anti-DPP8 antibody (OTI1D2), monoclonal, mouse, NBP2-01830 (Novus Biologicals, Englewood, CO, USA), an anti-DPP9 antibody (OTI2E3), monoclonal, mouse, NBP2-01521 (Novus Biologicals), an anti-GSDMD antibody, monoclonal, rabbit, ab210070 (Abcam, Cambridge, UK), an anti-Cleaved Caspase-3 antibody (Asp175, 5A1E), monoclonal, rabbit, #9664S (Cell Signaling Technology, Danvers, MA, USA), an anti-DFNA5/GSDME antibody (EPR19859, N-terminal), monoclonal, rabbit, ab215191 (Abcam), an anti-Caspase-1 antibody, polyclonal, rabbit, #2225S (Cell Signaling Technology), an anti-CARD8 antibody (2108C2a), monoclonal, mouse, sc-81213 (Santa Cruz Biotechnology), an anti-Caspase-3 antibody, polyclonal, rabbit, #9662S (Cell Signaling Technology), an anti-HCK antibody (E1I7F), monoclonal, rabbit, #14643 (Cell Signaling Technology), an anti-LCK antibody (3A5), monoclonal, mouse, sc-433 (Santa Cruz Biotechnology), an anti-Fyn antibody (15),

monoclonal, mouse, sc-434 (Santa Cruz Biotechnology, Dallas, TX, USA), an anti-c-Fgr antibody (B-8), monoclonal, mouse, sc-166079 (Santa Cruz Biotechnology), an anti-Lyn antibody (H-6), monoclonal, mouse, sc-7274 (Santa Cruz Biotechnology), an anti-Blk antibody (9D10D1), monoclonal, mouse, sc-65980 (Santa Cruz Biotechnology), an anti- β -actin antibody (8H10D10), monoclonal, mouse, #3700S (Cell Signaling Technology), an anti-AK2 antibody, polyclonal, rabbit, ab37594 (Abcam), an anti-FADD antibody (A66-2), monoclonal, mouse, 556402 (BD Biosciences, Franklin Lakes, NJ, USA), an anti-phospho-FADD (Ser194) antibody, polyclonal, rabbit, #2781S (Cell Signaling Technology), or an anti-DUSP26 antibody, polyclonal, rabbit, GTX109283 (GeneTex, Zeeland, MI, USA). Proteins detected by these antibodies were visualized with horseradish-peroxidase-conjugated anti-mouse or rabbit antibody (Santa Cruz Biotechnology) followed by the use of enhanced chemiluminescence (Amersham Pharmacia Biotech., Amersham, UK), as we described previously [16].

2.6. Microarray Analysis

RNA was isolated from cells using an RNeasy Mini Kit (QIAGEN, Hilden, Germany). Microarray analysis was performed using the 3D-Gene human oligo chip 25k (TORAY Industries, Tokyo, Japan), which permits the detection of 24,460 mRNAs. After hybridization, the DNA microarray was washed according to the manufacturer's instructions, followed by image scanning using 3D-Gene Scanner 3000 (TORAY Industries) and data processing using 3D-Gene Extraction 2.0.0.4 (TORAY Industries).

2.7. In Vivo Studies

In vivo experiments were performed as we previously described [16]. NOD.Cg-Prkdc^{scid}Il2rg^{tm1Wjl}/SzJ (NSG) female mice of age 6–7 weeks and weight 19–21 g were obtained from Charles River Japan Inc. (Kanagawa, Japan). The mice were kept under specific pathogen-free conditions with a 12 h day and night cycle with free access to food and water, and they received humane care in compliance with Institutional Guidelines. All experiments were approved by the Animal Care and Use Committee of Toyama University (reference number A2020UH-5). In order to evaluate for lethal toxicity, NSG mice were administered with 1G244 or tominostat subcutaneously once a week, with body weights being measured at the same time. For the evaluation of antitumor activity, 5×10^6 of MM.1S or Daudi cells were subcutaneously inoculated on the left side on the backs of NSG mice. Three days after the inoculation, 1G244 or tominostat was administered subcutaneously once a week. Tumor measurements were obtained at the same time with a caliper, and tumor volume was calculated according to the following formula: $MD \times TL^2 \times 1/2$, with MD and TL being the maximum diameter and transverse length, respectively.

3. Results

3.1. DPP8-Dependent Antineoplastic Effect of High-Dose 1G244

We compared the cytotoxic effect of the DPP8/9 inhibitors 1G244 and talabostat on hematological cancer cell lines using water-soluble tetrazolium (WST) to detect the respiratory chain metabolic activity in viable cells. As shown in Figure 1A, in three cell lines sensitive to DPP8/9 inhibitors, specifically MM.1S, KARPAS299, and THP-1 cells, talabostat was superior to 1G244 at low concentrations of 0.1 and 1 μ M. On the other hand, the opposite was true at concentrations as high as 10 and 100 μ M, with 1G244 being more effective than talabostat. Meanwhile, talabostat exhibited a minimal cytotoxic effect against the three less sensitive cell lines, specifically KG1, Daudi, and NAMALWA cells. However, 1G244 was effective at concentrations of 10 and 100 μ M against these cell lines.

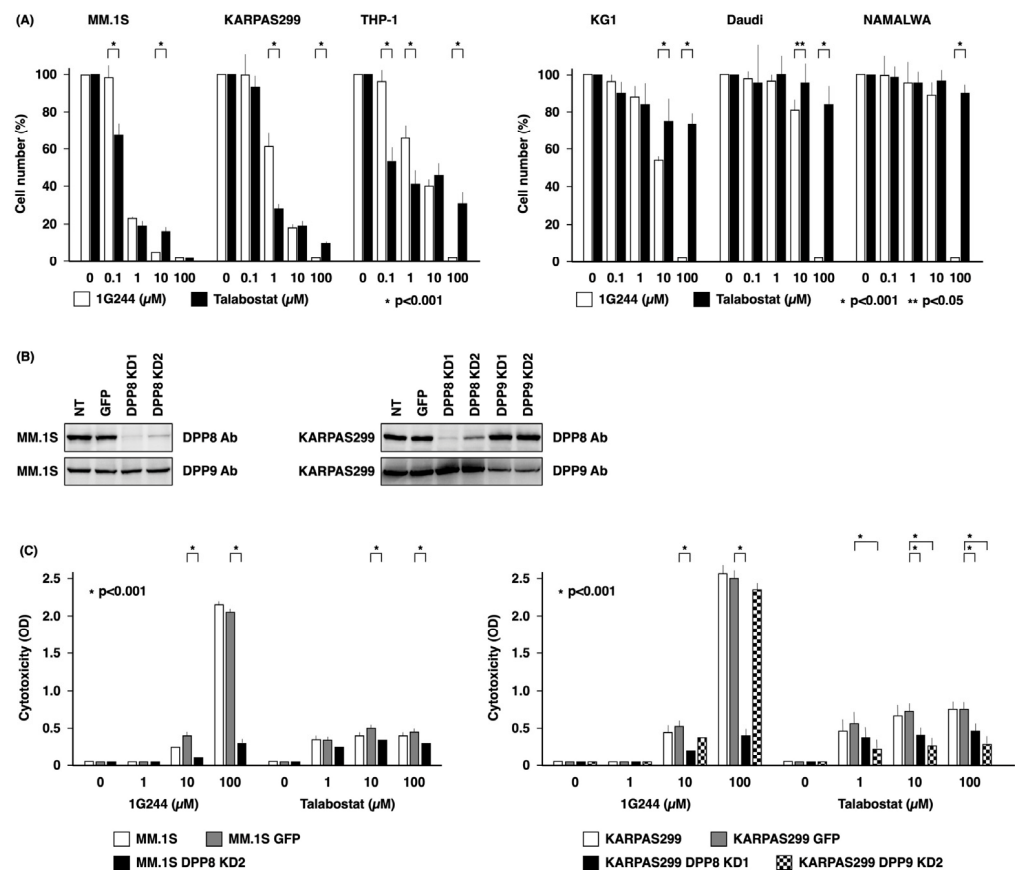


Figure 1. DPP8-dependent antineoplastic effect of high-dose 1G244. (A) 1.0×10^5 of hematological cancer cell lines (MM.1S, KARPAS299, THP-1, KG1, Daudi, or NAMALWA) were cultured with DPP8/9 inhibitors (1G244 or talabostat) at doses of 0–100 μM for 72 h. Cell number was estimated by a colorimetric assay using WST-1 reagent ($n = 6$). (B) Knockdown studies of DPP8 and DPP9 in MM.1S or KARPAS299 cells. NT, no treatment; GFP, control vector; KD, knockdown. Expression level of DPP8 or DPP9 was estimated by Western blot analysis. (C) 1.0×10^5 of MM.1S and KARPAS299 cells and their transfectants were cultured with DPP8/9 inhibitors (1G244 or talabostat) at doses of 0–100 μM for 6 h. Cytotoxicity was estimated by a LDH release assay ($n = 6$).

To determine whether the DPP8/9 inhibitors 1G244 and talabostat exerted their cytotoxic effect through DPP8 or DPP9, we conducted knockdown studies on DPP8 or DPP9 expression in MM.1S and KARPAS299 cells, which are highly sensitive cell lines. As shown in Figure 1B, DPP8 was effectively suppressed in MM.1S cells. On the other hand, MM.1S cells with DPP9 knockdown did not proliferate and died. DPP8 and DPP9 in KARPAS299 cells were both effectively suppressed.

As shown in Figure 1C, the cytotoxic effect of DPP8/9 inhibitors was assessed by measuring lactate dehydrogenase (LDH) released from dead cells into the culture supernatant. In both MM.1S GFP and KARPAS299 GFP cells transfected with the control vector, talabostat at a low concentration of 1 μM and 1G244 at a high concentration of 100 μM exhibited greater cytotoxic effects than the others at the same concentrations, consistent with results shown in Figure 1A. On the other hand, both KARPAS299 DPP8 and DPP9 knockdown cells were less sensitive to 10 and 100 μM of talabostat, which was particularly more pronounced in DPP9 knockdown cells. MM.1S DPP8 knockdown cells also showed decreased sensitivity to talabostat. The selective reduced sensitivity of KARPAS299 DPP8 knockdown cells to 100 μM of 1G244 was also demonstrated. Greatly reduced sensitivity was also observed in MM.1S DPP8 knockdown cells. This DPP8-knockdown-induced decrease in sensitivity to 1G244 was also observed in KARPAS299 and in MM.1S at 10 μM . These results showed that the cytotoxic effect of talabostat depends mainly on DPP9, as well

as partly on DPP8, and that the potent anticancer activity of 1G244 at high concentrations is dependent on DPP8.

3.2. Caspase-3-Mediated Apoptosis as Anticancer Effect by High-Dose 1G244

Figure 2A shows the results of our investigation into the types of cell death caused by DPP8/9 inhibitors. In MM.1S cells, cleaved GSDMD, a marker of pyroptosis, was detected between 3 and 48 h of treatment by 1 to 100 μ M talabostat. Cleaved GSDMD was also detected following 1G244 exposure. On the other hand, cleaved caspase-3, a marker of apoptosis, was detected following 24 h of exposure to 10 μ M 1G244, while a greater level was detected at an earlier time point of 6 h after stimulation with 100 μ M. Cleaved caspase-3 was also detected following 24 h of exposure to 1 to 100 μ M of talabostat. These results suggested that DPP8/9 inhibitors induce the cleavage of GSDMD, as well as caspase-3, and that the potent cytotoxic effect of high concentrations of 1G244 may be dependent on caspase-3.

Figure 2B shows the findings from experiments conducted to examine these hypotheses. Disulfiram (DSF) almost completely inhibited cell death induced by 10 and 100 μ M of talabostat, while weakly suppressing 1G244 at 10 μ M. Cell death suppressed by DSF is pyroptosis mediated by GSDMD pore formation. In contrast, 1G244 at concentrations of 10 and 100 μ M was largely unaffected by DSF but was strongly inhibited by the caspase-3/7 inhibitor Z-DEVD.

These results were consistent with our hypothesis that the strong anticancer effect exhibited by high concentrations of 1G244 is caspase-3-dependent apoptosis. At the same time, Z-DEVD also weakly inhibited 10 and 100 μ M of talabostat, suggesting that caspase-3-mediated pyroptotic pathways may also be involved. While a potential candidate may involve the cleavage of Gasdermin-E (GSDME) [18], our work did not implicate this pathway (Figure 2A). Of note is the fact that talabostat at 10 and 100 μ M was strongly inhibited by the pan caspase inhibitor Z-VAD. This observation was consistent with the fact that caspase-1 is required for pyroptosis in the canonical inflammasome pathway and caspase-4/5/11 in the noncanonical inflammasome pathway [18]. Meanwhile, no inhibitory effect was observed for necrostatin-1 (Nec) or necrosulfonamide (NSA), inhibitors of necroptosis (Figure 2C).

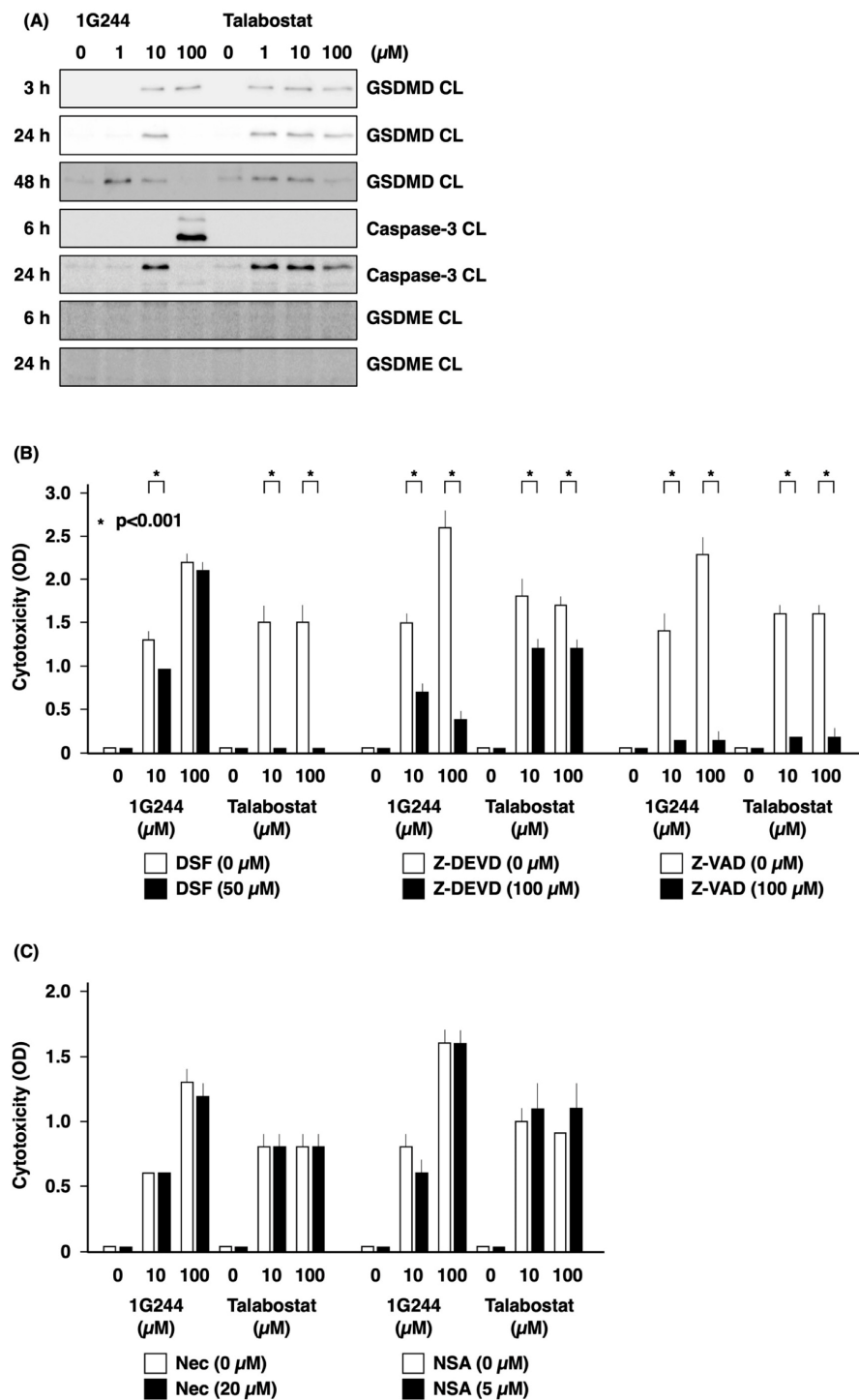


Figure 2. Caspase-3-mediated apoptosis as anticancer effect by high-dose 1G244. (A) 1×10^6 MM.1S cells were cultured with DPP8/9 inhibitors (1G244 or talabostat) at doses of 0–100 μM for 3–48 h. The cleaved form (CL) of gasdermin-D (GSDMD), caspase-3, or gasdermin-E (GSDME) was detected by Western blot analysis. The upper caspase-3 CL: 19 kDa; and the lower caspase-3 CL: 17 kDa. (B,C) 1.0×10^5 of MM.1S cells were cultured with DPP8/9 inhibitors (1G244 or talabostat) at doses of 0–100 μM for 6 h with disulfiram (DSF), Z-DEVD, Z-VAD, necrostatin-1 (Nec), or necrosulfonamide (NSA). Cytotoxicity was estimated by a LDH release assay ($n = 6$).

3.3. Dependence on HCK for DPP8/9 Inhibitor-Induced Pyroptosis

Figure 3A shows the results of experiments evaluating possible predictors of sensitivity to DPP8/9 inhibitors. The sensitive cell lines studied were THP-1, MM.1S, and KARPAS299, and resistant cell lines studied were KG1, NAMALWA, and Daudi. We first examined the expression of DPP8 and DPP9 as prerequisite factors and caspase-1, CARD8, and GSDMD as factors related to pyroptosis signaling, as well as caspase-3 as a factor involved in apoptosis signaling. However, no association was found between the expression level of any of the factors and susceptibility.

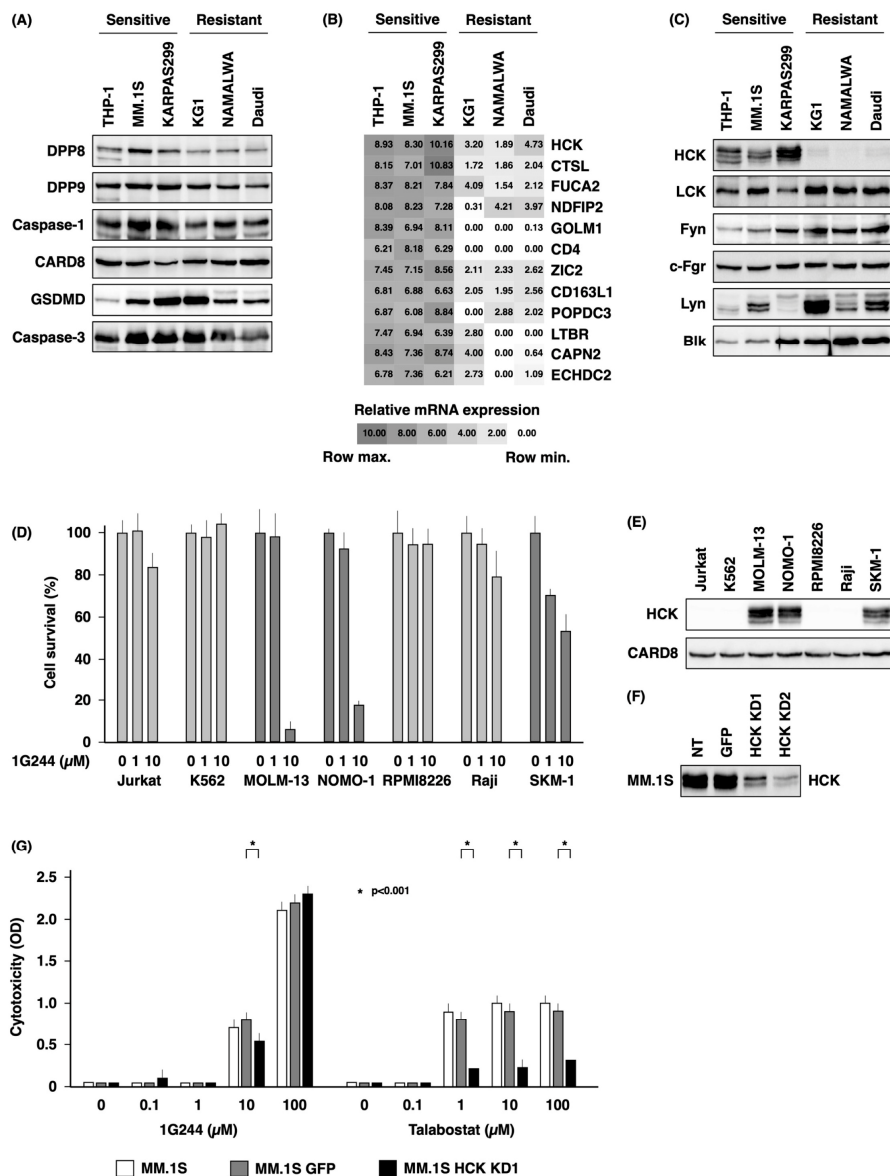


Figure 3. Dependence on HCK for DPP8/9 inhibitor-induced pyroptosis. (A) Expression level of DPP8, DPP9, caspase-1, CARD8, GSDMD, or caspase-3 in THP-1, MM.1S, KARPAS299, KG1, NAMALWA, or Daudi cells was estimated by Western blot analysis. (B) Gene expression of THP-1, MM.1S, KARPAS299, KG1, NAMALWA, or Daudi cells was analyzed by microarray method using 3D-Gene. (C) Expression level of HCK, LCK, Fyn, c-Fgr, Lyn, or Blk in THP-1, MM.1S, KARPAS299, KG1, NAMALWA, or Daudi cells was estimated by Western blot analysis. (D) 1.0×10^5 of hematological cancer cell lines (Jurkat, K562, MOLM-13, NOMO-1, RPMI8226, Raji, or SKM-1) were cultured with 1G244 at doses of 0–10 μ M for 72 h. Cell number was estimated by a colorimetric assay using WST-1

reagent (n = 6). (E) Expression level of HCK or CARD8 in Jurkat, K562, MOLM-13, NOMO-1, RPMI8226, Raji, or SKM-1 cells was estimated by Western blot analysis. (F) Knockdown studies of HCK in MM.1S cells. NT, no treatment; GFP, control vector; KD, knockdown. Expression level of HCK was estimated by Western blot analysis. (G) 1.0×10^5 of MM.1S cells and their transfectants were cultured with DPP8/9 inhibitors (1G244 or talabostat) at doses of 0–100 μM for 6 h. Cytotoxicity was estimated by a LDH release assay (n = 6).

Microarray analysis was then performed as a comprehensive evaluation to compare sensitive cell lines with resistant cell lines. Factors with high expression in the former and low expression in the latter are shown in Figure 3B. Among these, we paid particular attention to hematopoietic cell kinase (HCK). HCK is one of the Src-family tyrosine kinases and mediates proliferation, survival, and adhesion signals sent by cell surface receptors [19]. Furthermore, HCK has been reported to mediate caspase-3-mediated apoptosis [20]. We therefore decided to further investigate the possible involvement of HCK.

Our initial studies employed the Western blotting method to examine the HCK protein level in each cell line, as shown in Figure 3C. HCK was selectively highly expressed in the three highly sensitive cell lines. In contrast, there was no association with the susceptibility and expression of other members of the Src-family tyrosine kinases with known expression in hematopoietic cells, including LCK, Fyn, c-Fgr, Lyn, and Blk (Figure 3C).

Meanwhile, MOLM-13, NOMO-1, and SKM-1 were sensitive to 1G244, while Jurkat, K562, RPMI8226, and Raji were resistant to 1G244 (Figure 3D), with HCK being highly expressed in a selective manner in the three sensitive cell lines (Figure 3E). On the other hand, CARD8, which has been reported to define DPP8/9 inhibitor sensitivity [13], was almost equally expressed in these seven cell lines.

To further confirm the dependence on HCK for DPP8/9 inhibitor sensitivity, we conducted HCK knockdown studies in highly sensitive MM.1S cells (Figure 3F). The knockdown cells showed reduced sensitivity to 10 μM of 1G244 and to 1, 10, and 100 μM of talabostat. However, no effect on sensitivity to 100 μM of 1G244 was observed (Figure 3G). These results indicated that DPP8/9-mediated pyroptosis is HCK-dependent, but HCK is not involved in DPP8-mediated apoptosis induced by high levels of 1G244. In addition, the forced expression of HCK in hyposensitive Daudi and NAMALWA (Figure S1A) did not alter their sensitivity to 1G244 or talabostat. (Figure S1B,C). These results suggested that the presence of HCK is a necessary but not sufficient condition for DPP8/9-inhibitor-induced pyroptosis.

3.4. Antitumor Effects of Tominostat

High concentrations of 1G244 induced apoptotic cell death via DPP8, even in blood cancer cell lines resistant to pyroptosis induced by talabostat and low concentrations of 1G244 via DPP8/9. We therefore attempted to determine whether increasing the DPP8 selectivity of 1G244 could result in a greater antineoplastic effect. The selectivity for DPP8 compared to DPP9 is expressed as the selectivity index (SI), i.e., IC₅₀ for DPP9 divided by IC₅₀ for DPP8. The SI of 1G244 is 3.8 [21], whereas the SI of 12 m with the H in the piperazine skeleton of 1G244 replaced by (S)CH₃ is reported to be 8.1 [17]. We named this 12 m molecule tominostat and performed the experiments described below.

The antitumor effect of tominostat was compared to that of 1G244 in the sensitive cell lines MM.1S and KARPAS299 and in the resistant cell line Daudi in *in vitro* studies (Figure 4A). For all of these cell lines, at concentrations >10 μM , tominostat exhibited a greater antitumor effect as compared to the original 1G244. These results indicated that the antitumor effect at high concentrations, which is a characteristic of 1G244, is accentuated by increasing DPP8 selectivity.

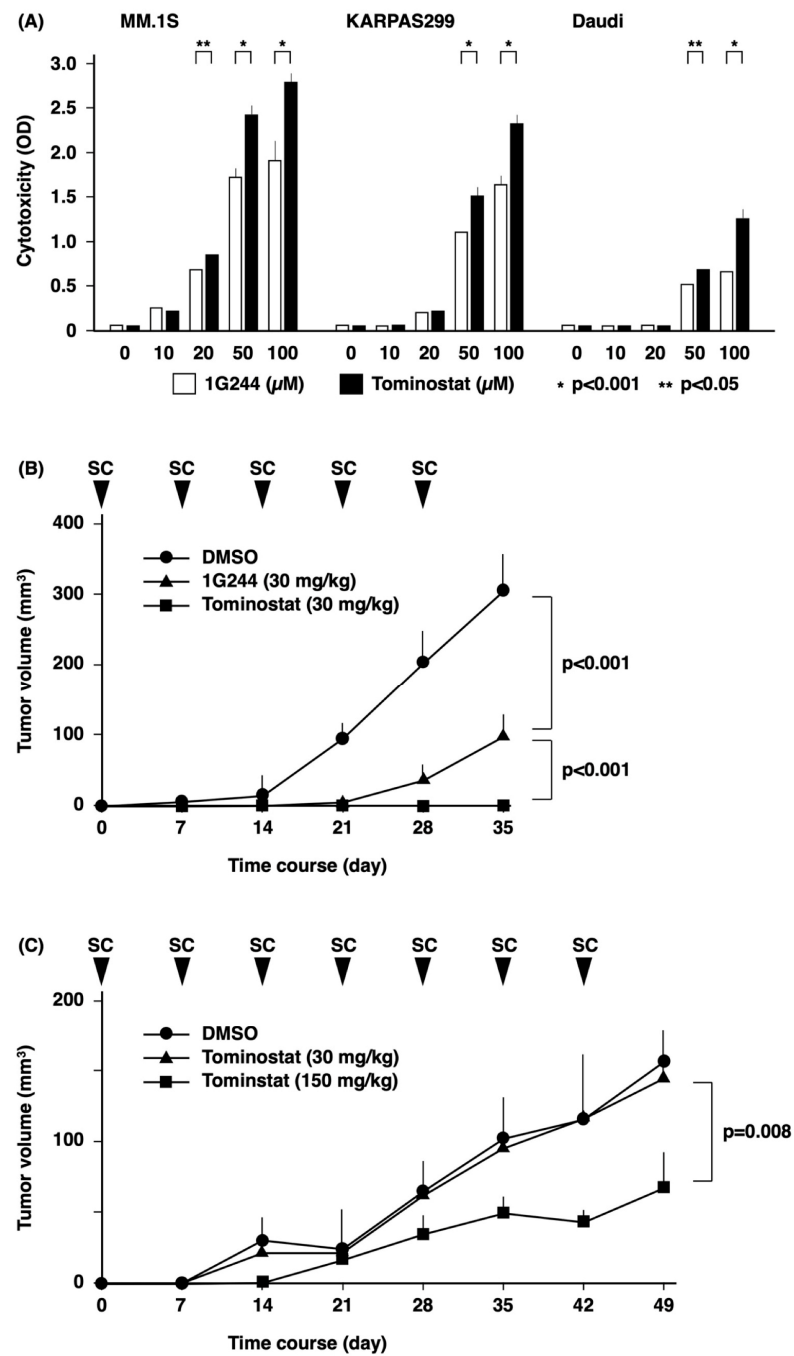


Figure 4. Antitumor effects of tominostat. (A) 1.0×10^5 of MM.1S, KARPAS299, or Daudi cells were cultured with DPP8/9 inhibitors (1G244 or tominostat) at doses of 0–100 μM for 6 h. Cytotoxicity was estimated by a LDH release assay ($n = 6$). (B,C) 5×10^6 of MM.1S (B) or Daudi (C) cells were subcutaneously inoculated into NSG mice ($n = 6$). Three days after inoculation, 1G244 or tominostat was administered subcutaneously once a week. Tumor volume was assessed at the same time.

For *in vivo* studies, we first conducted experiments examining the toxicity profile of the pertinent inhibitors. There was no death of the tested animals from acute toxicity from the administration of either 1G244 (Figure 5A) or tominostat (Figure 5B). However, dose-dependent weight loss was observed with 1G244. On the other hand, this weight-loss toxicity was not observed with tominostat, even when the dose was increased to 150 mg/kg.

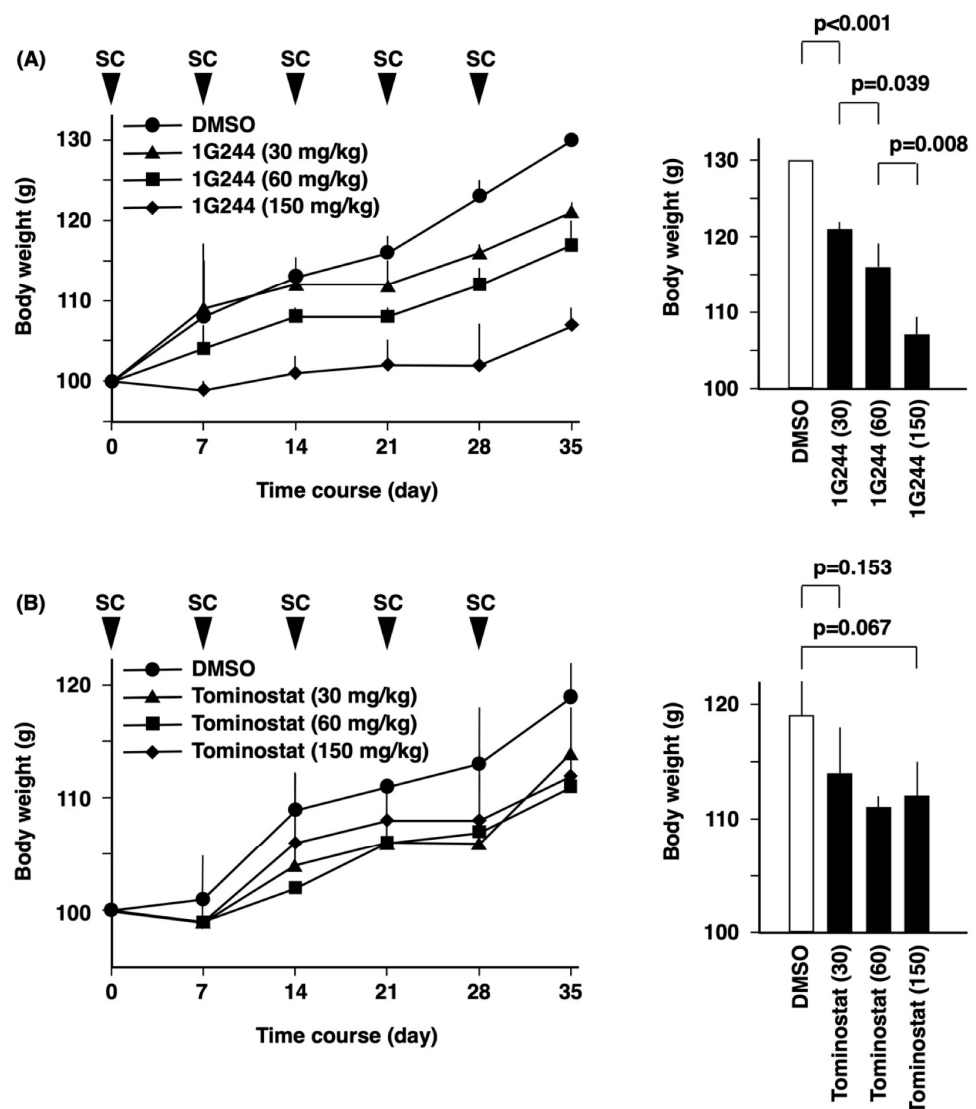


Figure 5. Weight loss as a side effect of tominostat treatment. NSG mice were treated with 1G244 (A) or tominostat (B) subcutaneously once a week ($n = 6$). The body weight was assessed at the same time.

The next *in vivo* experiment examined the antitumor effect of the inhibitors. Although the treatment of mice implanted subcutaneously with the sensitive cell line MM.1S cells with 30 mg/kg of 1G244 or tominostat resulted in tumor growth inhibition, tominostat exhibited significantly superior antitumor activity (Figure 4B). Meanwhile, the treatment of mice transplanted with the resistant cell line Daudi with 30 mg/kg tominostat did not inhibit tumor growth. However, an increase in treatment dose to 150 mg/kg tominostat led to significant Daudi cell tumor shrinkage (Figure 4C). These results showed that tominostat has superior antineoplastic activity as compared to the original 1G244 and that it exhibits effectiveness against resistant cells at higher doses without the side effect of weight loss.

4. Discussion

An initial finding of our current work is the dual nature of 1G244. At low concentrations, 1G244 induces pyroptosis mainly through the inhibition of DPP9, while it induces apoptosis through the inhibition of DPP8 at high concentrations. A potential explanation for this duality is that 1G244 inhibits DPP8 and DPP9 by different mechanisms. Indeed, it has been suggested that 1G244's inhibition of DPP8 is based on binding that is slow and tight [21], i.e., irreversible [11], while its inhibition of DPP9 is competitive [21]. However, studies using experimental 3D models have not demonstrated clear differences between

the molecular structures of 1G244-liganded DPP8 and 1G244-liganded DPP9 to support the suggested hypothesis [22]. Such differences may become apparent in studies using tominostat, an analog of 1G244 with increased selectivity for DPP8. We are currently planning to analyze the molecular structures of tominostat-liganded DPP8/9 to further evaluate this important issue.

The dependence of cell death caused by high concentrations of 1G244 on DPP8 inhibition is precisely demonstrated by DPP8 knockdown experiments (Figure 1C). Further evidence supporting this conclusion is based on the enhanced cytotoxic effect of high concentrations of DPP8-selective tominostat (Figure 4A). Whether this enhanced cytotoxicity can lead to use in clinical practice as an anticancer agent depends largely on the toxicity profile and severity of adverse events. Toxicity of 1G244 has been reported for daily intravenous administration for 14 days to rats [21]. Groups administered with doses of 1 and 10 mg/kg showed hematological and serum parameters that were all within normal limits. However, 30 mg/kg dosing led to treatment discontinuation from such dose-limiting toxicities as startle reflexes, chronic and tonic convulsions, and opisthosis.

In our previous and present studies, no such toxicity was observed with 1G244 treatment, likely due to the fact it was administered subcutaneously once a week in mice [16]. However, clear weight loss was observed in the 30 mg/kg group, which worsened with increasing doses of 60 mg/kg and 150 mg/kg (Figure 5). In contrast, no weight loss was observed with tominostat in any of the 30, 60, or 150 mg/kg groups.

A reason for the observed reduction in toxicity may be due to differences in the tissue expression of DPP8 and DPP9. Specifically, DPP9 is expressed throughout all organs in the body (Dataset: GeneAtlas U133A, gcrma), with its absence in mice causing impairment in tongue development, suckling defects, and subsequent neonatal lethality [23,24]. On the other hand, DPP8 expression is relatively restricted to hematopoietic cells (Dataset: GeneAtlas U133A, gcrma).

Importantly, the low-sensitivity cell line Daudi was resistant to 100 μ M of 1G244, but the same dose of tominostat exhibited effective *in vitro* antitumor activity (Figure 4A), and 150 mg/kg tominostat inhibited tumor growth *in vivo* (Figure 4C). These findings indicate that the increased DPP8 selectivity of tominostat compared to 1G244 not only enhanced its antitumor effect, but also reduced its toxicity, allowing higher doses to be safely administered to treat less sensitive tumor cells.

An issue that needs to be clarified involves the specific signaling events induced by DPP8 inhibition. Comparing high- and low-susceptible cell lines, we identified HCK as one factor defining differences in susceptibility. However, HCK knockdown suppressed pyroptosis induced by DPP9 inhibition, while apoptosis induced by DPP8 inhibition was unaffected (Figure 3).

Recent work by others suggested a mechanism for HCK involvement in signaling events of pyroptosis [25]. These authors demonstrate that the genetic and pharmacological inhibition of HCK suppresses NLRP3 inflammasome activation and that HCK binds to the NBD and LRR domains of NLRP3. In addition, DPP9 is shown to regulate pyroptosis by binding to Nlrp1b [15]. Our current findings that HCK dictates susceptibility to pyroptosis induced by DPP9 inhibition are therefore consistent with previously published reports.

On the other hand, assuming that DPP8 inhibition induces apoptosis by inhibiting the cleavage of relevant substrates, adenylylase kinase 2 (AK2), which is involved in energy metabolism, can be considered as a potential candidate substrate. AK2 forms a complex with dual-specificity phosphatase 26 (DUSP26) to dephosphorylate fas-associated protein with death domain (FADD) [26]. Phosphorylated FADD plays an essential role in cellular mechanisms that enhance chemotherapy-induced apoptosis [27]. AK2 is one of the representative substrates of DPP8 [1,28]. It is possible that the inhibition of AK2 cleavage by DPP8 leads to increased levels of phosphorylated FADD.

Our preliminary examination showed that AK2, FADD, phosphorylated FADD, and DUSP26 were all equally expressed in the three high-sensitive and three low-sensitive cell lines used in Figure 1A (Figure S2). These findings are consistent with results showing that

all six of these cell lines were equally sensitive to high concentrations of 1G244 (Figure 1A). We are currently planning future in vitro reconstitution experiments involving these factors.

5. Conclusions

In this paper, we show that the DPP8/9 inhibitor 1G244 exhibits a dual role: at low concentrations, it induces DPP9 inhibition-dependent pyroptosis, and at high concentrations, it induces DPP8 inhibition-dependent apoptosis. Importantly, we identified HCK expression as a necessary determinant of susceptibility to pyroptosis, but with no effect on the induction of apoptosis (Figure 6). Furthermore, a greater antitumor effect associated with the lower toxicity profile of tominostat, a methylpiperazine analog of 1G244 with high DPP8 selectivity, was observed and compared to 1G244. Our findings suggest that additional enhancement in DPP8 selectivity by further modifications of tominostat chemical structure may lead to the development of novel anticancer agents that are effective against a wide range of hematologic malignancies.

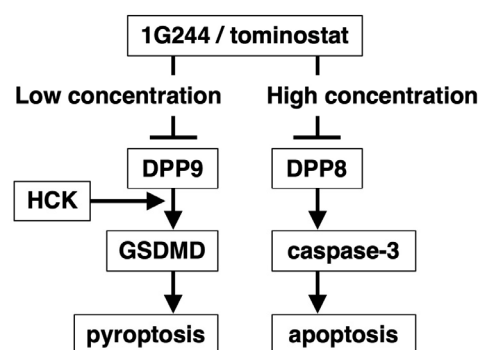


Figure 6. A diagram describing the dual signaling nature of 1G244/tominostat.

Supplementary Materials: The following supporting information can be downloaded at: <https://www.mdpi.com/article/10.3390/cells12071100/s1>, Figure S1: Effect of forced expression of HCK in resistant cell lines on DPP8/9 inhibitor-induced cytotoxicity, Figure S2: Expression of AK2-mediated apoptosis-inducing factors.

Author Contributions: Investigation, methodology, S.K., A.W., Y.K., K.O., P.J., M.U.R., E.K., T.S. (Takeshi Susukida), T.M., Y.N., N.I., T.O., R.H. and M.Y.; supervision, H.K., Y.M., M.M., Y.H., N.H.D., Y.S. and C.M.; writing—review and editing, N.H.D.; funding acquisition, writing—original draft, T.S. (Tsutomu Sato). All authors have read and agreed to the published version of the manuscript.

Funding: This research was supported by Japan Science and Technology Agency (JST) Moonshot R&D Grant Number JPMJMS2021, Japan Agency for Medical Research and Development (AMED) Grant Number 211m0203005j0005 (A145) and 22ym0126807j0001 (A160), and Japan Society for the Promotion of Science (JSPS) Grant-in-Aid for Scientific Research (C) Grant Number 21K07237.

Institutional Review Board Statement: The animal study protocol was approved by the Institutional Review Board of the Animal Care and Use Committee of Toyama University (reference number A2020UH-5).

Informed Consent Statement: Not applicable.

Data Availability Statement: Data are available on reasonable request. All data relevant to the study are included in the article or uploaded as online Supplementary Materials.

Acknowledgments: We gratefully thank Toyomi Kozawa for her help in performing this study.

Conflicts of Interest: The authors declare no conflict of interest.

References

1. Wilson, C.H.; Zhang, H.E.; Gorrell, M.D.; Abbott, C.A. Dipeptidyl Peptidase 9 Substrates and Their Discovery: Current Progress and the Application of Mass Spectrometry-Based Approaches. *Biol. Chem.* **2016**, *397*, 837–856. [[CrossRef](#)] [[PubMed](#)]
2. Lambeir, A.M.; Proost, P.; Durinx, C.; Bal, G.; Senten, K.; Augustyns, K.; Scharpé, S.; van Damme, J.; de Meester, I. Kinetic Investigation of Chemokine Truncation by CD26/Dipeptidyl Peptidase IV Reveals a Striking Selectivity within the Chemokine Family. *J. Biol. Chem.* **2001**, *276*, 29839–29845. [[CrossRef](#)] [[PubMed](#)]
3. Morimoto, C.; Schlossman, S.F. The Structure and Function of CD26 in the T-Cell Immune Response. *Immunol. Rev.* **1998**, *161*, 55–70. [[CrossRef](#)] [[PubMed](#)]
4. Kirby, M.; Yu, D.M.T.; O'Connor, S.P.; Gorrell, M.D. Inhibitor Selectivity in the Clinical Application of Dipeptidyl Peptidase-4 Inhibition. *Clin. Sci.* **2010**, *118*, 31–41. [[CrossRef](#)]
5. Bjelke, J.R.; Christensen, J.; Nielsen, P.F.; Branner, S.; Kanstrup, A.B.; Wagtmann, N.; Rasmussen, H.B. Dipeptidyl Peptidases 8 and 9: Specificity and Molecular Characterization Compared with Dipeptidyl Peptidase IV. *Biochem. J.* **2006**, *396*, 391–399. [[CrossRef](#)]
6. Bolgi, O.; Silva-Garcia, M.; Ross, B.; Pilla, E.; Kari, V.; Killisch, M.; Spitzner, M.; Stark, N.; Lenz, C.; Weiss, K.; et al. Dipeptidyl Peptidase 9 Triggers BRCA2 Degradation and Promotes DNA Damage Repair. *EMBO Rep.* **2022**, *23*, e54136. [[CrossRef](#)]
7. Freeman, M.; Justa-Schuch, D.; Silva-Garcia, M.; Pilla, E.; Engelke, M.; Kilisch, M.; Lenz, C.; Möller, U.; Nakamura, F.; Urlaub, H.; et al. DPP9 Is a Novel Component of the N-End Rule Pathway Targeting the Tyrosine Kinase Syk. *Elife* **2016**, *5*, e16370. [[CrossRef](#)]
8. Zhang, H.; Maqsudi, S.; Rainczuk, A.; Duffield, N.; Lawrence, J.; Keane, F.M.; Justa-Schuch, D.; Geiss-Friedlander, R.; Gorrell, M.D.; Stephens, A.N. Identification of Novel Dipeptidyl Peptidase 9 Substrates by Two-Dimensional Differential in-Gel Electrophoresis. *FEBS J.* **2015**, *282*, 3737–3757. [[CrossRef](#)]
9. Geiss-Friedlander, R.; Parmentier, N.; Möller, U.; Urlaub, H.; van den Eynde, B.J.; Melchoir, F. The Cytoplasmic Peptidase DPP9 Is Rate-Limiting for Degradation of Proline-Containing Peptides. *J. Biol. Chem.* **2009**, *284*, 27211–27219. [[CrossRef](#)]
10. Ajami, K.; Pitman, M.R.; Wilson, C.H.; Park, J.; Menz, R.I.; Starr, A.E.; Cox, J.H.; Abbott, C.A.; Overall, C.M.; Gorrell, M.D. Stromal Cell-Derived Factors 1 α and 1 β , Inflammatory Protein-10 and Interferon-Inducible T Cell Chemo-Attractant Are Novel Substrates of Dipeptidyl Peptidase 8. *FEBS Lett.* **2008**, *582*, 819–825. [[CrossRef](#)]
11. Cui, C.; Tian, X.; Wei, L.; Wang, Y.; Wang, K.; Fu, R. New Insights into the Role of Dipeptidyl Peptidase 8 and Dipeptidyl Peptidase 9 and Their Inhibitors. *Front. Pharmacol.* **2022**, *13*, 1002871. [[CrossRef](#)]
12. Ajami, K.; Abbott, C.A.; McCaughan, G.W.; Gorrell, M.D. Dipeptidyl Peptidase 9 Has Two Forms, a Broad Tissue Distribution, Cytoplasmic Localization and DPIP-like Peptidase Activity. *Biochim. Et Biophys. Acta-Gene Struct. Expr.* **2004**, *1679*, 18–28. [[CrossRef](#)]
13. Johnson, D.C.; Taabazuing, C.Y.; Okondo, M.C.; Chui, A.J.; Rao, S.D.; Brown, F.C.; Reed, C.; Peguero, E.; de Stanchina, E.; Kentsis, A.; et al. DPP8/DPP9 Inhibitor-Induced Pyroptosis for Treatment of Acute Myeloid Leukemia. *Nat. Med.* **2018**, *24*, 1151–1156. [[CrossRef](#)]
14. Okondo, M.C.; Johnson, D.C.; Sridharan, R.; Go, E.B.; Chui, A.J.; Wang, M.S.; Poplawski, S.E.; Wu, W.; Liu, Y.; Lai, J.H.; et al. DPP8 and DPP9 Inhibition Induces Pro-Caspase-1-Dependent Monocyte and Macrophage Pyroptosis. *Nat. Chem. Biol.* **2017**, *13*, 46–53. [[CrossRef](#)]
15. Okondo, M.C.; Rao, S.D.; Taabazuing, C.Y.; Chui, A.J.; Poplawski, S.E.; Johnson, D.C.; Bachovchin, D.A. Inhibition of Dpp8/9 Activates the Nlrp1b Inflammasome. *Cell. Chem. Biol.* **2018**, *25*, 262–267.e5. [[CrossRef](#)]
16. Sato, T.; Tatekoshi, A.; Takada, K.; Iyama, S.; Kamihara, Y.; Jawaid, P.; Rehman, M.U.; Noguchi, K.; Kondo, T.; Kajikawa, S.; et al. DPP8 Is a Novel Therapeutic Target for Multiple Myeloma. *Sci. Rep.* **2019**, *9*, 18094. [[CrossRef](#)]
17. van Goethem, S.; Matheussen, V.; Joossens, J.; Lambeir, A.M.; Chen, X.; de Meester, I.; Haemers, A.; Augustyns, K.; van der Veken, P. Structure-Activity Relationship Studies on Isoindoline Inhibitors of Dipeptidyl Peptidases 8 and 9 (DPP8, DPP9): Is DPP8-Selectivity an Attainable Goal? *J. Med. Chem.* **2011**, *54*, 5737–5746. [[CrossRef](#)]
18. Jiang, M.; Qi, L.; Li, L.; Li, Y. The Caspase-3/GSDME Signal Pathway as a Switch between Apoptosis and Pyroptosis in Cancer. *Cell. Death Discov.* **2020**, *6*, 112. [[CrossRef](#)]
19. Poh, A.R.; O'Donoghue, R.J.J.; Ernst, M. Hematopoietic Cell Kinase (HCK) as a Therapeutic Target in Immune and Cancer Cells. *Oncotarget* **2015**, *6*, 15752–15771. [[CrossRef](#)]
20. Radha, V.; Sudhakar, C.; Ray, P.; Swarup, G. Induction of Cytochrome c Release and Apoptosis by Hck-SH3 Domain-Mediated Signalling Requires Caspase-3. *Apoptosis* **2002**, *7*, 195–207. [[CrossRef](#)]
21. Wu, J.J.; Tang, H.K.; Yeh, T.K.; Chen, C.M.; Shy, H.S.; Chu, Y.R.; Chien, C.H.; Tsai, T.Y.; Huang, Y.C.; Huang, Y.L.; et al. Biochemistry, Pharmacokinetics, and Toxicology of a Potent and Selective DPP8/9 Inhibitor. *Biochem. Pharmacol.* **2009**, *78*, 203–210. [[CrossRef](#)] [[PubMed](#)]
22. Ross, B.; Krapp, S.; Augustin, M.; Kierfersauer, R.; Arciniega, M.; Geiss-Friedlander, R.; Huber, R. Structures and Mechanism of Dipeptidyl Peptidases 8 and 9, Important Players in Cellular Homeostasis and Cancer. *Proc. Natl. Acad. Sci. USA* **2018**, *115*, E1437–E1445. [[CrossRef](#)] [[PubMed](#)]
23. Gall, M.G.; Chen, Y.; de Ribeiro, A.J.V.; Zhang, H.; Bailey, C.G.; Spielman, D.S.; Yu, D.M.T.; Gorrell, M.D. Targeted Inactivation of Dipeptidyl Peptidase 9 Enzymatic Activity Causes Mouse Neonate Lethality. *PLoS ONE* **2013**, *8*, e78378. [[CrossRef](#)]
24. Kim, M.; Minoux, M.; Piaia, A.; Kueng, B.; Gapp, B.; Weber, D.; Haller, C.; Barbieri, S.; Namoto, K.; Lorenz, T.; et al. DPP9 Enzyme Activity Controls Survival of Mouse Migratory Tongue Muscle Progenitors and Its Absence Leads to Neonatal Lethality Due to Suckling Defect. *Dev. Biol.* **2017**, *431*, 297–308. [[CrossRef](#)]

25. Kong, X.; Liao, Y.; Zhou, L.; Zhang, Y.; Cheng, J.; Yuan, Z.; Wang, S. Hematopoietic Cell Kinase (HCK) Is Essential for NLRP3 Inflammasome Activation and Lipopolysaccharide-Induced Inflammatory Response In Vivo. *Front. Pharmacol.* **2020**, *11*, 581011. [[CrossRef](#)]
26. Kim, H.; Lee, H.J.; Oh, Y.; Choi, S.G.; Hong, S.H.; Kim, H.J.; Lee, S.Y.; Choi, J.W.; Su Hwang, D.; Kim, K.S.; et al. The DUSP26 Phosphatase Activator Adenylate Kinase 2 Regulates FADD Phosphorylation and Cell Growth. *Nat. Commun.* **2014**, *5*, 3351. [[CrossRef](#)] [[PubMed](#)]
27. Shimada, K.; Matsuyoshi, S.; Nakamura, M.; Ishida, E.; Kishi, M.; Konishi, N. Phosphorylation of FADD Is Critical for Sensitivity to Anticancer Drug-Induced Apoptosis. *Carcinogenesis* **2004**, *25*, 1089–1097. [[CrossRef](#)]
28. Wilson, C.H.; Indarto, D.; Doucet, A.; Pogson, L.D.; Pitman, M.R.; McNicholas, K.; Menz, R.I.; Overall, C.M.; Abbott, C.A. Identifying Natural Substrates for Dipeptidyl Peptidases 8 and 9 Using Terminal Amine Isotopic Labeling of Substrates (TAILS) Reveals in Vivo Roles in Cellular Homeostasis and Energy Metabolism. *J. Biol. Chem.* **2013**, *288*, 13936–13949. [[CrossRef](#)]

Disclaimer/Publisher’s Note: The statements, opinions and data contained in all publications are solely those of the individual author(s) and contributor(s) and not of MDPI and/or the editor(s). MDPI and/or the editor(s) disclaim responsibility for any injury to people or property resulting from any ideas, methods, instructions or products referred to in the content.

ORIGINAL ARTICLE

Functional roles of CD26/DPP4 in bleomycin-induced pulmonary fibrosis

Yu Koyanagi¹ | Takeshi Kawasaki¹  | Yoshitoshi Kasuya² | Ryo Hatano³ | Shun Sato¹ | Yukiko Takahashi¹ | Kei Ohnuma³ | Chikao Morimoto³ | Steven M. Dudek⁴ | Koichiro Tatsumi¹ | Takuji Suzuki^{1,5}

¹Department of Respiriology, Graduate School of Medicine, Chiba University, Chiba, Japan

²Department of Biomedical Science, Graduate School of Medicine, Chiba University, Chiba, Japan

³Department of Therapy Development and Innovation for Immune Disorders and Cancers, Graduate School of Medicine, Juntendo University, Tokyo, Japan

⁴Division of Pulmonary, Critical Care, Sleep and Allergy, Department of Medicine, University of Illinois at Chicago, Chicago, Illinois, USA

⁵Synergy Institute for Futuristic Mucosal Vaccine Research and Development, Chiba University, Chiba, Japan

Correspondence

Takeshi Kawasaki, Department of Respiriology, Graduate School of Medicine, Chiba University, 1-8-1 Inohana, Chuo-ku, Chiba-shi, Chiba, Japan.

Email: kawatake@chiba-u.jp

Funding information

Intractable Respiratory Diseases and Pulmonary Hypertension Research Group, Ministry of Health, Labor and Welfare, Japan, Grant/Award Number: 20FC1027 and 21FC1027; AMED, Grant/Award Number: 223fa627003h0001; AMED-CREST, Grant/Award Number: JP21gm1210003; JSPS KAKENHI, Grant/Award Number: 19K17663, 22K16163 and 22H03076

Abstract

The pathogenesis of pulmonary fibrosis involves complex interplay between cell types and signaling pathways. Recurrent alveolar epithelial injury can occur during pulmonary inflammation, causing dysregulation of epithelial repair. Dysregulated repair interacts with mesenchymal, inflammatory, and endothelial cells to trigger fibroblast-to-myofibroblast activation. CD26/dipeptidyl peptidase-4 (DPP4) is a type II membrane protein mediating pleiotropic effect. However, the mechanistic role of CD26/DPP4 in pulmonary fibrosis remains unclear. In this study, we aimed to characterize *Dpp4* deficiency in a mouse bleomycin (BLM)-induced pulmonary fibrosis model and in cell culture systems of human lung fibroblasts (HLFs). *Dpp4* knockout (*Dpp4* KO) mouse lungs exhibited lower Ashcroft scale indices, collagen content, and numbers of fibroblasts and myofibroblasts compared with those in C57BL/6 wild-type (WT) mice. Upregulation of *Tgfb1* and *Tgfb2* mRNA levels in the lungs after BLM treatment was lower in *Dpp4* KO mice compared with those in WT mice. Although TGF- β -driven endothelial-to-mesenchymal transition (EndMT) has been implicated as one of the mechanisms of pulmonary fibrosis, a number of partial EndMT cells in lungs did not differ between *Dpp4* KO mice and WT mice. The proliferation capacity and mRNA levels of *COL1A1*, a collagen deposition-related gene, in cultured HLFs were suppressed in *DPP4* small interfering RNA-treated cells. This study indicates that the genetic deficiency of *DPP4* has protective effects against BLM-induced pulmonary fibrosis, partly through the reduction in TGF- β expression

This is an open access article under the terms of the [Creative Commons Attribution](https://creativecommons.org/licenses/by/4.0/) License, which permits use, distribution and reproduction in any medium, provided the original work is properly cited.

© 2023 The Authors. *Physiological Reports* published by Wiley Periodicals LLC on behalf of The Physiological Society and the American Physiological Society.

and inhibition of fibroblast activation in the lung. Our study suggests that CD26/DPP4 inhibition is a potential therapeutic strategy for pulmonary fibrosis.

KEYWORDS

CD26, dipeptidyl peptidase-4, fibroblast, pulmonary fibrosis

1 | INTRODUCTION

Interstitial lung diseases (ILDs) comprise a large number of chronic progressive lung diseases that are characterized by varying degrees of inflammation, followed by pulmonary fibrosis in the lung interstitium. Although the clinical course is variable and unpredictable, these diseases can lead to progressive respiratory failure with poor prognosis (Raghu et al., 2006, 2011). The immune system plays a pivotal role in the initiation, development, and resolution of inflammation following recurrent alveolar epithelial injury and dysregulation of epithelial repair. The most accepted hypothesis for idiopathic pulmonary fibrosis (IPF) pathogenesis relies on the inability of alveolar epithelium to regenerate after injury. Further, IPF is characterized by altered composition and dysfunction of resident and immune cells in the lungs, leading to excessive accumulation of extracellular matrix (ECM) and progressive scarring. Although much progress has been made in understanding IPF pathogenesis and management, and disease-modifying therapies have been approved worldwide, important clinical needs and demands are not yet met (Distler et al., 2019; Flaherty et al., 2019; Podolanczuk et al., 2021; Wollin et al., 2019).

The etiology of IPF is diverse and incompletely defined since all stages of fibrosis are accompanied by a broad spectrum of innate and adaptive immune responses. The pathogenesis of IPF involves complex interplay between cell types and signaling pathways. Repetitive alveolar epithelial cell injury may occur in the context of predisposing immunological inflammatory factors, leading to aberrant epithelial cell activation and dysregulation of epithelial repair (Heukels et al., 2019). Further, inflammation plays an important role in IPF pathogenesis (Heukels et al., 2019), although steroids as inflammatory modulators have exhibited deleterious effects in clinical IPF.

Repetitive alveolar epithelial injury triggers the early development of fibrosis. These injuries, in combination with dysregulated wound repair and fibroblast dysfunction, lead to tissue remodeling and pulmonary fibrosis, although tissue remodeling is complex and differs among compartments. Abnormal deposition of ECM proteins is a key factor in the development of tissue remodeling. The current notion is that myofibroblasts, which are derived from epithelial cells by epithelial–mesenchymal transition

(EMT), exhibit abnormal proliferation and ECM overproduction, presumably resulting in IPF progression (Jia et al., 2021; Mackinnon et al., 2012; Podolanczuk et al., 2021; Salton et al., 2019; Wollin et al., 2019). When EMT occurs in the lung, E-cadherin levels in epithelial cells decrease, and α -smooth muscle actin (α -SMA)-expressing mesenchymal cells increase. A few studies have found that approximately one-third of fibroblasts are of epithelial origin in pulmonary fibrosis. In addition, EMT plays a critical role in the development of pulmonary fibrosis (Della Latta et al., 2015; Jia et al., 2021; Nataraj et al., 2010; Sanchez-Duffhues et al., 2018; Suzuki et al., 2017). The cytokine transforming growth factor β (TGF- β) functions as an important mediator of fibrogenesis. Further, TGF- β 1 induces fibroblasts to undergo a phenotypic transition to myofibroblasts, which are effectors of the fibrotic state (Qian et al., 2018). Thus, the anti-EMT pathway or inhibition of TGF- β 1 signaling is a novel potential target for IPF treatment.

The differentiation of fibroblasts into myofibroblasts favors the progression of fibrosis (Suzuki et al., 2020). Compared with fibroblasts, myofibroblasts upregulate α -SMA expression and increase the production of ECM proteins (Akamatsu et al., 2013; Garrison et al., 2013; Hinz et al., 2007). Myofibroblasts can originate from sources other than fibroblasts. Endothelial cells are a potential source of endothelial-to-mesenchymal transition (EndMT) (Hashimoto et al., 2010). During this process, endothelial cells acquire a mesenchymal phenotype and present typical markers of myofibroblast differentiation, such as α -SMA and vimentin, while reducing the expression of vascular endothelial cadherin (VE-cadherin; Pardali et al., 2017). In one study, 16% of lung fibroblasts expressing α -SMA and collagen type I were derived from lung endothelial cells in mice with bleomycin (BLM)-induced pulmonary fibrosis (Hashimoto et al., 2010). Similar to EMT, TGF- β plays a central role in promoting EndMT through a wide network of molecular interactions (Liu & Qi, 2020; Pardali et al., 2017).

CD26/dipeptidyl peptidase-4 (DPP4) is a transmembrane protein expressed in various cells that exists as a soluble protein in tissue and circulation. The peptidase activity of CD26/DPP4 exerts effects on multiple proteins, including incretin hormones, and has led to the development of CD26/DPP4 inhibitors as therapeutic agents for

diabetes. CD26/DPP4 also participates in immune regulation and promotion of inflammation (Morimoto & Schlossman, 1998; Ohnuma et al., 2008). In healthy human lung, CD26/DPP4 is expressed in type I and II alveolar epithelial cells, alveolar macrophages, vascular endothelium, and pleural mesothelium (Meyerholz et al., 2016).

We previously reported that CD26/DPP4 inhibition by the pharmaceutical agent sitagliptin ameliorated LPS-induced lung injury in mice, with anti-inflammatory effects on lung endothelial cells, and that CD26/DPP4 mediates inflammatory responses in the pulmonary endothelium (Kawasaki et al., 2018; Suzuki et al., 2016; Takahashi et al., 2021). These findings suggest plausible interactions between CD26/DPP4 and the pathophysiology of inflammatory lung diseases. Vildagliptin, another CD26/DPP4 inhibitor, ameliorates BLM-induced pulmonary fibrosis (Liu & Qi, 2020), and *Dpp4* deficiency reduces BLM-induced fibrosis in the skin and lungs of mice (Soare et al., 2020), suggesting a functional participation of CD26/DPP4 in pulmonary fibrosis. However, it remains unclear how CD26/DPP4 affects mechanisms related to pulmonary fibrosis, such as fibroblast activation or mesenchymal transition.

Mouse BLM-induced pulmonary fibrosis is a widely used model of pulmonary fibrosis, because BLM damage provokes a histological lung pattern similar to that described in patients with IPF, and this pattern is characterized by patchy parenchymal inflammation, epithelial cell injury with reactive hyperplasia, EMT, activation and differentiation of fibroblasts to myofibroblasts, and basement membrane and alveolar epithelium injuries (Della Latta et al., 2015).

In this study, we aimed to clarify the functional roles of CD26/DPP4 in pulmonary fibrosis by focusing on fibroblast activation and EndMT using *Dpp4*-deficient mice in the model of BLM-induced pulmonary fibrosis (Liu et al., 2017), and in cultured human lung fibroblasts (HLFs).

2 | MATERIALS AND METHODS

2.1 | BLM-induced pulmonary fibrosis in *Dpp4* knockout mice

Eight- 10-week-old male C57BL/6J wild-type (WT) mice (Clea Japan) and *Dpp4* knockout (*Dpp4* KO) mice on a C57BL/6 background were intratracheally administered phosphate-buffered saline (PBS) or 4 U/mg/body bleomycin (Nihon Kayaku). The lungs were harvested 21 days after BLM treatment. All animal experiments were conducted according to protocols approved by the Review Board for animal experiments of Chiba University, Japan.

2.2 | Bronchoalveolar lavage fluid analysis

Bronchoalveolar lavage fluid (BALF) was collected 21 days after BLM treatment by instilling 1 mL of PBS through the tracheal cannula into the lungs, followed by slow recovery of the fluid. Cells were collected from the BALF by centrifugation (500×g, 20 min, 4°C) and counted using an automated cell counter (TC20; Bio-Rad). The BALF supernatant was centrifuged again (17,000×g, 10 min, 4°C) and stored at −80°C until further analysis. The BALF protein concentration was measured using a bicinchoninic acid assay kit (Thermo Fisher Scientific).

2.3 | Histological examination

Mouse lung tissues were fixed in formalin, embedded in paraffin, sectioned, mounted onto slides, and subjected to hematoxylin–eosin and Masson's trichrome staining. The severity of pulmonary fibrosis was semi-quantitatively assessed according to the method proposed by Ashcroft (Ashcroft et al., 1988; Hubner et al., 2008).

2.4 | Quantification of collagen content of lungs

The collagen content of lung tissues was measured using the Sircol Soluble Collagen Assay kit (Biocolor Ltd.) according to the manufacturer's instructions.

2.5 | Preparation of single cell suspension from mouse lungs

At the time of harvest, the lungs were perfused from the right ventricle until blood-free using 20 mL PBS containing 10 U/mL heparin (Mochida). They were then minced and digested in an enzyme cocktail of Dulbecco's Modified Eagle's Medium (Sigma) containing 1% bovine serum albumin (BSA) (Sigma), 2 mg/mL collagenase (Worthington), 100 µg/mL DNase (Sigma), and 2.5 mg Dispase II (Sigma) at 37°C for 60 min, and then meshed through a 70-µm nylon cell strainer.

2.6 | Flow cytometry analysis of mouse cells in BALF and lungs

Mouse cells in BALF or lungs were pretreated with anti-CD16/32 antibody (BioLegend) for 10 min to block Fc receptors and then incubated with specific antibodies

in the dark at 4°C for 15 min. The following antibodies were used for cell surface staining: anti-CD31-PE/Cy7 (BioLegend), anti-CD45-Alexa Flour 700 (BioLegend), anti-CD326-PerCP/Cyanine5.5 (BioLegend), and anti-CD26-FITC (BioLegend), and anti-Gr-1-APC (BioLegend). After surface staining, the lung cells were incubated with α -SMA (Thermo Fisher Scientific) and anti-vimentin (Abcam) for 15 min in the dark at 4°C. The secondary antibody used was donkey anti-rabbit IgG-PE (Invitrogen) for 15 min in the dark at 4°C. Numbers of fibroblasts, myofibroblasts, and partial EndMT cells in the lungs were assessed using flow cytometry (FCM). Fibroblasts, myofibroblasts, and partial EndMT cells were defined as vimentin-positive CD31⁻/CD45⁻/CD326⁻ cells (Lazarides, 1980; Morbini et al., 2011; Suzuki et al., 2017), α -SMA-positive CD31⁻/CD45⁻/CD326⁻ cells (Suzuki et al., 2017; Zhang et al., 2020), and α -SMA-positive CD31⁺/CD45⁻/CD326⁻ cells (Hashimoto et al., 2010; Suzuki et al., 2016, 2017), respectively. Cell fluorescence was measured using a BD FACS Canto™ II (BD Biosciences), and the data were analyzed using FlowJo software (TreeStar). To evaluate expression levels, mean fluorescence intensity (MFI) of a sample was calculated as follows: MFI of a sample stained with an antibody–MFI of a sample unstained (autofluorescence of the sample).

2.7 | Culture of HLFs

Human lung fibroblasts were obtained from Lonza and cultured in Dulbecco's Modified Eagle's Medium, with L-glutamine, phenol red, and sodium pyruvate, (FUJIFILM Wako) supplemented with 15% fetal bovine serum. The cells were incubated at 37°C in a 5% CO₂ incubator and used at passages 6–8 for all experiments.

2.8 | Transfections with small interfering RNA

Non-specific control small interfering RNA (NS-siRNA) (Cat# 4390843: Silencer™ Select Negative Control No. 1 siRNA), *DPP4* siRNA (Cat# 4392421: siRNA ID s4254) (*DPP4*-siRNA1), and *DPP4* siRNA (Cat# 4392421: siRNA ID s4255) (*DPP4*-siRNA2) were purchased from Thermo Fisher Scientific. For siRNA transfection, the Lipofectamine™ RNAiMAX Transfection Reagent (Invitrogen) was used according to the manufacturer's protocol. Cultured cells were transfected with siRNA at 60% confluence for 72 h. Selective silencing of CD26/*DPP4* was confirmed using FCM and quantitative PCR (qPCR).

2.9 | Real-time quantitative PCR

Total RNA was extracted from cells using TRIzol, followed by the Direct-zol RNA MiniPrep Plus Kit (Zymo Research Corporation). Subsequently, RNA was reverse-transcribed via PCR using the SuperScript IV VILO Master Mix (Thermo Fisher Scientific) to synthesize single-stranded cDNA. The cDNA samples were amplified using qPCR with Fast SYBR Green PCR Master Mix (Thermo Fisher Scientific) and the GeneAmp PCR System (Thermo Fisher Scientific). Specific primers were designed using the web software from the Universal Probe Library Assay Design Center (Roche Applied Science). The expression level of each target gene was normalized to hypoxanthine phosphoribosyltransferase 1 (HPRT1) threshold cycle (CT) values and calculated using the 2^{- $\Delta\Delta$ Ct} method. $\Delta\Delta$ CT = (target gene CT of experimental group–reference gene CT of experimental group)–(target gene CT of control group–reference gene CT of control group).

2.10 | Cell proliferation assay

Cell proliferation assay was performed to assess the number of viable cells using the Cell Counting Kit-8 (WST-8) (Dojindo Molecular Technologies) according to the manufacturer's protocol. HLFs (5000 cells/well) treated with siRNA against *DPP4* or non-specific control siRNA for 72 h were detached using ACCUTASE (Thermo Fisher Scientific) and cultured in 96-well plates for 24 h. The cells were then cultured with 10 μ L of WST-8 in each well at 37°C for 2 h. Cell viability was measured as the absorbance (optical density [OD]) at 450 nm using a microplate reader. The results were calculated using the following formula: Cell viability = (treatment group OD–blank group OD)/(control group OD–blank group OD).

2.11 | Western blot analysis

Cells were washed with PBS, and lysates were prepared in Laemmli's SDS sample buffer (Boston Bioproducts). Protein samples were subjected to SDS-PAGE and then transferred to polyvinylidene difluoride membranes (Thermo Fisher Scientific). After blocking with Tris-buffered saline containing 0.1% Tween 20 (TBS-T) and 5% BSA (Sigma) for 30 min at 25°C, the membrane was incubated with primary antibodies against α -SMA (dilution 1:1000, Abcam) and β -actin (dilution 1:1000, Thermo Fisher Scientific) for 1 h at 25°C. Secondary antibodies conjugated to horseradish peroxidase (dilution 1:2000, Thermo Fisher Scientific) were added to membranes for 30 min at 25°C. Finally, the SuperSignal West Dura

kit (Thermo Fisher Scientific) was used to visualize the bands, and band densities were determined using the ImageJ software (National Institutes of Health).

2.12 | Statistical analysis

Results were expressed as mean \pm SD. One-way ANOVA was used for multiple-group comparisons, followed by

Tukey's post hoc test. Student's t-test was used to compare the two groups. Statistical analyses were performed using GraphPad Prism 5 software. Statistical significance was set at $p < 0.05$. To minimize distributions of values caused by possible differences in experimental conditions, data were normalized using the mean value derived from WT mice treated with BLM for each experiment, and then, the normalized values from each experiment were combined for statistical analysis.

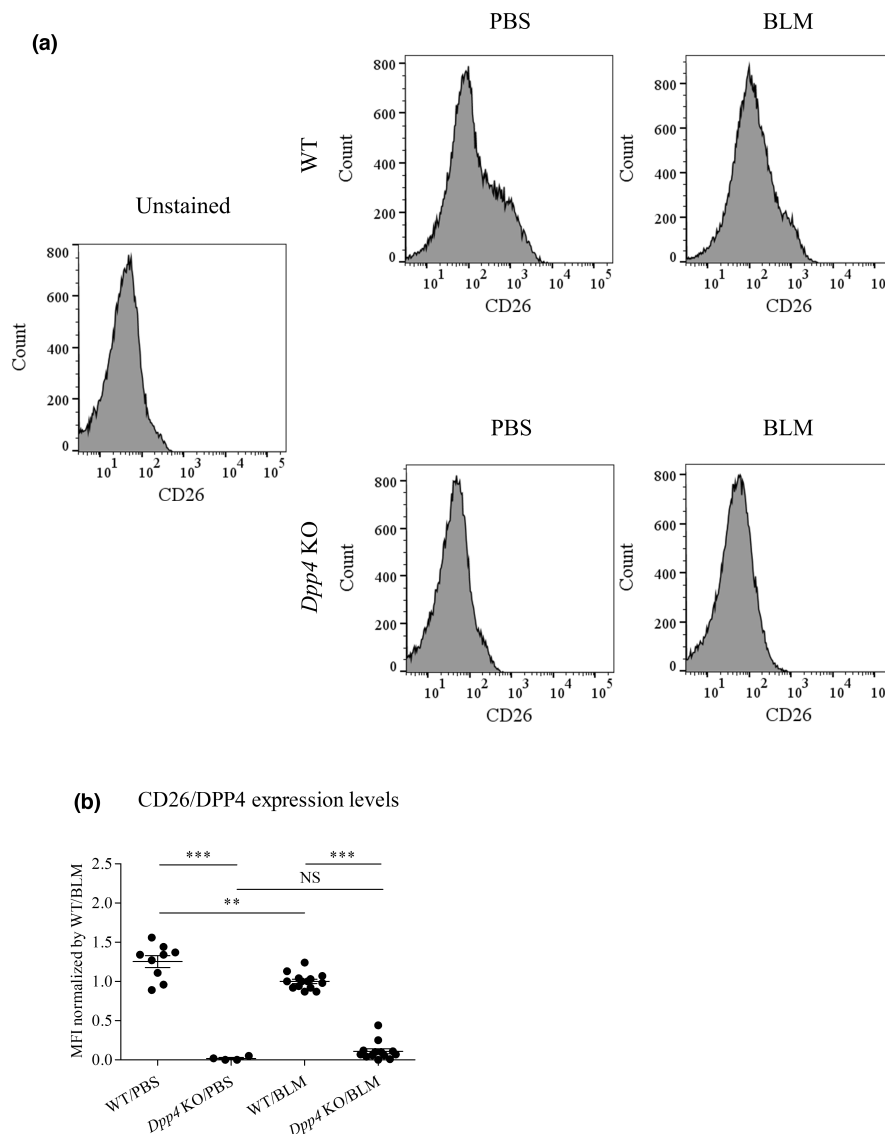


FIGURE 1 BLM-induced pulmonary fibrosis in *Dpp4*-deficient and WT mice. (a, b) CD26/DPP4 expression levels in lung cells of bleomycin (BLM)- or PBS-treated *Dpp4* KO and WT mice were measured by mean fluorescence intensity (MFI) using flow cytometry analysis. CD26/DPP4 expression levels were substantially lower or nearly zero in *Dpp4* KO mice compared with those in WT mice ($n = 4-19$). (c) BLM-induced pulmonary fibrosis was assessed using hematoxylin–eosin and Masson's trichrome staining in lung tissue sections in *Dpp4* KO and WT mice, respectively. Collagen fibers are differentially stained and shown as blue color in Masson's trichrome staining. Representative images are shown for each condition. Original magnification 100 \times . Black scale bar, 100 μ m. (d and e) Fibrotic lung injury was histologically assessed by two independent researchers using the Ashcroft scoring system. Indices of Ashcroft scores and collagen content were lower in *Dpp4* KO mouse lungs than those in WT mouse lungs ($n = 3-17$). * $p < 0.05$, ** $p < 0.01$, *** $p < 0.001$. Values represent the mean \pm SD of three independent experiments. WT, wild-type mice; NS, not significant.

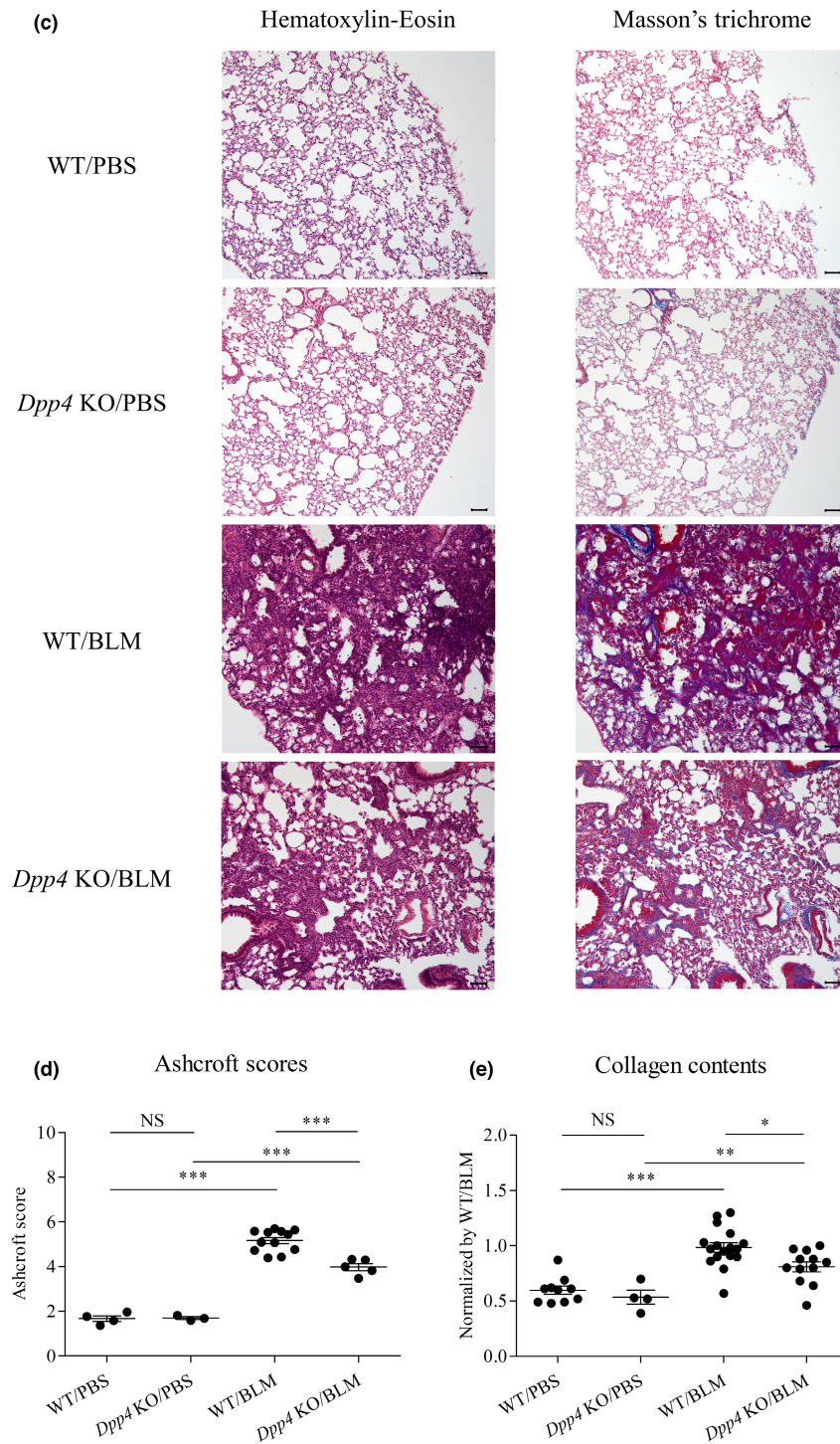


FIGURE 1 (Continued)

3 | RESULTS

3.1 | BLM-induced pulmonary fibrosis was attenuated in *Dpp4*-deficient mice

CD26/DPP4 expression levels were evaluated in the cellular components of the mouse lung using FCM. CD26/DPP4 levels were confirmed to be substantially low or nearly zero

in *Dpp4* KO mice, and the levels in WT mouse lung after BLM treatment were significantly lower than those after PBS treatment (Figure 1a,b). The effects of global *Dpp4* deficiency on BLM-induced fibrosis were then assessed. Both Ashcroft scores and collagen content were significantly lower in *Dpp4* KO mouse lungs compared with those in WT mouse lungs (Figure 1c–e), suggesting that *Dpp4* deficiency has protective effects against BLM-induced fibrosis in mice.

3.2 | Severity of lung injury did not differ between *Dpp4*-deficient mice and WT mice with BLM-induced pulmonary fibrosis

In pulmonary fibrosis, the immune system plays a pivotal role in the initiation, development, and resolution of parenchymal inflammation following an insult or damage to organs. The role of inflammation as an important component of IPF etiology is controversial and is sometimes seen as an epiphenomenon of fibrosis. We investigated whether severity of lung injury, as evaluated by some representative parameters of inflammation and permeability (Matute-Bello et al., 2011), was ameliorated by *Dpp4* deficiency in BLM-induced pulmonary fibrosis. The results revealed that protein concentrations and the number of CD45⁺ and Gr-1 double positive neutrophils in BALF were increased by BLM treatment but did not differ between the *Dpp4* KO mice and WT mice (Figure 2). These results suggest that the severity of lung injury may not differ between *Dpp4*-deficient mice and WT mice with BLM-induced pulmonary fibrosis.

3.3 | The numbers of lung fibroblasts and myofibroblasts in BLM-induced lung fibrosis were lower in *Dpp4*-deficient mice than in WT mice

We next assessed numbers of the lung constituent cells using FCM analysis that were defined as follows: CD31⁺/CD45⁻ endothelial cells, CD31⁻/CD45⁺ hematopoietic cells, CD31⁻/CD45⁻/CD326⁺ epithelial cells, and CD31⁻/CD45⁻/CD326⁻ mesenchymal cells (Kawasaki et al., 2015). The number of whole lung constituent cells in WT mice was increased after BLM challenge but did not

differ between WT mice and *Dpp4* KO mice (Figure 3a). Similarly, the number of CD31⁻/CD45⁺ hematopoietic cells was increased after BLM challenge but did not differ between WT mice and *Dpp4* KO mice with BLM-induced pulmonary fibrosis (Figure 3b). Neither the number of CD31⁺/CD45⁻ endothelial cells in WT mice differ after BLM challenge, nor the number of CD31⁺/CD45⁻ endothelial cells differ between WT mice and *Dpp4* KO with BLM-induced pulmonary fibrosis (Figure 3c). Meanwhile, the number of CD31⁻/CD45⁻/CD326⁺ epithelial cells in WT mice was decreased after BLM challenge, and the number did not differ between WT mice and *Dpp4* KO mice with BLM-induced pulmonary fibrosis (Figure 3d). Of note, the number of CD31⁻/CD45⁻/CD326⁻ mesenchymal cells in WT mice was increased after BLM challenge, and the magnitude of this increase was significantly lower in *Dpp4* KO mice than that in WT mice (Figure 3e). Additionally, the numbers of fibroblasts and myofibroblasts in *Dpp4* KO mouse lungs after BLM treatment were all lower than those in WT mice (Figure 3f,g,h,i), while the number of partial EndMT cells in lungs after BLM challenge did not differ between in *Dpp4* KO mice and in WT mice (Figure 3j,k). These results suggested that lung fibroblast activation in the lungs were suppressed by *Dpp4* deficiency in BLM-induced lung fibrosis.

3.4 | Expression levels of CD26/DPP4 in the WT mouse lung after BLM-challenge were lower in epithelial and endothelial cells, while higher in hematopoietic and mesenchymal cells

As shown in Figure 1b, CD26/DPP4 levels in WT mouse lung after BLM treatment were significantly lower than

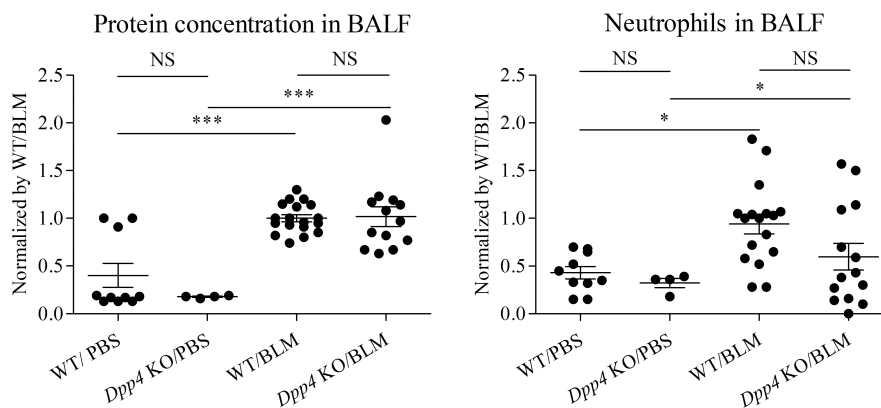


FIGURE 2 Severity of lung injury in *Dpp4*-deficient and WT mice with BLM-induced pulmonary fibrosis. Some representative lung injury parameters (total protein concentration and number of neutrophils) were measured in bronchoalveolar lavage fluid (BALF) of WT and *Dpp4* KO mice 21 days after bleomycin (BLM) or PBS treatment. Neither total protein concentration levels nor the number of neutrophils in BALF significantly differed between WT and *Dpp4* KO mice, in either the PBS or BLM-treated groups ($n = 4-18$). * $p < 0.05$, *** $p < 0.001$. Values represent the mean \pm SD of three independent experiments. WT, wild-type mice; NS, not significant.

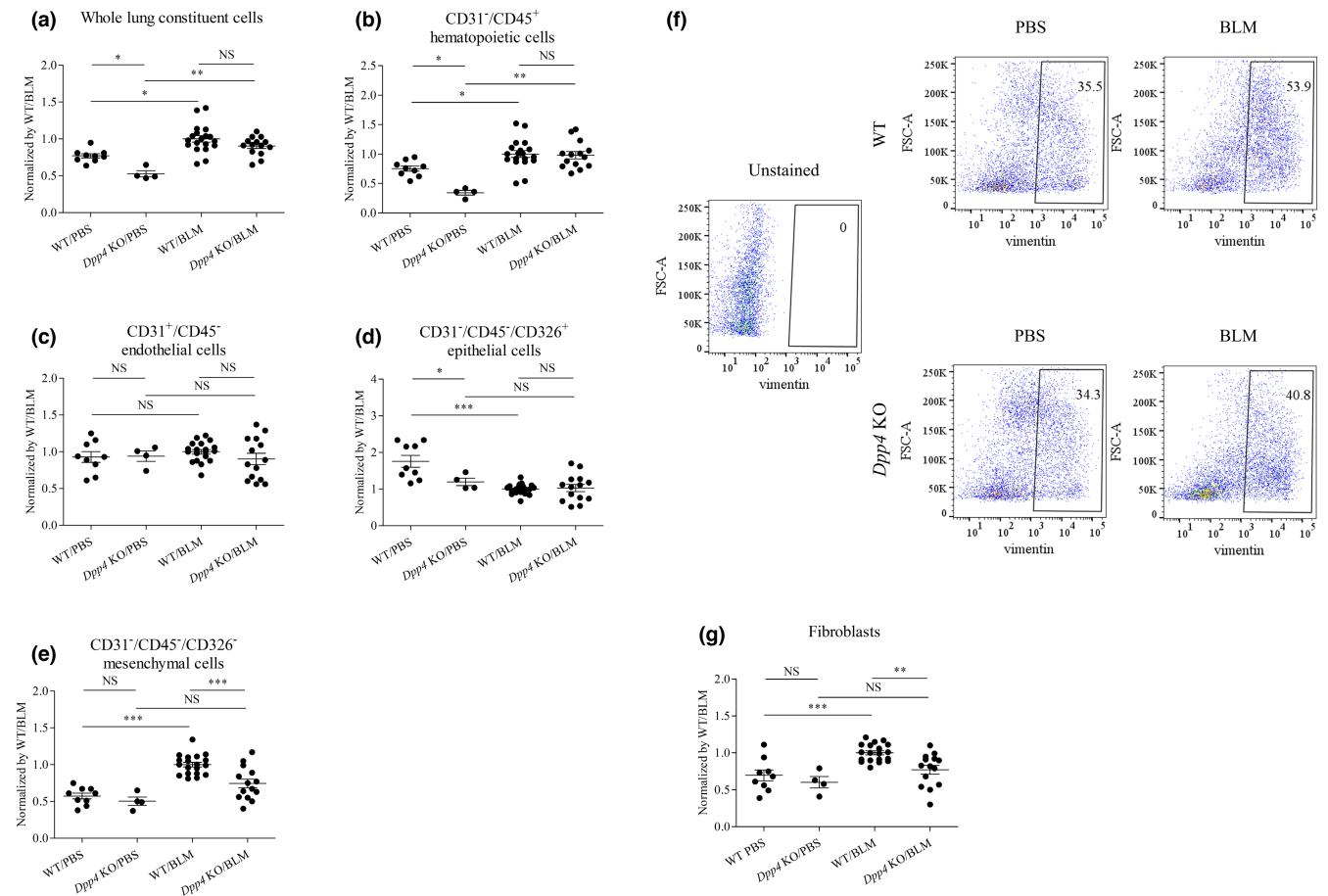


FIGURE 3 Lung constituent cells from *Dpp4*-deficient and WT mice in BLM-induced lung fibrosis. Numbers of mouse whole lung cells and lung constituent cells were evaluated using flow cytometry (FCM) analysis ($n = 4-19$). (a) The number of whole lung constituent cells in WT mice was increased after BLM challenge but did not differ between WT mice and *Dpp4* KO mice. (b) Similarly, the number of CD31⁺/CD45⁺ hematopoietic cells was increased after BLM challenge but did not differ between WT mice and *Dpp4* KO mice with BLM-induced pulmonary fibrosis. (c) Neither the number of CD31⁺/CD45⁻ endothelial cells in WT mice differ after BLM challenge, nor the number of CD31⁺/CD45⁻ endothelial cells differ between WT mice and *Dpp4* KO mice with BLM-induced pulmonary fibrosis. (d) Meanwhile, the number of CD31⁺/CD45⁻/CD326⁺ epithelial cells in WT mice was decreased after BLM challenge, and the number did not differ between WT mice and *Dpp4* KO mice with BLM-induced pulmonary fibrosis. (e) Of note, the number of CD31⁺/CD45⁻/CD326⁻ mesenchymal cells in WT mice was increased after BLM challenge, and the magnitude of this increase was significantly lower in *Dpp4* KO mice than that in WT mice. (f, g, h, and i) Additionally, the numbers of fibroblasts and myofibroblasts in *Dpp4* KO mouse lungs after BLM treatment were all lower than those in WT mice. (j and k) Meanwhile, the number of partial EndMT cells in lungs after BLM challenge did not differ between in *Dpp4* KO mice and in WT mice. (F, H, and J) Representative FCM panels are shown. These cell numbers are not normalized by lung size or body weight. * $p < 0.05$, ** $p < 0.01$, *** $p < 0.001$. Values represent the mean \pm SD of three independent experiments. WT, wild-type mice; NS, not significant.

those after PBS treatment. Therefore, we next determined CD26/DPP4 levels in lung constituent cells using FCM analysis. The results demonstrated that lung expression levels of CD26/DPP4 after BLM-challenge were lower in epithelial and endothelial cells (Figure 4b,c), while they were higher in hematopoietic and mesenchymal cells, including fibroblasts and myofibroblasts (Figure 4a,d,e,f), compared with those after PBS treatment. These results suggest that the decreased expression levels of CD26/DPP4 in WT mouse lungs after BLM treatment may be due to effects in epithelial and endothelial cells. Additionally, CD26/DPP4 levels in the lung constituent cells were all

confirmed to be substantially low or nearly zero in *Dpp4* KO mice regardless of BLM treatment (Figure 4a-f).

3.5 | Expression levels of *Tgfb* in *Dpp4*-deficient mouse lungs were lower than those in WT mice after BLM treatment

We next assessed the mRNA expression levels of the central pro-fibrotic genes, *Tgfb1* and *Tgfb2*, in the lungs. The levels of both *Tgfb1* and *Tgfb2* were upregulated in WT mouse lungs after BLM treatment, while those in

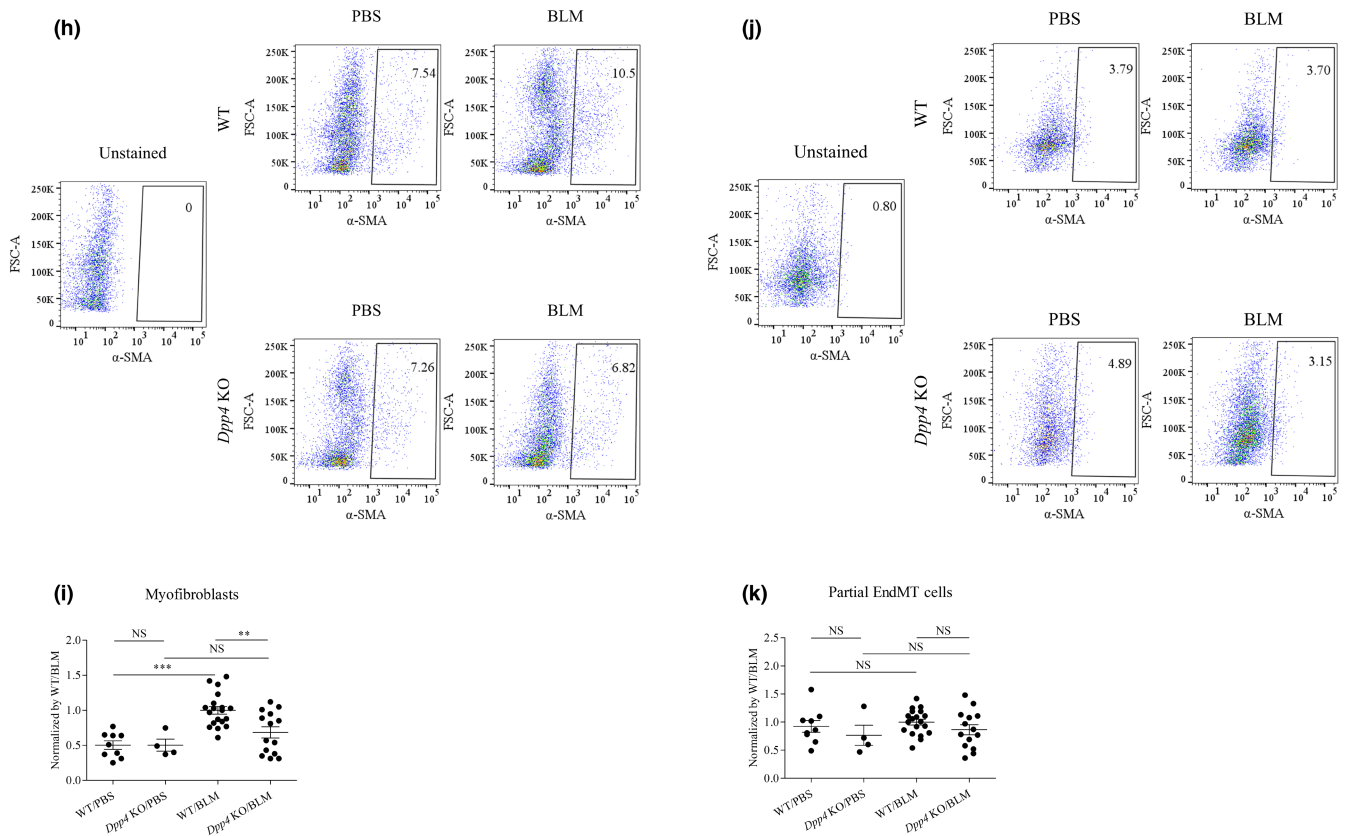


FIGURE 3 (Continued)

Dpp4-deficient mice were significantly lower than those in WT mice (Figure 5). These results suggest that up-regulation of the central fibrotic genes, *Tgfb1* and *Tgfb2*, was suppressed by *Dpp4* deficiency in BLM-induced lung fibrosis.

3.6 | Cell proliferation capacity and collagen-related gene expression of HLFs were suppressed by *DPP4* siRNA knockdown

Lung fibroblast activation is considered to be a major mechanism of pulmonary fibrosis (Suzuki et al., 2020; Wynn & Ramalingam, 2012), and data in this current study indicated that the number of lung fibroblasts was lower in *Dpp4* deficient mice with BLM-induced pulmonary fibrosis than that in WT mice (Figure 3g). Therefore, we next assessed the functional role of CD26/*DPP4* in lung fibroblasts using cultured HLFs. After 72 h of siRNA treatment, CD26/*DPP4* expression in cultured HLFs was suppressed at the protein (Figure 6a,b) and mRNA levels (Figure 6c) compared with those in HLFs treated with non-specific siRNA. The effects of *DPP4* suppression in HLFs by siRNA were evaluated in terms of the proliferative capacity of HLFs using the WST-8 assay. The results

revealed that the knockdown of *DPP4* inhibited the proliferation of HLFs (Figure 6d). We next examined whether expression levels of genes known as fibroblast activation markers, *TGFB1*, *TGFB2*, and *COL1A1*, were transcriptionally inhibited by *DPP4* siRNA treatment in HLFs in vitro. As a result, the mRNA levels of *COL1A1*, a collagen deposition-related gene, were significantly downregulated in transfected HLFs transfected with either *DPP4*-siRNA1 or siRNA2, whereas *TGFB1* and *TGFB2* were not downregulated (Figure 6e). The expression levels of α -SMA, an activation marker of fibroblasts, were not significantly suppressed in HLFs transfected with either *DPP4*-siRNA1 or siRNA2 (Figure 6f). These results suggested that inhibition of proliferation capacity and the downregulation of a collagen deposition-related gene in HLFs by suppressing CD26/*DPP4* expression could be associated with the attenuation of pulmonary fibrosis in vivo.

4 | DISCUSSION

In this study, we demonstrated that in *Dpp4* KO mice BLM-induced pulmonary fibrosis was significantly attenuated and the numbers of fibroblasts and myofibroblasts in the lungs were lower compared to those in WT mice. Additionally, expression levels of *Tgfb1* and *Tgfb2*

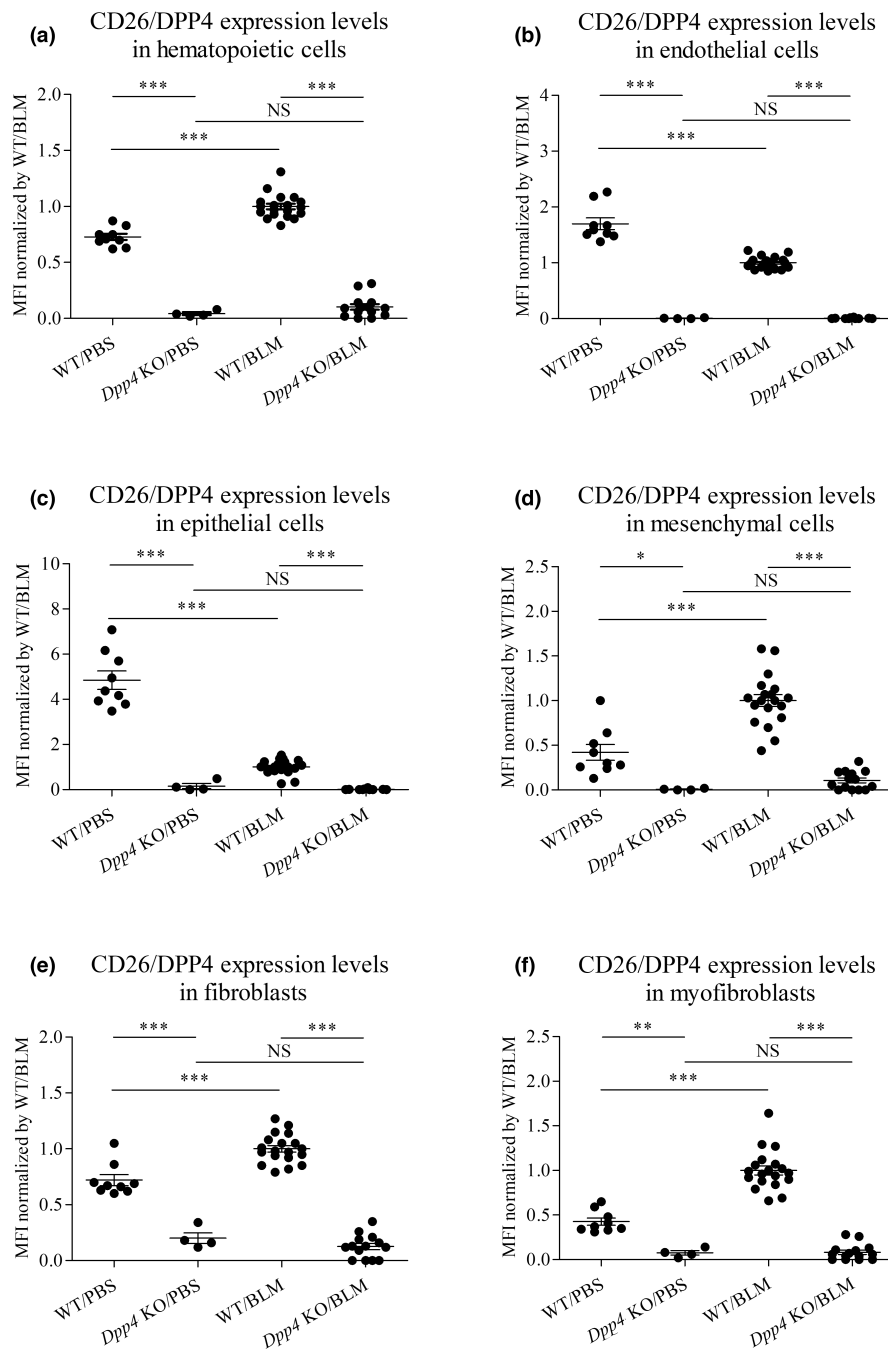


FIGURE 4 CD26/DPP4 expression levels in lung constituent cells from *Dpp4*-deficient and WT mice in BLM-induced lung fibrosis. CD26/DPP4 expression levels in lung constituent cells of bleomycin (BLM)- or PBS-treated *Dpp4* KO and WT mice were measured by mean fluorescence intensity (MFI) using flow cytometry analysis: (a) CD31⁻/CD45⁺ hematopoietic cells, (b) CD31⁺/CD45⁻ endothelial cells, (c) CD31⁻/CD45⁻/CD326⁺ epithelial cells, (d) CD31⁻/CD45⁻/CD326⁻ mesenchymal cells, (e) vimentin-positive CD31⁻/CD45⁻/CD326⁻ fibroblasts, and (f) α -SMA-positive CD31⁻/CD45⁻/CD326⁻ myofibroblasts. CD26/DPP4 expression levels were substantially lower or nearly zero in *Dpp4* KO mice compared with those in WT mice regardless of BLM treatment ($n = 4-19$). * $p < 0.05$, ** $p < 0.01$, *** $p < 0.001$. Values represent the mean \pm SD of three independent experiments. WT, wild-type mice; NS, not significant.

in the lungs were lower in *Dpp4*-deficient mice than those in WT mice, and suppression of CD26/DPP4 expression by siRNA treatment had inhibitory effects on lung fibroblast activation in vitro. Meanwhile, *Dpp4* deficiency was unlikely to be related to EndMT regulation in mouse BLM-induced pulmonary fibrosis. Our current study not only confirmed that BLM-induced pulmonary fibrosis is attenuated in *Dpp4* KO mice (Soare et al., 2020), but it expands upon prior work by suggesting that the mechanisms responsible for these effects in vivo involve a decrease in fibroblasts and myofibroblasts, *Tgfb* downregulation in the lungs, and inhibitory effects on lung fibroblast activation.

Fibroblasts in pulmonary fibrosis acquire an active myofibroblast phenotype, which is thought to be a major mechanism underlying the development of pulmonary fibrosis (Suzuki et al., 2020; Wynn & Ramalingam, 2012). Although the molecular mechanisms underlying the persistent activation of fibroblasts remain incompletely understood, TGF- β signaling has emerged as a core pathway for fibroblast activation in pulmonary fibrosis. In our study, the downregulation of the expression levels of *Tgfb1* and *Tgfb2* in the lungs was demonstrated, suggesting a central mechanism to ameliorate BLM-induced pulmonary fibrosis. Previous studies reported that under proinflammatory conditions, TGF- β is produced by immune cells,

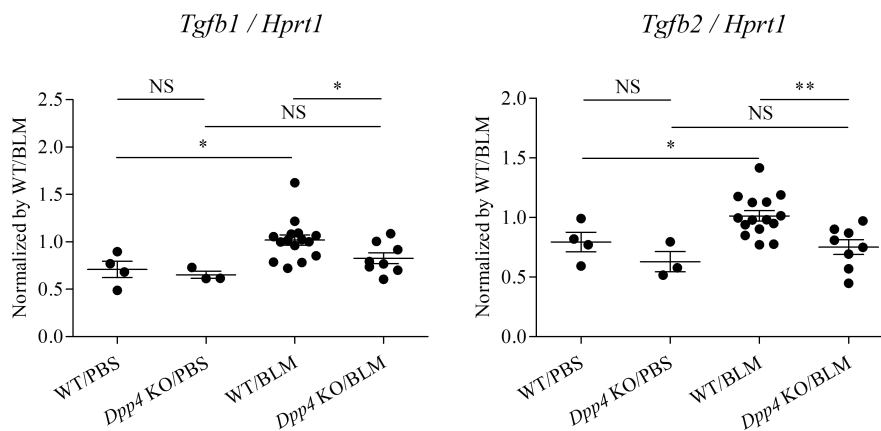


FIGURE 5 *Tgfb* expression levels in *Dpp4*-deficient and WT mice in BLM-induced lung fibrosis. *Tgfb1* and *Tgfb2* mRNA expression levels in lung cells were compared between WT and *Dpp4* KO mice relative to hypoxanthine phosphoribosyltransferase (*Hprt*) as reference values for internal standardization of real-time PCR data. The mRNA levels of *Tgfb1* and *Tgfb2* were higher in the WT lungs after bleomycin (BLM) treatment, respectively. Both were lower in the lungs of *Dpp4* KO mice after BLM exposure ($n = 3-15$). * $p < 0.05$, ** $p < 0.01$. Values represent the mean \pm SD of three independent experiments. WT, wild-type mice; NS, not significant.

epithelial cells (Juban et al., 2018), or platelets (Meyer et al., 2012) in a latent form. Therefore, *DPP4* deficiency in those cell types might relate to the low expression levels of *Tgfb1* and *Tgfb2* in the lungs with BLM-induced pulmonary fibrosis. The substrates of CD26/DPP4 include a broad range of mediators, and CD26/DPP4 modulates intracellular signaling through direct interactions with regulatory molecules. Further, CD26/DPP4 is expressed in tissue-resident cells such as fibroblasts (but not in *Dpp4* KO mice) and may regulate fibroblast activation and collagen release in a TGF- β -dependent manner. Of note, our study demonstrated that CD26/DPP4 expression levels in lung mesenchymal cells, including fibroblasts and myofibroblasts, were increased in BLM-induced fibrosis (Figure 4d-f). One study demonstrated that TGF- β drives the expansion of CD26/DPP4-positive fibroblasts and the upregulation of CD26/DPP4 promotes the activation of TGF- β pathways in fibroblasts (Soare et al., 2020). CD26/DPP4 inhibition reduces the TGF- β -induced activation of extracellular signal-regulated kinase (ERK) signaling in cultured human fibroblasts, and ERK inhibition ameliorates experimental fibrosis. However, other intracellular cascades than ERK are also regulated by TGF- β signaling, and some of these are not affected by CD26/DPP4 inhibition (Soare et al., 2020). One review paper mentions that the inhibition of CD26/DPP4 may regulate TGF- β production in a disease-specific manner mainly depending on the cell type that are involved. CD26/DPP4 inhibition has no major effects on systemic TGF- β levels; however, it generally results in a local reduction of TGF- β expression in fibrotic disease (Ohm et al., 2022). Taken together with the results in the current study, these studies suggest a close link among CD26/DPP4, regulation of TGF- β expression, and lung fibroblast activation.

The present study also demonstrated that both proliferative capacity and a collagen-related gene expression were suppressed in HLFs with its CD26/DPP4 expression reduced by *DPP4*-siRNA treatment in vitro (Figure 6d,f). These results suggest that the reduction in CD26/DPP4 expression inhibits fibroblast activation. Previous studies reported that CD26/DPP4 expression is locally regulated in fibrotic tissues and CD26/DPP4 is a marker of activated skin fibroblasts (Soare et al., 2020), while its expression may not be associated with an activated fibroblast phenotype in human lung fibroblasts from IPF patients (Kadefors et al., 2022). Together, fibroblasts can be a heterogeneous population, even in the same lung tissue, and CD26/DPP4 expression is a marker of activation in some fibroblasts. The possible mechanisms how CD26/DPP4 expression and proliferative capacity and a collagen-related gene expression are related remains unclarified; therefore, further research is warranted.

Although the exact etiology of pulmonary fibrosis is unknown and likely diverse, all stages of fibrosis are accompanied by innate and adaptive immune responses. The role of inflammation as an important component in the etiology of pulmonary fibrosis has been controversial. BLM administration develops lung inflammation in the early stage of the BLM-induced mouse model. In this process, the expression of *Tgfb1* and *Smad3* increased, followed by the activation of JAK-STAT pathways, while the knockdown of IL-31 decreased STAT1 expression (Shi et al., 2014). In the present study, lung injury parameters of protein concentrations and the number of neutrophils in BALF 21 days after BLM treatment demonstrated no significant differences between *Dpp4* KO and WT mice (Figure 2), suggesting that neutrophilic inflammation is not associated with the amelioration of fibrosis in *Dpp4*

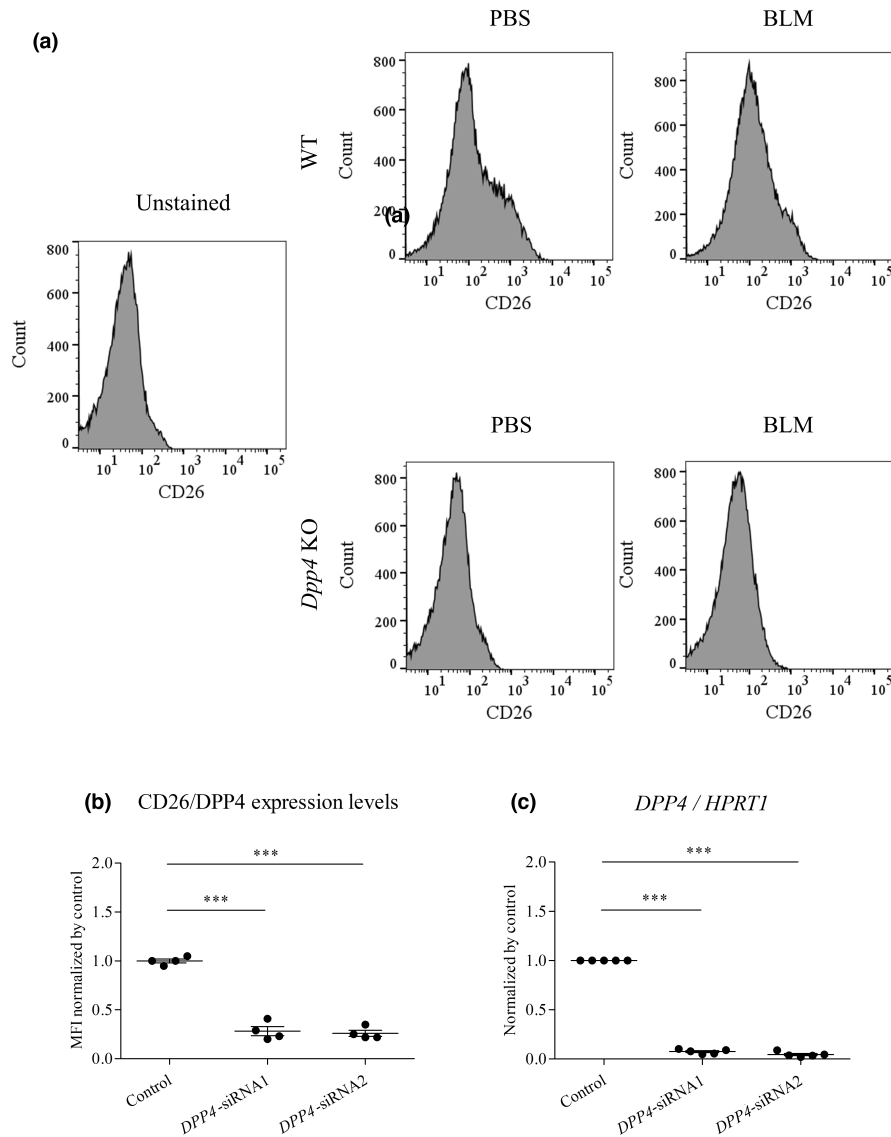


FIGURE 6 Cell proliferation capacity and pro-fibrotic gene expression of HLFs after siRNA-mediated *DPP4* knockdown. (a and b) Protein levels of CD26/DPP4 expression in cultured human lung fibroblasts (HLFs) were lower in siRNA1 and siRNA2 treatment compared with the treatment by non-specific control RNA measured by mean fluorescence intensity (MFI) using flow cytometry analysis ($n = 4$). (c) *DPP4* mRNA expression levels in cultured HLFs were measured using quantitative PCR relative to hypoxanthine phosphoribosyltransferase (*HPRT*) as a reference value after siRNA1 and siRNA2 treatments. mRNA levels were lower in HLFs treated with *DPP4*-siRNA1 and siRNA2 ($n = 5$). (d) The proliferation of human lung fibroblasts (HLFs) was determined in the WST-8 assay. The WST-8 assay results suggested that knockdown of *DPP4* decreased the viability of HLFs ($n = 5$). (e) mRNA expression levels of *TGFBI*, *TGFB2*, and *COL1A1*, relative to those of the internal control *HPRT*, in human lung fibroblasts (HLFs) after *DPP4*-siRNA treatment were measured using real-time quantitative PCR. mRNA levels of *COL1A1* were downregulated in HLFs by siRNA treatment. mRNA levels of *TGFBI* and *TGFB2* were not downregulated in HLFs by siRNA treatment ($n = 5$). (f) Protein levels of α -SMA were not significantly suppressed in HLFs after siRNA treatment ($n = 3$). * $p < 0.05$, ** $p < 0.01$, *** $p < 0.001$. Values represent the mean \pm SD of three independent experiments. NS, not significant; Control, non-specific control siRNA.

deficiency in the fibrotic stage of BLM-induced lung fibrosis. However, previous studies demonstrated some immunomodulatory effects of CD26/DPP4 as follows. CD26/DPP4 possesses non-enzymatic functions, acting as a T-cell costimulatory protein and interacting with ECM proteins such as collagen and fibronectin (Itou et al., 2013; Ohnuma et al., 2008). The T-cell costimulatory

activity of CD26/DPP4 affects the inflammatory process in pulmonary fibrosis, although its target immune cells or pulmonary constitutive cells have not been elucidated (Hatano et al., 2015). Additionally, the beneficial effects of pharmacological CD26/DPP4 inhibition on ischemia-reperfusion and LPS-induced lung injuries through its anti-inflammatory effects on pulmonary endothelial

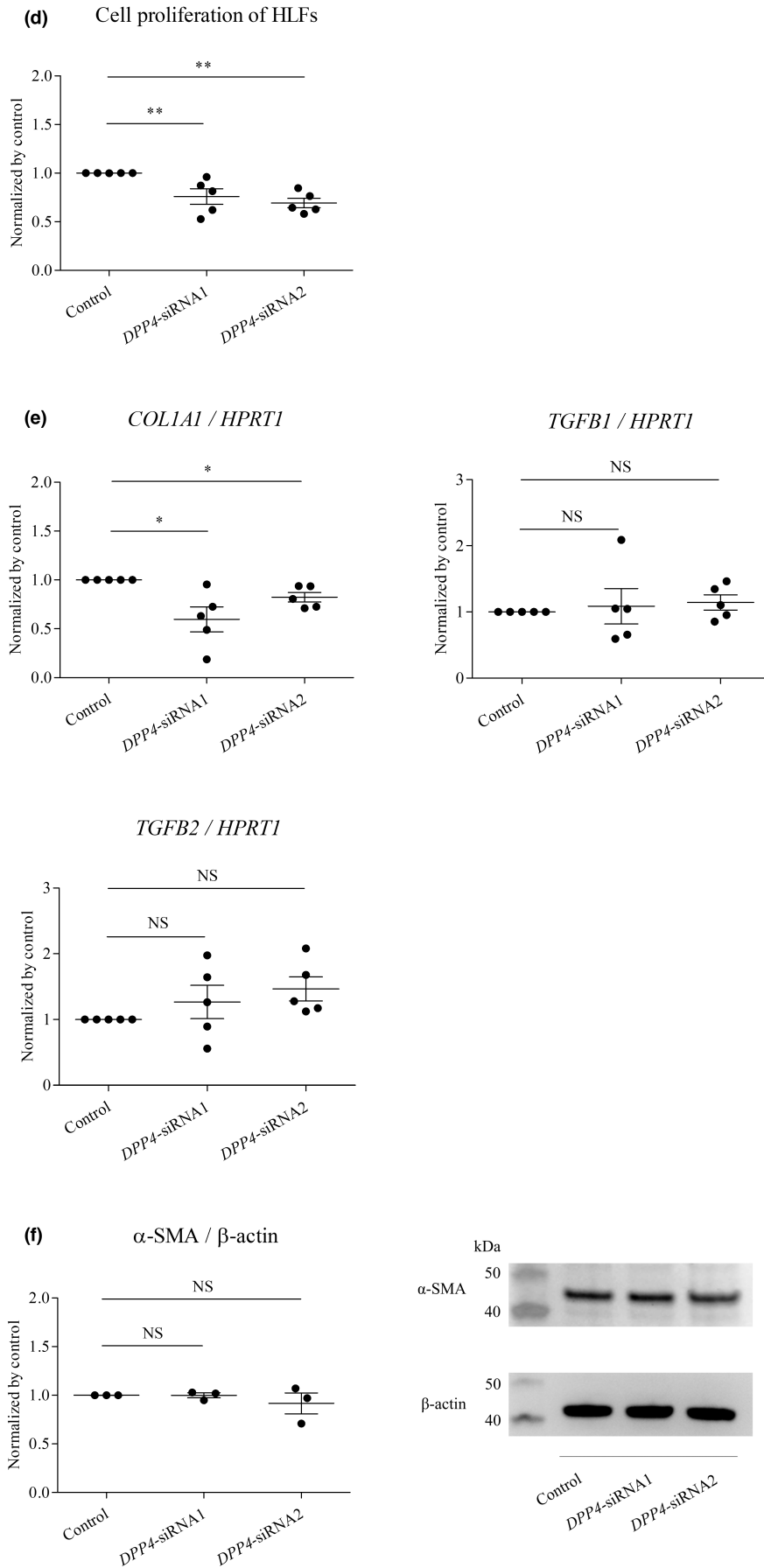


FIGURE 6 (Continued)

cells have been previously reported (Jungrathmayr et al., 2012). Taken together, it might be possible in our current study that anti-inflammatory effects of *Dpp4* deficiency on BLM-induced lung inflammation at the early stage could lead to the amelioration of pulmonary fibrosis at the later stage.

Our current observations are limited in several aspects. First, the source of the downregulation of the central fibrotic expression of *Tgfb1* and *Tgfb2* in mouse BLM-induced fibrosing lungs has not been identified. The global *Dpp4* KO mice used in this study do not allow for cell-specific determination of genetic deficiency. Our in vitro study (Figure 6e) indicates that other cell types than fibroblasts could be candidate cell types and should be examined. Second, our study demonstrated that the effects of BLM on CD26/DPP4 expression levels were different among various cell types in mouse lung during BLM-induced fibrosis (Figures 4a–f). However, the key mechanisms associated with CD26/DPP4 signaling that are involved in the pathophysiology of pulmonary fibrosis are still unclear. Although downregulation of *Tgfb* in lungs of BLM-induced pulmonary fibrosis is considered to be an important mechanism (Figure 5), TGF- β 1/Smad signaling pathway includes both positive and negative regulatory ones in each constituent cell such as fibroblasts, endothelial cells, and EndMT cells. TGF- β 1 activates the PKB, JNK, and AKT signaling pathways through the PI3K (Wang et al., 2022). Other signaling pathways including Wnt/ β signaling pathway through miR-133 could be involved in the pathogenesis of pulmonary fibrosis (Wei et al., 2019). Third, it remains unknown whether decreased expression of TGF- β 1 and TGF- β 2 is a correlative or causative finding. Experiments with overexpression or gain of TGF- β function would be a helpful future direction to determine whether TGF- β expression level is a causative mechanism. Fourth, investigation using human lung specimens or data mining from published databases would be helpful to characterize the potential importance of CD26/DPP4 in fibrosis during human disease. Lastly, it would be helpful to clarify what substrates of CD26/DPP4 are involved in these effects, and to examine the effects of CD26/DPP4 activation on fibroblasts or other cell types. Further studies are warranted to better understand the functional role of CD26/DPP4 in pulmonary fibrosis, since multiple important questions that need to be addressed remain unanswered.

In conclusion, our study demonstrated that genetic deficiency of *Dpp4* has protective effects on BLM-induced pulmonary fibrosis in mice through a reduction in *Tgfb* expression levels in the lungs and direct inhibitory effects on lung fibroblast activation. These results suggest that CD26/DPP4 inhibition is a potential therapeutic strategy for pulmonary fibrosis.

AUTHOR CONTRIBUTIONS

T.K. and Y.K.—Conceptualization; Y.K. and T.K.—Investigation; T.K., K.T., and T.S.—Funding acquisition; T.K., R.H., Y.T., S.S., and K.O.—Methodology; T.K.—Project administration; Y.K., C.M., K.T., and T.S.—Supervision; Y.T. and T.K.—Writing-original draft; Y.K., R.H., Y.T., S.S., K.O., C.M., S.M.D., K.T., and T.S.—Writing-review and editing.

ACKNOWLEDGMENTS

We are grateful to Ikuko Sakamoto, Tomoko Misawa, Akiko Moriya, and Sumina Atarashi for technical advice and assistance and to Chieko Handa and Tamie Hirano for administrative support. We would like to thank Editage (www.editage.com) for English language editing.

FUNDING INFORMATION

This research was funded by JSPS KAKENHI (grant numbers 19K17663, 22K16163, and 22H03076), AMED-CREST (JP21gm1210003), AMED (223fa627003h0001), and a research grant from the Intractable Respiratory Diseases and Pulmonary Hypertension Research Group, Ministry of Health, Labor and Welfare, Japan (grant numbers 20FC1027 and 21FC1027).

CONFLICT OF INTEREST STATEMENT

The authors declare no conflict of interest.

ETHICS STATEMENT

All animal experiments were conducted according to protocols approved by the Review Board for animal experiments of Chiba University, Japan.

ORCID

Takeshi Kawasaki  <https://orcid.org/0000-0002-1468-172X>

REFERENCES

- Akamatsu, T., Arai, Y., Kosugi, I., Kawasaki, H., Meguro, S., Sakao, M., Shibata, K., Suda, T., Chida, K., & Iwashita, T. (2013). Direct isolation of myofibroblasts and fibroblasts from bleomycin-injured lungs reveals their functional similarities and differences. *Fibrogenesis & Tissue Repair*, 6, 15.
- Ashcroft, T., Simpson, J. M., & Timbrell, V. (1988). Simple method of estimating severity of pulmonary fibrosis on a numerical scale. *Journal of Clinical Pathology*, 41, 467–470.
- Della Latta, V., Cecchetti, A., Del Ry, S., & Morales, M. A. (2015). Bleomycin in the setting of lung fibrosis induction: From biological mechanisms to counteractions. *Pharmacological Research*, 97, 122–130.
- Distler, O., Highland, K. B., Gahlemann, M., Azuma, A., Fischer, A., Mayes, M. D., Raghu, G., Sauter, W., Girard, M., Alves, M., Clerisme-Beaty, E., Stowasser, S., Tetzlaff, K., Kuwana, M., Maher, T. M., & Investigators ST. (2019). Nintedanib for

- systemic sclerosis-associated interstitial lung disease. *The New England Journal of Medicine*, 380, 2518–2528.
- Flaherty, K. R., Wells, A. U., Cottin, V., Devaraj, A., Walsh, S. L. F., Inoue, Y., Richeldi, L., Kolb, M., Tetzlaff, K., Stowasser, S., Coeck, C., Clerisme-Beaty, E., Rosenstock, B., Quaresma, M., Haeufel, T., Goeldner, R. G., Schlenker-Herceg, R., Brown, K. K., & Investigators IT. (2019). Nintedanib in progressive fibrosing interstitial lung diseases. *The New England Journal of Medicine*, 381, 1718–1727.
- Garrison, G., Huang, S. K., Okunishi, K., Scott, J. P., Kumar Penke, L. R., Scruggs, A. M., & Peters-Golden, M. (2013). Reversal of myofibroblast differentiation by prostaglandin E(2). *American Journal of Respiratory Cell and Molecular Biology*, 48, 550–558.
- Hashimoto, N., Phan, S. H., Imaizumi, K., Matsuo, M., Nakashima, H., Kawabe, T., Shimokata, K., & Hasegawa, Y. (2010). Endothelial-mesenchymal transition in bleomycin-induced pulmonary fibrosis. *American Journal of Respiratory Cell and Molecular Biology*, 43, 161–172.
- Hatano, R., Ohnuma, K., Otsuka, H., Komiya, E., Taki, I., Iwata, S., Dang, N. H., Okumura, K., & Morimoto, C. (2015). CD26-mediated induction of EGR2 and IL-10 as potential regulatory mechanism for CD26 costimulatory pathway. *Journal of Immunology*, 194, 960–972.
- Heukels, P., Moor, C. C., von der Thusen, J. H., Wijsenbeek, M. S., & Kool, M. (2019). Inflammation and immunity in IPF pathogenesis and treatment. *Respiratory Medicine*, 147, 79–91.
- Hinz, B., Phan, S. H., Thannickal, V. J., Galli, A., Bochaton-Piallat, M. L., & Gabbiani, G. (2007). The myofibroblast: One function, multiple origins. *The American Journal of Pathology*, 170, 1807–1816.
- Hubner, R. H., Gitter, W., El Mokhtari, N. E., Mathiak, M., Both, M., Bolte, H., Freitag-Wolf, S., & Bewig, B. (2008). Standardized quantification of pulmonary fibrosis in histological samples. *BioTechniques*, 44(507–511), 514–507.
- Itou, M., Kawaguchi, T., Taniguchi, E., & Sata, M. (2013). Dipeptidyl peptidase-4: A key player in chronic liver disease. *World Journal of Gastroenterology*, 19, 2298–2306.
- Jia, W., Wang, Z., Gao, C., Wu, J., & Wu, Q. (2021). Trajectory modeling of endothelial-to-mesenchymal transition reveals galectin-3 as a mediator in pulmonary fibrosis. *Cell Death & Disease*, 12, 327.
- Juban, G., Saclier, M., Yacoub-Youssef, H., Kernou, A., Arnold, L., Boisson, C., Ben Larbi, S., Magnan, M., Cuvellier, S., Theret, M., Petrof, B. J., Desguerre, I., Gondin, J., Mounier, R., & Chazaud, B. (2018). Ampk activation regulates LTBP4-dependent TGF-beta1 secretion by pro-inflammatory macrophages and controls fibrosis in duchenne muscular dystrophy. *Cell Reports*, 25, 2163–2176 e2166.
- Jungraithmayr, W., De Meester, I., Matheussen, V., Baerts, L., Arni, S., & Weder, W. (2012). CD26/DPP-4 inhibition recruits regenerative stem cells via stromal cell-derived factor-1 and beneficially influences ischaemia-reperfusion injury in mouse lung transplantation. *European Journal of Cardio-Thoracic Surgery*, 41, 1166–1173.
- Kadefors, M., Berlin, F., Wildt, M., Dellgren, G., Rolandsson Enes, S., Aspberg, A., & Westergren-Thorsson, G. (2022). Dipeptidyl peptidase 4 expression is not associated with an activated fibroblast phenotype in idiopathic pulmonary fibrosis. *Frontiers in Pharmacology*, 13, 953771.
- Kawasaki, T., Chen, W., Htwe, Y. M., Tatsumi, K., & Dudek, S. M. (2018). DPP4 inhibition by sitagliptin attenuates Ipsi-induced lung injury in mice. *American Journal of Physiology. Lung Cellular and Molecular Physiology*, 315, L834–L845.
- Kawasaki, T., Nishiwaki, T., Sekine, A., Nishimura, R., Suda, R., Urushibara, T., Suzuki, T., Takayanagi, S., Terada, J., Sakao, S., & Tatsumi, K. (2015). Vascular repair by tissue-resident endothelial progenitor cells in endotoxin-induced lung injury. *American Journal of Respiratory Cell and Molecular Biology*, 53, 500–512.
- Lazarides, E. (1980). Intermediate filaments as mechanical integrators of cellular space. *Nature*, 283, 249–256.
- Liu, T., De Los Santos, F. G., & Phan, S. H. (2017). The bleomycin model of pulmonary fibrosis. *Methods in Molecular Biology*, 1627, 27–42.
- Liu, Y., & Qi, Y. (2020). Vildagliptin, a CD26/DPP4 inhibitor, ameliorates bleomycin-induced pulmonary fibrosis via regulating the extracellular matrix. *International Immunopharmacology*, 87, 106774.
- Mackinnon, A. C., Gibbons, M. A., Farnworth, S. L., Leffler, H., Nilsson, U. J., Delaine, T., Simpson, A. J., Forbes, S. J., Hirani, N., Gauldie, J., & Sethi, T. (2012). Regulation of transforming growth factor-beta1-driven lung fibrosis by galectin-3. *American Journal of Respiratory and Critical Care Medicine*, 185, 537–546.
- Matute-Bello, G., Downey, G., Moore, B. B., Groshong, S. D., Matthay, M. A., Slutsky, A. S., Kuebler, W. M., & Acute Lung Injury in Animals Study G. (2011). An official American Thoracic Society workshop report: Features and measurements of experimental acute lung injury in animals. *American Journal of Respiratory Cell and Molecular Biology*, 44, 725–738.
- Meyer, A., Wang, W., Qu, J., Croft, L., Degen, J. L., Coller, B. S., & Ahamed, J. (2012). Platelet TGF-beta1 contributions to plasma TGF-beta1, cardiac fibrosis, and systolic dysfunction in a mouse model of pressure overload. *Blood*, 119, 1064–1074.
- Meyerholz, D. K., Lambert, A. M., & McCray, P. B., Jr. (2016). Dipeptidyl peptidase 4 distribution in the human respiratory tract: Implications for the middle east respiratory syndrome. *The American Journal of Pathology*, 186, 78–86.
- Morbini, P., Inghilleri, S., Campo, I., Oggionni, T., Zorzetto, M., & Luisetti, M. (2011). Incomplete expression of epithelial-mesenchymal transition markers in idiopathic pulmonary fibrosis. *Pathology, Research and Practice*, 207, 559–567.
- Morimoto, C., & Schlossman, S. F. (1998). The structure and function of CD26 in the T-cell immune response. *Immunological Reviews*, 161, 55–70.
- Nataraj, D., Ernst, A., & Kalluri, R. (2010). Idiopathic pulmonary fibrosis is associated with endothelial to mesenchymal transition. *American Journal of Respiratory Cell and Molecular Biology*, 43, 129–130.
- Ohm, B., Moneke, I., & Jungraithmayr, W. (2022). Targeting cluster of differentiation 26 / dipeptidyl peptidase 4 (CD26/DPP4) in organ fibrosis. *British Journal of Pharmacology*. Online ahead of print. <https://doi.org/10.1111/bph.15967>
- Ohnuma, K., Dang, N. H., & Morimoto, C. (2008). Revisiting an old acquaintance: CD26 and its molecular mechanisms in T cell function. *Trends in Immunology*, 29, 295–301.
- Pardali, E., Sanchez-Duffhues, G., Gomez-Puerto, M. C., & Ten Dijke, P. (2017). TGF-beta-induced endothelial-mesenchymal

- transition in fibrotic diseases. *International Journal of Molecular Sciences*, 18(10), 2157. <https://doi.org/10.3390/ijms18102157>
- Podolanczuk, A. J., Wong, A. W., Saito, S., Lasky, J. A., Ryerson, C. J., & Eickelberg, O. (2021). Update in interstitial lung disease 2020. *American Journal of Respiratory and Critical Care Medicine*, 203, 1343–1352.
- Qian, W., Cai, X., Qian, Q., Zhang, W., & Wang, D. (2018). Astragaloside iv modulates TGF-beta1-dependent epithelial-mesenchymal transition in bleomycin-induced pulmonary fibrosis. *Journal of Cellular and Molecular Medicine*, 22, 4354–4365.
- Raghu, G., Collard, H. R., Egan, J. J., Martinez, F. J., Behr, J., Brown, K. K., Colby, T. V., Cordier, J. F., Flaherty, K. R., Lasky, J. A., Lynch, D. A., Ryu, J. H., Swigris, J. J., Wells, A. U., Ancochea, J., Bours, D., Carvalho, C., Costabel, U., Ebina, M., ... Fibrosis AEJACoIP. (2011). An official ats/ers/jrs/alat statement: Idiopathic pulmonary fibrosis: Evidence-based guidelines for diagnosis and management. *American Journal of Respiratory and Critical Care Medicine*, 183, 788–824.
- Raghu, G., Freudenberger, T. D., Yang, S., Curtis, J. R., Spada, C., Hayes, J., Sillery, J. K., Pope, C. E., 2nd, & Pellegrini, C. A. (2006). High prevalence of abnormal acid gastro-oesophageal reflux in idiopathic pulmonary fibrosis. *The European Respiratory Journal*, 27, 136–142.
- Salton, F., Volpe, M. C., & Confalonieri, M. (2019). Epithelial(–) mesenchymal transition in the pathogenesis of idiopathic pulmonary fibrosis. *Medicina (Kaunas)*, 55(4), 83. <https://doi.org/10.3390/medicina55040083>
- Sanchez-Duffhues, G., Garcia de Vinuesa, A., & Ten Dijke, P. (2018). Endothelial-to-mesenchymal transition in cardiovascular diseases: Developmental signaling pathways gone awry. *Developmental Dynamics*, 247, 492–508.
- Shi, K., Jiang, J., Ma, T., Xie, J., Duan, L., Chen, R., Song, P., Yu, Z., Liu, C., Zhu, Q., & Zheng, J. (2014). Pathogenesis pathways of idiopathic pulmonary fibrosis in bleomycin-induced lung injury model in mice. *Respiratory Physiology & Neurobiology*, 190, 113–117.
- Soare, A., Gyorfi, H. A., Matei, A. E., Dees, C., Rauber, S., Wohlfahrt, T., Chen, C. W., Ludolph, I., Horch, R. E., Bauerle, T., von Horsten, S., Mihai, C., Distler, O., Ramming, A., Schett, G., & Distler, J. H. W. (2020). Dipeptidylpeptidase 4 as a marker of activated fibroblasts and a potential target for the treatment of fibrosis in systemic sclerosis. *Arthritis & Rheumatology*, 72, 137–149.
- Suzuki, K., Kim, J. D., Ugai, K., Matsuda, S., Mikami, H., Yoshioka, K., Ikari, J., Hatano, M., Fukamizu, A., Tatsumi, K., & Kasuya, Y. (2020). Transcriptomic changes involved in the dedifferentiation of myofibroblasts derived from the lung of a patient with idiopathic pulmonary fibrosis. *Molecular Medicine Reports*, 22, 1518–1526.
- Suzuki, T., Tada, Y., Gladson, S., Nishimura, R., Shimomura, I., Karasawa, S., Tatsumi, K., & West, J. (2017). Vildagliptin ameliorates pulmonary fibrosis in lipopolysaccharide-induced lung injury by inhibiting endothelial-to-mesenchymal transition. *Respiratory Research*, 18, 177.
- Suzuki, T., Tada, Y., Nishimura, R., Kawasaki, T., Sekine, A., Urushibara, T., Kato, F., Kinoshita, T., Ikari, J., West, J., & Tatsumi, K. (2016). Endothelial-to-mesenchymal transition in lipopolysaccharide-induced acute lung injury drives a progenitor cell-like phenotype. *American Journal of Physiology. Lung Cellular and Molecular Physiology*, 310, L1185–L1198.
- Takahashi, Y., Kawasaki, T., Sato, H., Hasegawa, Y., Dudek, S. M., Ohara, O., Tatsumi, K., & Suzuki, T. (2021). Functional roles for CD26/DPP4 in mediating inflammatory responses of pulmonary vascular endothelial cells. *Cells*, 10(12), 3508. <https://doi.org/10.3390/cells10123508>
- Wang, J., Hu, K., Cai, X., Yang, B., He, Q., Wang, J., & Weng, Q. (2022). Targeting PI3K/AKT signaling for treatment of idiopathic pulmonary fibrosis. *Acta Pharmaceutica Sinica B*, 12, 18–32.
- Wollin, L., Distler, J. H. W., Redente, E. F., Riches, D. W. H., Stowasser, S., Schlenker-Herceg, R., Maher, T. M., & Kolb, M. (2019). Potential of nintedanib in treatment of progressive fibrosing interstitial lung diseases. *The European Respiratory Journal*, 54, 1900161.
- Zhang, L., Chi, X., Luo, W., Yu, S., Zhang, J., Guo, Y., Ren, Q., & Zhang, W. (2020). Lung myofibroblast transition and fibrosis is regulated by circ0044226. *The International Journal of Biochemistry & Cell Biology*, 118, 105660.
- Wynn, T. A., & Ramalingam, T. R. (2012). Mechanisms of fibrosis: Therapeutic translation for fibrotic disease. *Nature Medicine*, 18, 1028–1040.
- Wei, P., Xie, Y., Abel, P. W., Huang, Y., Ma, Q., Li, L., Hao, J., Wolff, D. W., Wei, T., & Tu, Y. (2019). Transforming growth factor (TGF)-beta1-induced miR-133a inhibits myofibroblast differentiation and pulmonary fibrosis. *Cell Death & Disease*, 10, 670.

How to cite this article: Koyanagi, Y., Kawasaki, T., Kasuya, Y., Hatano, R., Sato, S., Takahashi, Y., Ohnuma, K., Morimoto, C., Dudek, S. M., Tatsumi, K., & Suzuki, T. (2023). Functional roles of CD26/DPP4 in bleomycin-induced pulmonary fibrosis. *Physiological Reports*, 11, e15645. <https://doi.org/10.14814/phy2.15645>

[CASE REPORT]

Anti-glomerular Basement Membrane Disease Concomitant with MPO-ANCA Positivity Concurrent with High Serum Levels of Interleukin-26 Following Coronavirus Disease 2019 Vaccination

Seiji Kobayashi¹, Kazunori Fugo², Ryo Hatano³, Kazuto Yamazaki², Chikao Morimoto³ and Hiroyuki Terawaki¹

Abstract:

As coronavirus disease 2019 (COVID-19) vaccine booster campaigns progress worldwide, new reports of complications following COVID-19 vaccination have emerged. We herein report a case of new-onset anti-glomerular basement membrane (GBM) disease concomitant with myeloperoxidase-antineutrophil cytoplasmic antibody positivity concurrent with high levels of interleukin (IL)-26 following the second dose of the Pfizer-BioNTech COVID-19 vaccine. The temporal association with vaccination in this case suggests that an enhanced neutrophilic immune response through IL-26 may have triggered necrotizing glomerulonephritis and a T-cell-mediated immune response to GBMs, leading to the development of anti-GBM antibodies, with an enhanced B-cell response after the vaccination triggering anti-GBM IgG and the onset of anti-GBM disease.

Key words: Anti-GBM disease, ANCA-associated glomerulonephritis, IL-26, mRNA-based COVID-19 vaccine, pharmacovigilance

(Intern Med Advance Publication)
(DOI: 10.2169/internalmedicine.1027-22)

Introduction

As coronavirus disease 2019 (COVID-19) vaccine booster campaigns progress worldwide, new reports of adverse events following mRNA-based COVID-19 vaccination have emerged, such as cases of anti-glomerular basement membrane (GBM) disease or anti-neutrophil cytoplasmic antibody (ANCA)-associated vasculitis (AAV) (1, 2). The pathogenesis of anti-GBM disease has been well defined at the molecular level, but the factors that initiate the autoimmune process remain unclear (3).

AAV is a multisystem autoimmune disease, with neutrophil extracellular traps (NETs) involved in its pathogenesis (4). Interleukin (IL)-26 is a member of the IL-10 family of cytokines that participates in inflammatory signaling through directly binding DNA to facilitate cellular transduc-

tion and intracellular inflammation signaling (5). Recently, it has been shown that IL-26 binds to NETs to induce the secretion of inflammatory cytokines (IL-1 β and IL-6) and chemokines (IL-8) by myeloid cells in ANCA-associated glomerulonephritis (6).

We herein report a case of new-onset anti-GBM disease concomitant with myeloperoxidase (MPO)-ANCA positivity with high levels of serum IL-26 following the receipt of the second dose of the Pfizer-BioNTech COVID-19 vaccine.

Case Report

A 67-year-old man with a history of pulmonary tuberculosis at 25 years old was admitted with a fever and anuria 6 weeks after his second vaccination. He had reported protracted systemic reactions with a low-grade fever and gross hematuria two weeks after the first dose. He received a sec-

¹Division of Nephrology, Department of Internal Medicine, Teikyo University Chiba Medical Center, Japan, ²Department of Pathology, Teikyo University Chiba Medical Center, Japan and ³Department of Therapy Development and Innovation for Immune Disorders and Cancers, Graduate School of Medicine, Juntendo University, Japan

Received: September 20, 2022; Accepted: December 12, 2022; Advance Publication by J-STAGE: February 1, 2023

Correspondence to Dr. Seiji Kobayashi, kobayashi.seiji.oh@teikyo-u.ac.jp

ond dose three weeks after the first dose. One month after the second dose, he developed a fever, anasarca, and anuria, which lasted over the next two weeks. He had received 6 months of chemotherapy for the treatment of pulmonary tuberculosis at 25 years old. There was no history of smoking or medication use, including propylthiouracil. Results of annual medical reviews had been normal, with serum creatinine levels of 0.6 mg/dL and normal urinalysis findings.

On admission, his blood pressure was 162/98 mmHg, and a physical examination revealed generalized edema. Laboratory tests revealed a white blood cell (WBC) count of 12,900/mm³, serum creatinine of 14.6 mg/dL, and albumin of 1.6 g/dL. A serologic evaluation revealed a C-reactive protein level of 37.0 mg/dL, positive anti-GBM IgG (>3,500 U/mL, reference range 3.0> U/mL), positive MPO-ANCA IgG (268 U/mL, reference range 3.5> U/mL), and positive IFN- γ release assays for tuberculosis. The levels of complement C3 and C4 were within the reference ranges, and testing for proteinase 3-ANCA, anti-nuclear antibody, hepatitis B virus, hepatitis C virus were negative. Polymerase chain reaction and serology testing for SARS-CoV-2 were also negative. A urinalysis revealed blood (3+) and protein (3+) at 4,377 mg/dL, and urine microscopy showed >100 red blood cells per high-power field (>10% dysmorphic) and 100 WBCs per high-power field with granular casts. Computed tomography of the chest revealed nodules in the apex segment of the right upper lobe and bilateral mild pleural effusion, without pulmonary involvement. Three sputum smear examinations with Ziehl-Neelsen staining for the diagnosis of tuberculosis over a three-day period were negative. In addition, there were no negative culture results for those sputum specimens.

A kidney biopsy was performed 52 days after the second vaccination. Light microscopy of the kidney biopsy specimen showed cellular crescents and fibrinoid necrosis involving 43 of 45 glomeruli, with CD4 T cells and macrophages scattered throughout the glomeruli. Cortical tubules displayed diffuse acute epithelial injury with interstitial inflammation. Interstitial fibrosis and tubular atrophy were moderate. Immunofluorescence showed linear staining of GBMs for IgG1. Electron microscopy revealed disruption of GBMs and diffuse effacement of podocyte foot processes without immune complex-mediated deposits, leading to a diagnosis of anti-GBM glomerulonephritis (Fig. 1). Further investigations revealed a high serum IL-26 level of 517.1 pg/mL on an enzyme-linked immunosorbent assay (reference range: not detectable), IL-1 β of 34.5 pg/mL, IL-6 of 1,577.9 pg/mL, tumor necrosis factor- α (TNF- α) of 300.6 pg/mL, granulocyte colony-stimulating factor (G-CSF) of 126.6 pg/mL, IL-8 of 615.4 pg/mL, and chemokine (C-X-C motif) ligand (CXCL) 1 of 1,480.9 pg/mL using the Bio Plex multi-plex system (Bio-Rad Laboratories, Inc. Hercules, CA, USA). He carried human leukocyte antigen (HLA) DRB1*04:03 and DRB1*14:05 alleles.

Intravenous methylprednisolone 1 g daily for 3 days was initiated the day after the kidney biopsy followed by oral

prednisolone 1 mg/kg daily. Ten days after admission, he was treated with 2 doses of rituximab at 375 mg/m² once a week. Hemodialysis was initiated on day 2 after admission. Prednisolone was tapered by 0.1 mg/kg/day weekly, and the patient was discharged after 50 days in hospital. The patient received 300 mg of isoniazid daily for latent tuberculosis infection over 9 months from the start of treatment for anti-GBM disease. Currently, he continues maintenance hemodialysis while on oral prednisolone at 10 mg/day. Nine months after discharge, neither pulmonary involvement nor relapse occurred, with serum levels of anti-GBM IgG, MPO-ANCA and inflammatory cytokines/chemokines, including IL-26, gradually decreasing or resolving (Fig. 2).

Discussion

Several recent case reports have described the new onset of anti-GBM disease or AAV following COVID-19 vaccination (2, 7, 8). However, the mechanism concerning the contribution of the mRNA-based vaccines to these diseases remains unknown. To our knowledge, this is the first report of anti-GBM disease concomitant with ANCA positivity accompanied by a high serum IL-26 level following the second dose of the Pfizer-BioNTech COVID-19 vaccine. The temporal association with vaccination in this case suggests that an enhanced neutrophilic immune response through IL-26 may have triggered necrotizing glomerulonephritis and a T-cell-mediated immune response to GBMs, leading to the development of anti-GBM antibodies, with an enhanced B-cell response after the vaccination triggering anti-GBM IgG and the onset of anti-GBM disease (Fig. 3).

The possible mechanisms underlying the new-onset adverse effects following mRNA-based COVID-19 vaccination reportedly include molecular mimicry, vaccine adjuvants, and polyclonal activation followed by the production of particular autoantibodies. Recently, Ventura et al. reported that 2 out of 35 patients who developed ANCA after SARS-CoV-2 vaccination developed ANCA and AAV after receiving the first dose of the Pfizer-BioNTech COVID-19 vaccine. One of the two cases developed ANCA six days after the first dose (9). A secondary effect from the polyclonal activation induced by the vaccine may be attributable to the production of ANCA by potential autoreactive clones specific for MPO. AAV has been known to occur under a variety of circumstances, including with infections (4, 10). Certain infectious agents such as *Mycobacterium tuberculosis* may lead to development of ANCA (11, 12). In our case, latent MPO-ANCA, which might have developed following pulmonary tuberculosis, may have been enhanced following receipt of the SARS-CoV-2 mRNA vaccine, potentially triggering ANCA-associated glomerulonephritis. Whether or not our case can be attributed to pulmonary tuberculosis-induced ANCAs is speculative but intriguing and warrants further investigation, given emerging cases of vaccination-induced AAV.

IL-26 directly binds neutrophil-derived extracellular DNA

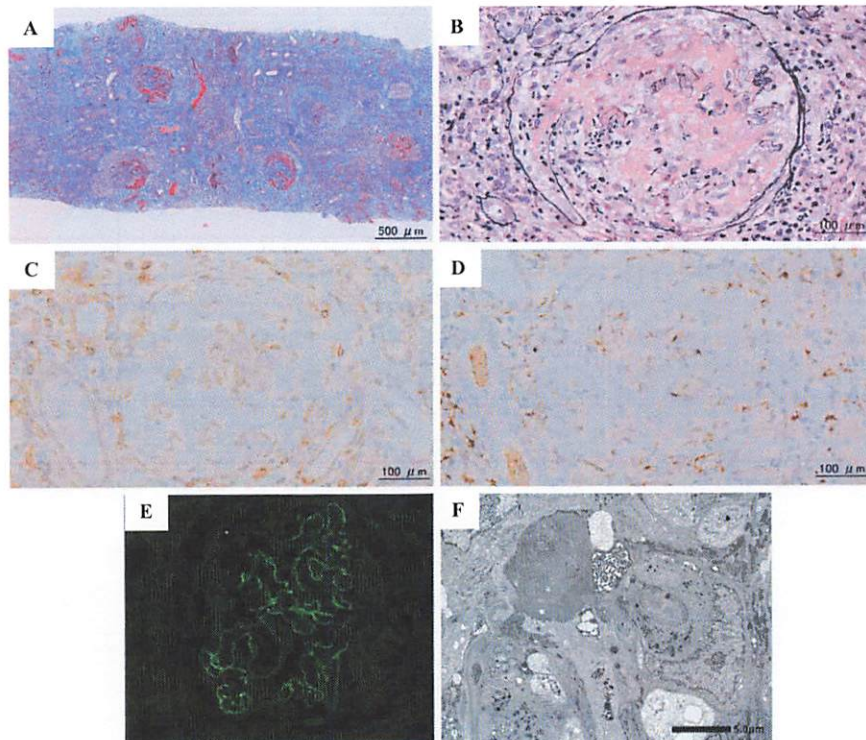


Figure 1. Kidney biopsy findings. Light microscopy of (A) the renal cortex showing multiple glomeruli with fibrinoid necrosis and crescentic formations associated with rupture of Bowman's capsule (Masson trichrome, original magnification $\times 40$) and of (B) a representative glomerulus showing fibrinoid necrosis, a circumferential cellular crescent, and destruction of the glomerular tuft and Bowman's capsule with leukocytes, including neutrophils (Jones methenamine silver, original magnification $\times 200$). Immunohistochemical staining for (C) CD4 and (D) CD68 showing scattered CD4 T cells and macrophages throughout the glomeruli as well as adjacent tubules and interstitium (original magnification $\times 200$, respectively). Immunofluorescence for (E) IgG1 of glomeruli showing global linear staining along glomerular basement membranes (original magnification $\times 200$). (F) Electron microscopy of the glomerulus showing disruption of the glomerular basement membranes, diffuse foot process effacement, and the absence of electron-dense deposits (original magnification, $\times 6,000$).

to facilitate intracellular inflammation signaling in a stimulator of interferon genes (STING)- and inflammasome-dependent manner (5). It is possible that an enhanced neutrophilic immune response through IL-26 after the vaccination may have been responsible for the ANCA-associated glomerulonephritis in our case. Recently, Poli et al. demonstrated that IL-26 is one of the most significant inflammatory mediators in active AAV (6). High levels of IL-26 are detected in the sera of active AAV patients with glomerulonephritis. Furthermore, IL-26 binds to NETs, and IL-26-DNA complexes induce secretion of inflammatory cytokines (TNF- α , IL-1 β , IL-6, and G-CSF) and chemokines (IL-8 and CXCL1) by myeloid cells in the crescentic necrotizing lesions of ANCA-associated glomerulonephritis (6). In our case, IL-26 may have potentiated the recruitment of immune cells to the necrotizing lesions through inflammatory cytokines and chemokines, leading to ANCA-associated glomerulonephritis.

Anti-GBM disease is caused by autoimmunity to the $\alpha 3$ chain of type IV collagen of GBM. Susceptibility to anti-

GBM disease is strongly associated with HLA-DRB1 genes, for which HLA-DRB1*15 and DRB1*04 are particularly responsible (13). In our case, the T-cell-mediated immune response to peptides derived from the ruptured GBM through HLA-DR4 from HLA DRB1*04:03 on antigen-presenting cells may have induced the development of anti-GBM antibodies. Furthermore, the vaccine is supposed to elicit CD4 cytokine responses involving type 1 helper T cells (14). It is possible that the enhanced B-cell response after the second dose of the vaccine was responsible for triggering the extremely high titers of anti-GBM IgG1 and the subsequent onset of anti-GBM disease.

Whether AAV predisposes patients to the development of anti-GBM disease or if ANCA positivity occurs in the course of anti-GBM disease is unclear at present (15). Patients with anti-GBM disease may be classified into at least two clusters based on clinical presentation: older adults presenting with kidney involvement alone with a high proportion of ANCA positivity and younger individuals with pulmonary involvement and a lower proportion of double posi-

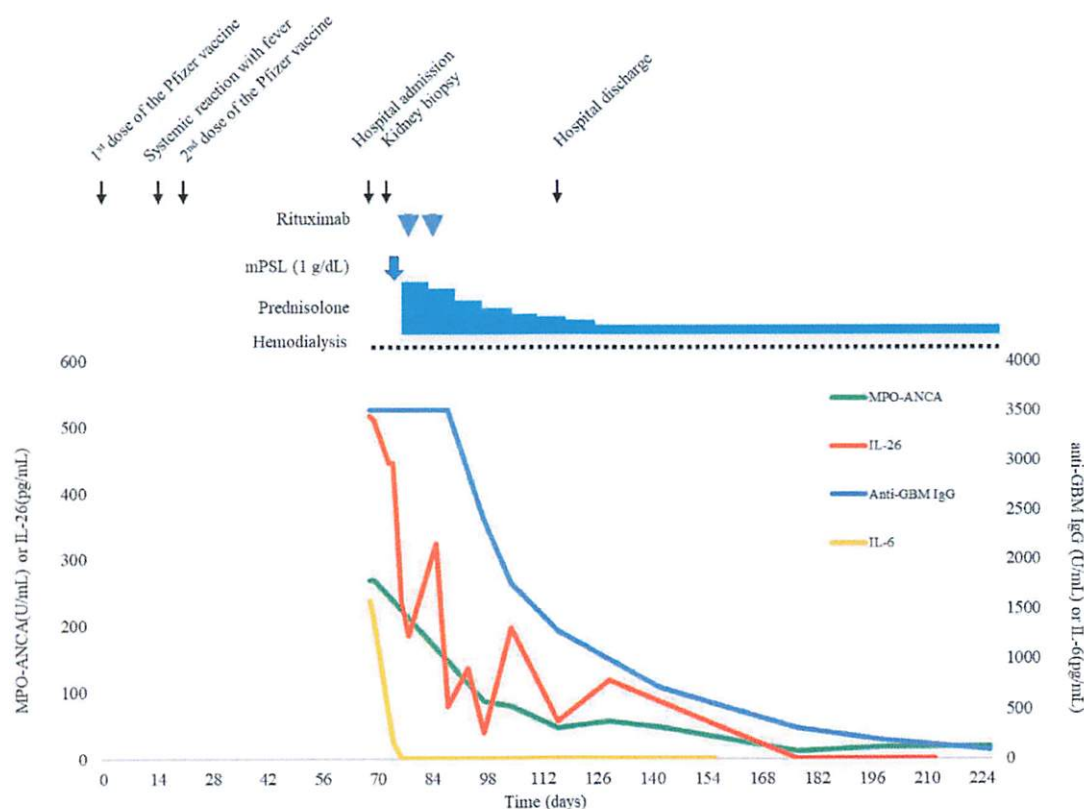


Figure 2. Timeline of clinical events and trends in the serum IgG antibody to GBM titer, MPO-ANCA titer, serum IL-26 concentration, and serum IL-6 concentration from the time of vaccination until the four-month follow-up after discharge.

tivity (16). The recent confirmation of spatial and temporal clustering of anti-GBM disease suggests that environmental factors, including certain infections, may trigger the disease in susceptible individuals (17, 18). We suspect that genetic susceptibility to anti-GBM disease and the history of pulmonary tuberculosis, followed by vaccination, may have triggered the secondary autoimmunity in our case.

Anti-GBM disease is a monophasic non-relapsing illness. However, this may not be so in patients with dual positivity for both ANCA and anti-GBM antibodies. The relapse of clinical features while anti-GBM antibodies are still present is common, and although relapses can also occur in double-positive cases, such instances are often in the context of co-existent ANCA positivity (19). In the present case, decreases in serum IL-26 levels were correlated to a decline in the serum levels of anti-GBM IgG and MPO-ANCA, with no relapses. IL-26 might be a specific biomarker of disease activity. Furthermore, we recently developed a humanized neutralizing anti-IL-26 monoclonal antibody (mAb) for therapeutic use (20). Humanized anti-IL-26 mAb might be a useful therapeutic agent for the treatment of AAV.

This case highlights the association between an aberrant immune response to a vaccine and development of anti-GBM disease concomitant with MPO-ANCA positivity through IL-26. A deeper analysis of the immune response through IL-26 may provide better insight into the mecha-

nism underlying the development of AAV and anti-GBM disease. However, at present, there is insufficient evidence to postulate causality, as it may have been coincidental that mRNA-based SARS-CoV-2 vaccine administration closely preceded the new-onset anti-GBM disease with ANCA positivity. Given the possibility of further usage of mRNA-based vaccines against viral infections, strict pharmacovigilance will be important to determine the true frequency and potential causality between these vaccines and small-vessel vasculitides.

The authors state that they have no Conflict of Interest (COI).

Patient Consent: The authors declare that they have obtained consent from the patient reported in this article for the publication of information about him that appears within this Case Report.

Funding statement: No specific funding was received from anyone in the public, commercial, or not-for-profit sectors to carry out the work described in this article.

Authors' contributions: SK was directly involved in the treatment of the patient, conceived the case report, collected and analyzed the data, and wrote the manuscript. RH and CM analyzed the data. All authors contributed to the article and ap-

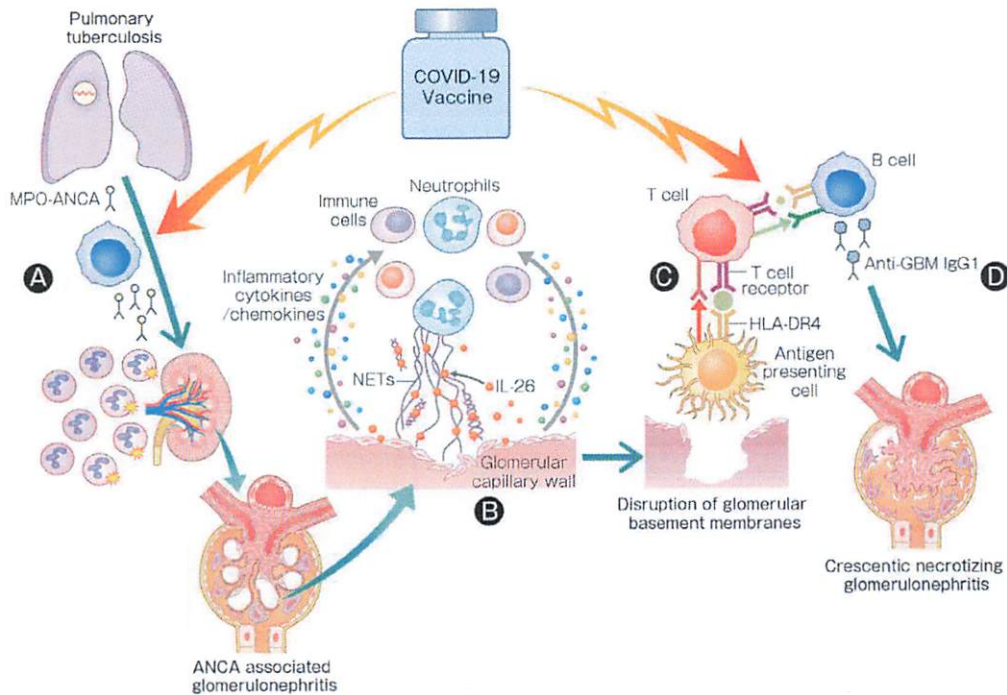


Figure 3. Hypothetical schematic illustration of the role of IL-26 and the mRNA-based COVID-19 vaccine in anti-GBM disease concomitant with MPO-ANCA following vaccination. (A) Latent MPO-ANCA, which might have developed following pulmonary tuberculosis, may have been enhanced following receipt of the SARS-CoV-2 mRNA vaccine, triggering ANCA-associated glomerulonephritis. (B) IL-26 potentiates recruitment of immune cells to necrotizing lesions through inflammatory cytokines and chemokines, leading to ANCA-associated glomerulonephritis. (C) The T-cell-mediated immune response to peptides derived from the ruptured GBM through HLA-DR4 from HLA DRB1*04: 03 on antigen-presenting cells may have induced the development of anti-GBM antibodies. (D) The COVID-19 vaccine may have been responsible for triggering extremely high titers of anti-GBM IgG1 and the onset of anti-GBM disease.

proved the manuscript.

Data availability statement: The data are included in the current report.

References

1. Johns Hopkins University Coronavirus Resource Center. COVID-19 dashboard by the Center for Systems Science and Engineering (CSSE) at Johns Hopkins University. September 1, 2022 [Internet]. Available from: <https://coronavirus.jhu.edu/map.html>
2. Li NL, Coates PT, Rovin BH. COVID-19 vaccination followed by activation of glomerular diseases: does association equal causation? *Kidney Int* **100**: 959-965, 2021.
3. Hellmark T, Segelmark M. Diagnosis and classification of Goodpasture's disease (anti-GBM). *J Autoimmun* **48-49**: 108-112, 2014.
4. Jennette JC, Nachman PH. ANCA glomerulonephritis and vasculitis. *Clin J Am Soc Nephrol* **12**: 1680-1691, 2017.
5. Shabgah AG, Abdelbasset WK, Rahman HS, et al. A comprehensive review of IL-26 to pave a new way for a profound understanding of the pathobiology of cancer, inflammatory diseases and infections. *Immunology* **165**: 44-60, 2022.
6. Poli C, Augusto JF, Dauvé J, et al. IL-26 Confers Proinflammatory Properties to Extracellular DNA. *J Immunol* **198**: 3650-3661, 2017.
7. Shakoor MT, Birkenbach MP, Lynch M. ANCA-associated vasculitis following the Pfizer-BioNTech COVID-19 vaccine. *Am J Kidney Dis* **78**: 611-613, 2021.
8. Gupta RK, Ellis BK. Concurrent antiglomerular basement membrane nephritis and antineutrophil cytoplasmic autoantibody-mediated glomerulonephritis after second dose of SARS-CoV-2 mRNA vaccination. *Kidney Int Rep* **7**: 127-128, 2022.
9. Irure-Ventura J, Belmar-Vega L, Fernández-Fresnedo G, et al. Increased induction of de novo serum ANCA and ANCA-associated vasculitis after mass vaccination against SARS-CoV-2. *iScience* **25**: 104847, 2022.
10. Frangou E, Vassilopoulos D, Boletis J, Boumpas DT. An emerging role of neutrophils and NETosis in chronic inflammation and fibrosis in systemic lupus erythematosus (SLE) and ANCA-associated vasculitides (AAV): Implications for the pathogenesis and treatment. *Autoimmun Rev* **18**: 751-760, 2019.
11. Flores-Suárez LF, Cabiedes J, Villa AR, van der Woude FJ, Alcocer-Varela J. Prevalence of antineutrophil cytoplasmic autoantibodies in patients with tuberculosis. *Rheumatology (Oxford)* **42**: 223-229, 2003.
12. Elkayam O, Bendayan D, Segal R, et al. The effect of anti-tuberculosis treatment on levels of anti-phospholipid and antineutrophil cytoplasmic antibodies in patients with active tuberculosis. *Rheumatol Int* **33**: 949-953, 2013.
13. Fisher M, Pusey CD, Vaughan RW, Rees AJ. Susceptibility to anti-glomerular basement membrane disease is strongly associated with HLA-DRB1 genes. *Kidney Int* **51**: 222-229, 1997.

14. Sahin U, Muik A, Derhovnessian E, et al. COVID-19 vaccine BNT162b1 elicits human antibody and TH1 T cell responses. *Nature* **586**: 594-599, 2020.
15. Levy JB, Hammad T, Coulthart A, Dougan T, Pusey CD. Clinical features and outcome of patients with both ANCA and anti-GBM antibodies. *Kidney Int* **66**: 1535-1540, 2004.
16. Alchi B, Griffiths M, Sivalingam M, Jayne D, Farrington K. Predictors of renal and patient outcomes in anti-GBM disease: clinicopathologic analysis of a two-centre cohort. *Nephrol Dial Transplant* **30**: 814-821, 2015.
17. Canney M, O'Hara PV, McEvoy CM, et al. Spatial and Temporal Clustering of Anti-Glomerular Basement Membrane Disease. *J Am Soc Nephrol* **11**: 1392-1399, 2016.
18. Predecki M, Candice Clarke C, Cairns T, et al. Anti-glomerular basement membrane disease during the COVID-19 pandemic. *Kidney Int* **98**: 780-781, 2020.
19. Levy JB, Lachmann RH, Pusey CD. Recurrent Goodpasture's disease. *Am J Kidney Dis* **27**: 573-578, 1996.
20. Hatano R, Itoh T, Otsuka H, et al. Humanized anti-IL-26 monoclonal antibody as a novel targeted therapy for chronic graft-versus-host disease. *Am J Transplant* 2022 Aug 23.

The Internal Medicine is an Open Access journal distributed under the Creative Commons Attribution-NonCommercial-NoDerivatives 4.0 International License. To view the details of this license, please visit (<https://creativecommons.org/licenses/by-nc-nd/4.0/>).

© The Japanese Society of Internal Medicine
Intern Med Advance Publication



Spare the lung: surgical treatment approach for malignant pleural mesothelioma

Nobukazu Fujimoto[^]

Department of Medical Oncology, Okayama Rosai Hospital, Okayama, Japan

Correspondence to: Nobukazu Fujimoto. Department of Medical Oncology, Okayama Rosai Hospital 1-10-25 Chikkomidorimachi, Okayama 7028055, Japan. Email: nobufujimot@gmail.com.

Comment on: Klotz LV, Hoffmann H, Shah R, *et al.* Multimodal therapy of epithelioid pleural mesothelioma: improved survival by changing the surgical treatment approach. *Transl Lung Cancer Res* 2022;11:2230-42.

Submitted Dec 26, 2022. Accepted for publication Jan 23, 2023. Published online Jan 29, 2023.

doi: 10.21037/tlcr-22-909

View this article at: <https://dx.doi.org/10.21037/tlcr-22-909>

In a recent study published on *Translational Lung Cancer Research*, Klotz and colleagues report the results of their retrospective analyses, where they compared treatment outcomes among patients diagnosed with epithelioid malignant pleural mesothelioma (MPM) (1). They compared survival of three patient cohorts: one was treated with an extrapleural pneumonectomy (EPP); one was treated with an extended pleurectomy/decortication (EPD) combined with hyperthermic intrathoracic chemoperfusion (HITOC) and adjuvant chemotherapy; and one was treated with chemotherapy alone. They demonstrated that the median overall survival (OS) was significantly longer in the EPD/HITOC cohort than in the EPP and chemotherapy cohorts. In addition, their multivariate analysis showed that EPD/HITOC was significantly associated with improved OS. Based on these findings, they concluded that a less radical lung-sparing surgery, EPD, should be performed in patients with epithelioid MPM.

MPM is strongly associated with past asbestos exposure, and its incidence has continued to increase in many developing countries. Surgical resection is applied to patients in the earlier stages of the disease. However, a tumor resection with wide microscopically negative margins is not feasible in MPM, due to the surrounding vital structures. The aim of a surgical resection for MPM is to remove the entire macroscopic tumor from the hemithorax. A macroscopic complete resection can be achieved with both an EPP and a PD. However, it remains controversial

which is the more appropriate procedure. Although an EPP was traditionally the technique of choice, perioperative mortality and morbidity were significantly lower with an EPD than with an EPP. A systematic review showed that OS was comparable between those treated with an EPP and those treated with an EPD (2). Those results were further supported in a meta-analysis (3). In addition, the EPP is generally more deleterious than an EPD, in terms of quality of life for the patient (4). Based on those reports, the recent European Society of Medical Oncology Clinical Practice Guidelines considered a lung-sparing EPD the first-choice surgical procedure (5). However, an EPP could also be offered to highly selected patients in high-volume centers. Due to the lack of a direct comparison between these two surgical modalities, the superiority of an EPD has not been established.

Klotz and colleagues analyzed the outcomes of patients with epithelioid MPM treated with a multimodal approach during the last 2 decades in a single high-volume center in Germany. They changed their surgical approach between 2012 and 2013, from an EPP-based multimodal treatment to an EPD/HITOC treatment. Many institutions around the world have similarly changed their surgical policies, based on a randomized feasibility study that compared EPP and no-EPP treatments (6).

In the Klotz study, the median OS of the EPD/HITOC, EPP, and chemotherapy cohorts were 38.1, 24.0, and 15.8 months, respectively. These median OS were

[^] ORCID: 0000-0002-4516-0433.

consistent with those reported previously. Better survival was significantly associated with good performance status, a younger age, and negative lymph node status. The perioperative morbidity rate was significantly higher in the EPP cohort (36.2%) than in the EPD/HITOC cohort (18%). The strength of the study was that the results of different surgical approaches were compared in a high-volume institution. This real-world data might support a less radical lung-sparing technique as the first-choice surgical procedure for epithelioid MPM. It seems quite natural that survival was worst in the chemotherapy cohort, because those patients had unresectable, advanced disease.

Of note, the study by Klotz and colleagues had some limitations. The main limitations were the retrospective study design and the limited number of selected patients. Moreover, the EPD/HITOC cohort contained more patients and better performance status, compared to the EPP cohort. Second, as the authors described, due to the time difference, potential improvements in perioperative management and recent advancements in treating tumor recurrence might have influenced the improved OS in the EPD/HITOC cohort. Third, the role of an HITOC adjunct to surgery for MPM has not been established. The objective of the HITOC is to eradicate the remaining cancer cells. To date, improvements in recurrence-free survival and OS have been observed in a retrospective single-center analysis (7). However, the efficacy of HITOC has not been demonstrated in a prospective trial.

In the future, the lung-sparing EPD will be a standard surgical approach for resectable MPM, based on the above-mentioned retrospective studies, including the meta-analyses. The current report by Klotz and colleagues also supported the efficacy of EPD and demonstrated that it could maintain the patient's quality of life. Nevertheless, many problems remain to be resolved concerning the surgical approach for MPM. First, there is no clear evidence on the impact of EPD on extended OS in patients with MPM. The evidence may be provided by the MARS2 trial, which will prospectively compare the extent of survival improvement between EPD and non-surgical therapy (8). Another major outstanding issue is whether systemic chemotherapy should be delivered in a neoadjuvant or adjuvant setting. Some clues to this issue might come from a randomized phase II trial that aims to compare the effect of neoadjuvant and adjuvant chemotherapy in combination with surgery in MPM (9). Furthermore, the exact role of HITOC should be clarified in a prospective clinical trial.

We sincerely hope that, through prospective clinical

trials and grounded real-world data, an optimal clinical approach will be established for patients with MPM.

Acknowledgments

Funding: The author is supported by grants-in-aid from the Ministry of Health, Labor, and Welfare, Japan.

Footnote

Provenance and Peer Review: This article was commissioned by the editorial office, *Translational Lung Cancer Research*. The article did not undergo external peer review.

Conflicts of Interest: The author has completed the ICMJE uniform disclosure form (available at <https://tldr.amegroups.com/article/view/10.21037/tlcr-22-909/coif>). The author reports grants and personal fees from ONO, Bristol-Meyers Squibb, and personal fees from Chugai and Behringer Ingelheim.

Ethical Statement: The author is accountable for all aspects of the work in ensuring that questions related to the accuracy or integrity of any part of the work are appropriately investigated and resolved.

Open Access Statement: This is an Open Access article distributed in accordance with the Creative Commons Attribution-NonCommercial-NoDerivs 4.0 International License (CC BY-NC-ND 4.0), which permits the non-commercial replication and distribution of the article with the strict proviso that no changes or edits are made and the original work is properly cited (including links to both the formal publication through the relevant DOI and the license). See: <https://creativecommons.org/licenses/by-nc-nd/4.0/>.

References

1. Klotz LV, Hoffmann H, Shah R, et al. Multimodal therapy of epithelioid pleural mesothelioma: improved survival by changing the surgical treatment approach. *Transl Lung Cancer Res* 2022;11:2230-42.
2. Cao C, Tian D, Park J, et al. A systematic review and meta-analysis of surgical treatments for malignant pleural mesothelioma. *Lung Cancer* 2014;83:240-5.
3. Taioli E, Wolf AS, Flores RM. Meta-analysis of survival after pleurectomy decortication versus extrapleural pneumonectomy in mesothelioma. *Ann Thorac Surg*

- 2015;99:472-80.
4. Rena O, Casadio C. Extrapleural pneumonectomy for early stage malignant pleural mesothelioma: a harmful procedure. *Lung Cancer* 2012;77:151-5.
 5. Popat S, Baas P, Faivre-Finn C, et al. Malignant pleural mesothelioma: ESMO Clinical Practice Guidelines for diagnosis, treatment and follow-up☆. *Ann Oncol* 2022;33:129-42.
 6. Treasure T, Lang-Lazdunski L, Waller D, et al. Extrapleural pneumonectomy versus no extra-pleural pneumonectomy for patients with malignant pleural mesothelioma: clinical outcomes of the Mesothelioma and Radical Surgery (MARS) randomised feasibility study. *Lancet Oncol* 2011;12:763-72.
 7. Sugarbaker DJ, Gill RR, Yeap BY, et al. Hyperthermic intraoperative pleural cisplatin chemotherapy extends interval to recurrence and survival among low-risk patients with malignant pleural mesothelioma undergoing surgical macroscopic complete resection. *J Thorac Cardiovasc Surg* 2013;145:955-63.
 8. Lim E, Darlison L, Edwards J, et al. Mesothelioma and Radical Surgery 2 (MARS 2): protocol for a multicentre randomised trial comparing (extended) pleurectomy decortication versus no (extended) pleurectomy decortication for patients with malignant pleural mesothelioma. *BMJ Open* 2020;10:e038892.
 9. Raskin J, Surmont V, Cornelissen R, et al. A randomized phase II study of pleurectomy/decortication preceded or followed by (neo-)adjuvant chemotherapy in patients with early stage malignant pleural mesothelioma (EORTC 1205). *Transl Lung Cancer Res* 2018;7:593-8.

Cite this article as: Fujimoto N. Spare the lung: surgical treatment approach for malignant pleural mesothelioma. *Transl Lung Cancer Res* 2023;12(2):197-199. doi: 10.21037/tlcr-22-909

